MASSEY
UNIVERSITY

Doctoral Thesis

Increasing the Capacity of 5G Networks using Mobile-Cells

Shan Jaffry

Department of
Mechanical & Electrical Engineering

Massey University
New Zealand

2019

Increasing the Capacity of 5G Networks using Mobile-Cells

Shan Jaffry

April 18, 2019

A THESIS PRESENTED IN PARTIAL FULFILMENT OF THE REQUIREMENTS FOR THE DEGREE OF

DOCTOR OF PHILOSOPHY

IN

ENGINEERING

AT

MASSEY UNIVERSITY,

NEW ZEALAND.

Acknowledgment

First and foremost, I am indebted and grateful to God for giving me the knowledge, strength, and courage to come this far to complete my doctoral thesis.

Secondly, I am thankful to my doctoral supervisor Dr. Syed Faraz Hasan for his continuous support and valuable guidance. Dr. Hasan's critical analysis on my work helped me a lot in improving the way I now conduct research. I must admit that I have learned the ways of thinking clearly and thoroughly under the guidance of Dr. Hasan. I am also very grateful to my co-supervisor Dr. Xiang Gui whose critiques on my research was a significant factor in improving the quality of this thesis. In particular, Dr. Gui's insight into my mathematical analysis helped to develop sound analytical proofs of the ideas presented in this thesis. I am sure that the end of my doctoral journey will not be the end of the relationship with my supervisors.

I am also thankful to Massey University, New Zealand for granting me Massey Doctoral Scholarship. Massey University has a very sound academic environment and provides excellent research facilities. The university also generously granted me funds to present my research in national and international conferences. Thank you, Massey University.

I could not have come this far without the life-time and unconditional support of my father and mother. Words will never justify my feelings of gratitude for their sacrifices. My four brothers (Sibte, Shabib, Shakeeb, and Riaz) have also been a strong support and source of inspiration for me. While I was busy doing my doctoral research, they looked after our parents.

I would also like to thank and acknowledge the sacrifices of my wife, Dr. Syeda Zehra Qamber. She supported my decision to begin PhD and took break from her medical practice to join me in New Zealand. She has been a constant support for me. Without any doubt, this thesis could not have been completed without her. We were also blessed with Raza-e-Muhammad, our son during this period. Thank you, Zehra.

In the end, I am grateful to all other people who have supported me in any way during my PhD. I want to acknowledge the support of all my friends in Pakistan who have motivated or inspired me. In particular, I am very thankful to Mr. Iftikhar Hussain Zaidi for being the source of motivation for me and to inspire me to start my journey towards PhD.

Thank you all!

Abstract

Recently, the exponential growth in mobile data demand, fuelled by novel use-cases, such as high-definition video streaming, etc., has caused massive strain on cellular networks. As a solution, the fifth generation (5G) of cellular technology has been introduced to improve network performance through various innovative features, such as millimeter-wave spectrum, device-centric communication, and heterogeneous networks (HetNet). The HetNets will comprise of several small-cells underlaid within macro-cell to serve densely populated regions, like stadiums, malls, etc. On the other hand, due to the constant rise in the use of mobile phones while traveling, the concept of mobile-cells has emerged. Mobile-cells may well be defined as public transport vehicles (e.g., buses or trains etc.) equipped with in-vehicle cellular antenna to serve commuters. The argument for using mobile-cell is based on the observation that commuters often experience poor quality of service (QoS) due to vehicular penetration loss (VPL). Mobile-cell will decouple commuters from the core network, thus eliminating VPL, along with relieving base station off large number of users.

Mobile-cells will contain multiple wireless links. Commuters will be served over access link (AL), while the communication with the core network will occur over the backhaul link (BL). On the other hand, neighboring mobile-cells will mutually exchange data over sidehaul links (SLs). Like any other device-centric communication, mobile-cells need to ‘discover’ their neighbors before establishing SLs. Neighborhood discovery is challenging for mobile-cells. Relevant literature on this topic has only focused on static devices, and discovery for mobile devices has not been investigated in detail. Hence, as our first research problem in this thesis, we have focused on the autonomous discovery by a mobile-cell. In general, due to randomness involved in an autonomous process, neighborhood discovery often fails due to collision and half-duplexing effects. This thesis focuses on mitigating these effects. Firstly, we have proposed a modified time-frequency frame structure to subside the collision and half-duplexing effects. Later on, we have presented a more reliable solution that utilizes proximity awareness to adapt transmission probability of individual devices. This scheme has resulted in a drastic increase in the probability of successful discovery as compared to the conventional approaches.

On the other hand, actual data exchange via mobile-cell’s links requires interference-free resource allocation for each link. Mobile-cells’ wireless links will cause severe interference to the out-of-vehicle cellular users. Few researchers have assigned separate bands for in-vehicle and out-of-vehicle links. However, given the scarcity of spectral resources, these methods are practically inefficient. Thus, we have addressed the issue of resource allocation as the second research problem in this thesis. Instead of assigning individual resources to each link, we have focused on resource sharing between multiple wireless links. To achieve this goal, we have exploited VPL and utilized successive interference cancellation. Our results have shown high QoS at each individual link. We have also demonstrated the effect of mobility on the proposed resource sharing schemes. The schemes proposed in this thesis will ensure that the mobile-cell increases the capacity of 5G networks through aggressive resource sharing such that more links will use available spectral resources.

This page is intentionally left blank.

Contents

List of Tables

List of Figures

List of Abbreviations

1G	First Generation
3G	Third Generation
3GPP	Third Generation Partnership Project
4G	Fourth Generation
5G	Fifth Generation
ABS	Autonomous base station
AL	Access-link
AWGN	Additive white Gaussian noise
BF	Brute-force
BL	Backhaul-link
BPP	Binomial Point Process
BTU	Beacon Transmission Unit
CCU	Communication Control Unit
CH	Cluster-head
CoMP	Coordinated multi-point
CSC	Cognitive small-cell
CSMA	Carrier Sense Multiple Access
CU	Cellular User
DJAS	Disjoint sub-channel access scheme
DUE	Discovering user equipment
DUSA	Dynamic user scheduling algorithm
FDD	Frequency-division duplexing
H-PPP	Homogenous Poisson Point Process
HetNet	Heterogenous Networks
IaaS	Infrastructure as a Service
INP	Infrastructure provider
ISM	Industrial, scientific, and medical

JAS	Joint sub-channel access scheme
LoS	Line-of-sight
LTE	Long Term Evolution
LTE-A	Long Term Evolution Advanced
MAC	Medium Access Control
mDUE	Mobile DUE
MBS	Macro-cell base station
MeNB	Macro-cell eNB
MIMO	Multiple-Input-Multiple-Output
MINLP	Mixed integer non-linear programming
mmWave	Millimeter wave
MUE	Macro-cell user equipment
MVNO	Mobile virtual network operator
NLoS	Non line-of-sight
OBMN	Optically backhauled mobile network
OFDMA	Orthogonal Frequency Division Multiple Access
PPP	Poisson Point Process
PRACH	Physical Random Access Channel
PSDCH	Physical Sidelink Shared Channel
PUCCH	Physical Uplink Control Channel
PUSCH	Physical Uplink Shared Channel
QoS	Quality of Service
RB	Resource block
RS	Random-selection / Random-select
RSRP	Reference Signal Received Power
RWP	Random way-point
SAP	Small-cell access point
SBS	Small-cell base station
SeNB	Small-cell eNB
SIC	Successive Interference Cancellation
SINR	Signal-to-Interference-Plus-Noise ratio
SIR	Signal-to-Interference ratio
SITable	Strong interference table
SL	Sidehaul Link

SRS	Sounding Reference Signal
SRSTable	Strong resource status table
SUE	Small-cell user equipment
TDD	Time-division duplexing
TIDI	Time interval dependent interference
UE	User equipment
USRP	Universal Software Radio Peripheral
VPL	Vehicular Penetration Loss
VR	Virtual resources
VUE	In-vehicle user equipment
WITable	Weak interference table
WRSTable	Weak resource status table

This page is intentionally left blank.

Chapter 1

Introduction

Since the inception of the first generation (1G) of wireless cellular technology in the late 1980s, its popularity has expanded tremendously due to its wide geographical coverage, reliability, and portability. The first generation focused merely on making voice calls with brick-sized mobile phones. However, due to the continued research and improvements in computing hardware and software, exciting new use-cases for this technology have emerged with every passing generation [1]. For example, the use of mobile Internet became widely available with 3rd and 4th generations (See Fig. 1.1). Currently, the mobile data traffic has outgrown voice traffic over cellular networks by a large proportion [2] as shown in Figure 1.2. This growth in data traffic is the consequence of a massive increase in the number of connected devices and a persistent rise in average data volume per device, fueled primarily by heightened viewership of online video contents [3].

In near future, due to the emergence of novel use-cases (such as, 4K/8K video streaming [4], vehicular communications, and virtual-reality based applications,

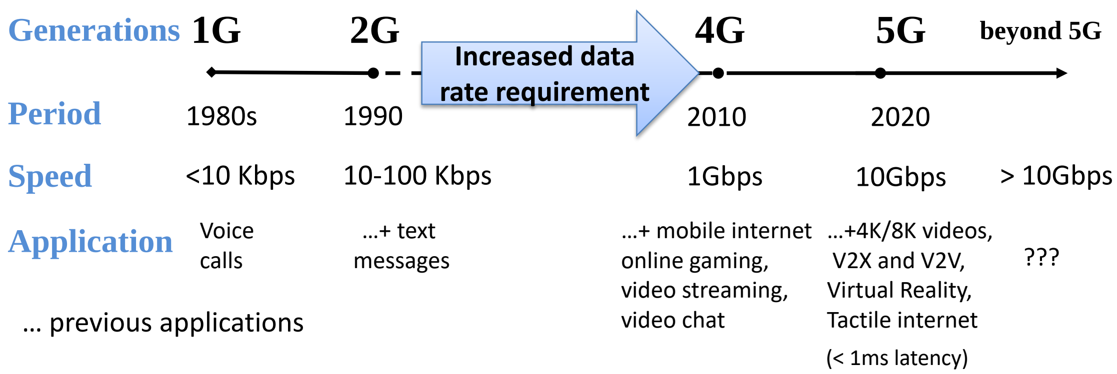

Figure 1.1: Past, present, and future of cellular technology

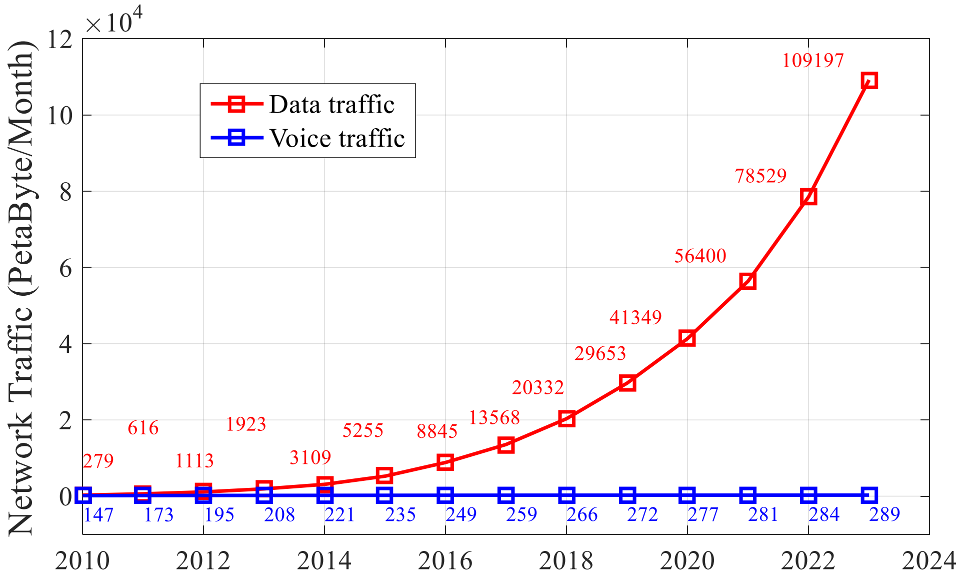

Figure 1.2: Extrapolated growth of voice and data traffic over the years [Source: Ericsson Mobility Report 2018]

etc.), available cellular bands will reach saturation limits [5]. As a potential remedy, the fifth generation (5G) of cellular technology has promised to enhance the network performance by offering several new features including millimeter wave (mmWave) spectrum, heterogeneous networks (HetNet), and device-centric communication [6, 7]. These features, as we shall explain in the later sections, will collectively contribute to enhance the network bandwidth, enable aggressive frequency reuse, and alleviate load on the base station by promoting network-free communication.

The ubiquity of wireless cellular technology, coupled with the portability of modern devices (such as, smartphones, tablets, and smart-watches, etc.), has also contributed in its widespread popularity among commuters inside public transport (such as buses, trains, and subways, etc.). The public transport passengers often utilize their traveling time by engaging in several activities over their smartphones and tablets [8–10]. As the demands of the in-vehicle users grow, the load on the core network also increases almost without bounds. Oftentimes these commuting users receive very poor quality of service (QoS) even while using very basic cellular services [11], due to the effects such as vehicular penetration loss (VPL), and Doppler effect etc. Hence, the researchers have proposed to install a dedicated antenna inside public transport to form a ‘mobile-cell’. The mobile-cells will improve QoS for the commuting users by

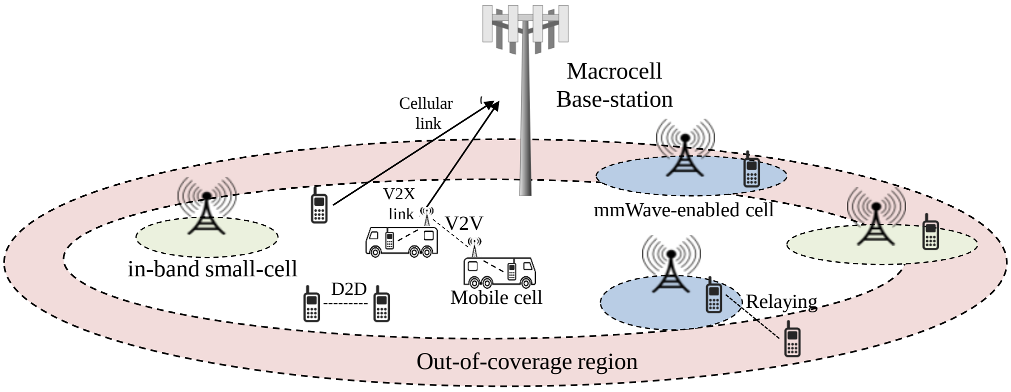

Figure 1.3: Envisioned 5G and beyond heterogeneous network.

bringing the communication antenna inside the vehicle, consequently eliminating VPL along with releasing the base station off large number of cellular users. As mobile-cells will be an integral part of future networks, it is essential to first discuss the anticipated underlying changes in the next generation of cellular technology.

1.1 Main Features of 5G Networks

1.1.1 Millimeter-wave Communication

Current wireless bandwidth will become a major bottleneck in fulfilling increasing traffic demands in future networks. On the other hand, there is huge bandwidth available in the unexplored mmWave bands between 30 and 300 GHz. Hence, this mmWave spectrum has been proposed as an integral part of 5G radio access network interface [12] to provide multi-gigabit communication services such as ultra-high definition video streaming, etc. The physical properties of mmWave radio signals do not allow the provision of coverage to larger geographical areas [13]. Therefore, this very high frequency spectrum has found much popularity in solutions that are indoor, such as inside confined offices or shopping malls, etc. [14] The shorter geographical regions that the mmWave-enabled base stations cover are often known as small-cell regions [15]. The challenges associated with mmWave transmissions demand highly directional antennas with efficient beam-forming mechanisms for both the base stations (on downlink) and cellular users (on uplink). Furthermore, massive multiple-input-multiple-output (MIMO)

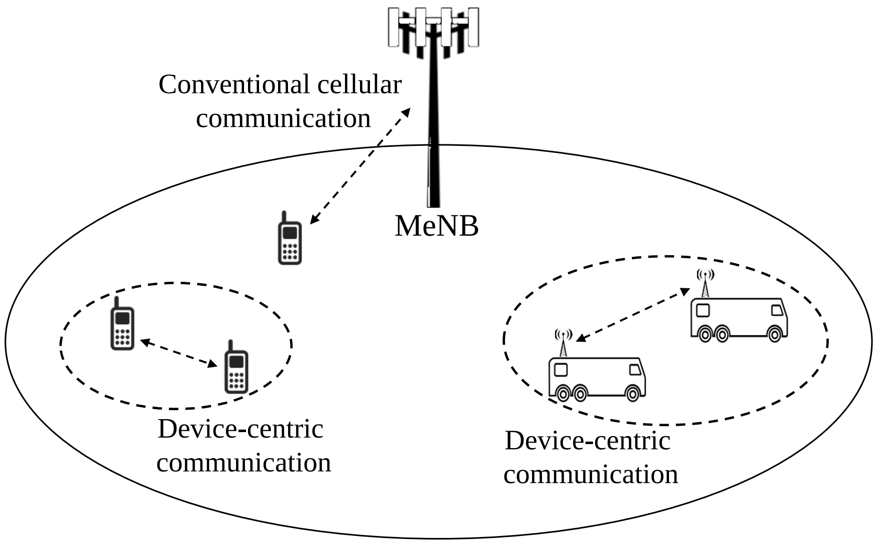

Figure 1.4: Examples of device-centric communication.

antennas are required for, at least, the transmitting base station to serve multiple users located in different positions within the cell. Alternatively, many researchers have explored small-cell densification using long term evolution advanced (LTE-A) spectrum (often called the sub 6 GHz spectrum). Hence, the overall architecture of future 5G networks can be pictured as layers of small-cells (mmWave-enabled or sub 6 GHz) that serve densely populated regions overlaid by macro-cell layer that provides services to wider regions [16]. Such a heterogeneous architecture will effectively enable 5G networks, which we will discuss in the next section.

1.1.2 Heterogeneity

To overcome the imminent saturation of current 4G spectrum, researchers have focused on distributing the load of macro-cell to several small-cells that provide services in regions where user density is medium to high (for example, inside shopping-malls, stadiums, or offices, etc.) [17]. Due to this network densification, spectrum can be reused very aggressively to accommodate ever larger number of users. As depicted in Figure 1.3, to enable ubiquitous cellular coverage, these small-cells are underlaid within macro-cellular layer to form a HetNet [18].

A conventional small-cell eNB (SeNB) is a fixed low-power base station. On the contrary, the mobile-cell is a wireless hotspot mounted on-board public vehicles (e.g., buses or trains, etc.) to serve the commuting passengers [19]. The mobile-cell is connected to the core network over backhaul link (BL) and communicate with neighboring vehicles over sidehaul links (SL). However, as mobile-cell may travel from one geographical area to another in short amount of time, it should remain self-reliant in operations, such as discovering neighbors, or establishing sidehaul communication links. This network-independence will also offload devices from the macro-cell eNBs (MeNBs), enabling device-centric communication. The device-centric communication will also enable frequency reuse to improve the spectral efficiency of future network [20, 21]. In particular, a mobile-cell will act in device-centric mode when, for example, two neighboring buses share data on the SL as shown in Figure 1.4. Mobile-cells will also relay services (using SLs) to out-of-vehicle cellular users in regions with no network coverage [22, 23]. To establish SLs mobile-cells must discover its neighbors or out-of-vehicle users.

A fast and efficient discovery procedure will ensure that more users will be connected to mobile-cells, effectively increasing the capacity of 5G networks, as we shall present in Chapter 4. The mobile-cells will also increase the capacity of 5G networks by accommodating more cellular users through resource sharing, as we shall demonstrate in Chapter 5 and Chapter 6. These various features, along with few others, have motivated us to undertake a detailed examination of mobile-cell in this research. These motivations are formally discussed in the next section.

1.2 Motivation Behind Mobile-Cells

The main motivation behind focusing on mobile-cells is based on the observations that the traveling time for commuters within public transport is enough to freely access smartphones and similar devices. A study conducted in Australia found that more than 80% of the commuters in Australian transport system use cellular devices while traveling inside buses or trains [11]. Similar trends have been reported for cities like New York, London, Shanghai, and São Paulo where more than 93%, 89%, 84%, and 53% commuters use cellular devices, respectively. However, most of these commuters are dissatisfied with the QoS they receive inside vehicle. For example, almost 55% of the New Yorkers are not satisfied with the cellular connectivity inside public transport [10]. The main cause of user dissatisfaction is the VPL which drastically reduces signal strength as radio waves

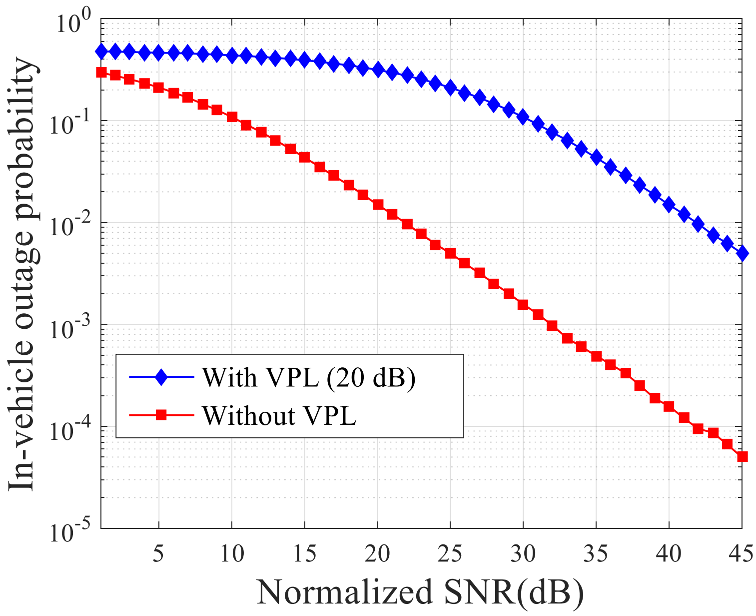

Figure 1.5: Effect of VPL on the outage probability. © 2018 IEEE [11].

penetrate through vehicular body. A mobile-cell will circumvent VPL using in-vehicle antenna, consequently improving QoS for commuters [24]. For example, Figure 1.5 shows how VPL compensation may reduce the outage probability for in-vehicle users. A mobile-cell will also have out-of-vehicle antennas to connect with the core network over BL and with neighboring mobile-cells over SLs as shown in Figure 1.6.

Furthermore, a study presented in [25] has found that commuters traveling inside public buses often make similar data requests. For example, it was found in an experiment conducted in 2015 that during peak traveling hours in Sweden, 85% of requests were generated only from the public transport of a specific route. The authors demonstrated that if these public buses were equipped with on-board cache mechanism, nearly 40% buses could have saved 20% of daily bandwidth. Note that the on-board cache mechanism within mobile-cells will provide data services to commuters without accessing the network [26].

Another motivation for mobile-cells stems from the fact that the group of commuting users inside fast moving public transport causes large number of simultaneous handovers as the vehicle moves from the coverage of one cell to another [11]. High handover rate (per hour) exerts undesirable signaling overhead

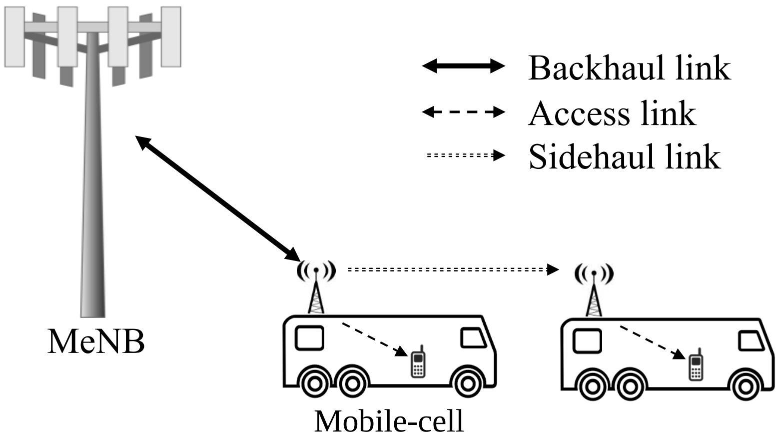

Figure 1.6: Mobile-cells and associated links

on the network [27]. In future networks, with smaller-sized cells and multiple radio access technologies (such as mmWave and microwave, etc.), the issue of handover will become more concerning unless effective measures are taken. Note that as a rule of thumb, the handover rate is proportional to the number of active connections per vehicle and the vehicle's speed [28], as illustrated in Figure 1.7. Hence, as mobile-cells cater for a large number of users through in-vehicle antenna, the number of handovers will also reduce [29].

Another significant utility of mobile-cell is anticipated under scenarios where the main network gets offline due to natural calamity or other reasons. In such settings, mobile-cells can provide basic connectivity to the users via SLs and connect to the main network using BLs where possible [30–32].

It should be noted that unlike other new additions in 5G, no significant hardware modifications are required in the current cellular equipment (e.g., smartphones) in order to benefit from mobile-cells. The in-vehicle antenna will communicate with commuters like a regular transmitter-receiver pair. On the other hand, the installation of in-vehicle antenna will be a minor variation considering that many vehicles today are already equipped with Wi-Fi transceivers. We will discuss about this issue in Chapter 2. Apart from the benefits associated with the mobile-cells, there are still some technical challenges which are yet to be resolved, e.g., neighborhood awareness for establishing SLs, and interference management, etc. In this thesis, our research contribution pivots around addressing these challenges, as we shall explain in the next section.

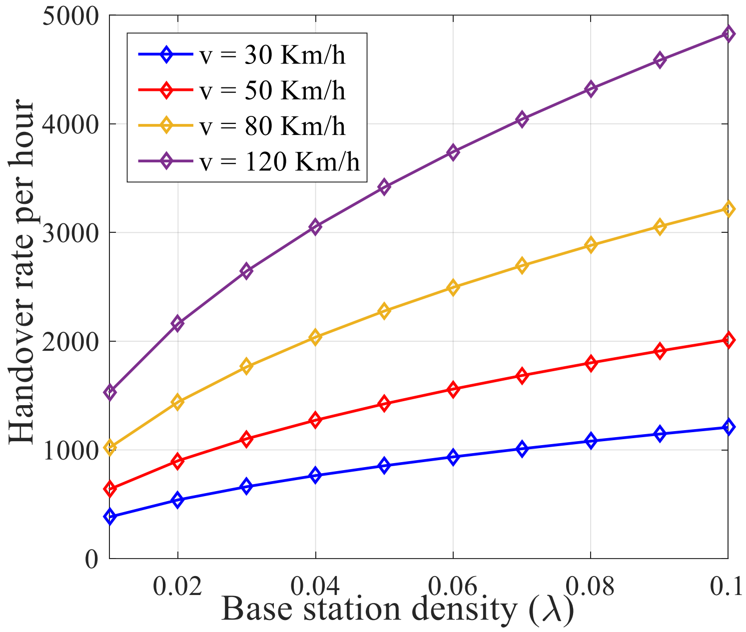

Figure 1.7: The impact of base station density and public vehicles' velocity on handover rate (with 10 passengers and an average of 10 active-links per-vehicle). © 2018 IEEE [11].

1.3 Problem Statement and Research Contribution

This thesis addresses two main problems concerning mobile-cells. The first problem relates to the discovery of neighboring mobile-cells or out-of-vehicle users to establish SLs. Neighbor discovery is an active research problem for any device-centric communication and several aspects, such as power consumption, resource allocation, and time-to-discovery, etc., have been addressed by researchers [33]. For mobile-cells, the time-to-discovery is of utmost importance as mobile-cells are moving nodes and their neighborhood may change very rapidly. Note that in the presence of network connectivity, the base station may assist nodes in the discovery process, at the cost of additional overhead on the network. However, in the absence of cellular coverage, neighborhood awareness gets more challenging. The devices that participate in out-of-network autonomous neighborhood awareness often suffer from discovery failure issues which we shall discuss in detail in Chapter 2. These issues severely degrade the performance of discovery processes, consequently increasing the time-to-discovery. We will propose an adaptive mechanism which optimizes the discovery procedure by considering density of nodes in the neighborhood. Furthermore, we will develop an analytical model for neighborhood discovery by a mobile-cell, which, to the best of our knowledge has never been presented in the literature before.

After accomplishing neighborhood discovery, mobile-cells can exchange data over sidehaul links. The mobile-cells have two additional links, namely backhaul link and access link (AL). The mobile-cell's wireless links will cause severe interference to the neighboring out-of-vehicle users. Therefore, our second research problem is related to resource allocation and interference management for mobile-cells. Ideally, each link should be assigned separate frequency resources to maintain optimal link quality with minimum interference. However, the allocation of unique frequency resources for multiple links associated with mobile-cells (i.e., AL, BL, and SL) will waste a large amount of cellular bandwidth. To address this issue, this thesis will propose resource sharing between mobile-cell's wireless links and out-of-vehicle cellular users. Unlike other schemes that are available in the literature, our proposed schemes will ensure that mobile-cells do not consume any additional resource from the spectrum, and share sub-channels with other links within the coverage of macro-cell base station.

1.4 Thesis Organization

This thesis is organized as follows. In the next section of this chapter, we present the summary of research outcomes which comprise of peer-reviewed journal and conference articles. The details of the remaining of chapters are as follows:

Chapter 2: Literature Review. This chapter reviews the latest literature pertinent to the problems that we will be addressing in this thesis. These problems include neighbor discovery, interference management and resource allocation for mobile-cells. The following publications [11,34] have contributed to this chapter.

- **Shan Jaffry**, Syed Faraz Hasan, Xiang Gui, "Mobile-Cells Assisting Future Cellular Networks", Vol. 37, Issue 5, IEEE Potentials, September 2018.

- **Shan Jaffry**, Syed Faraz Hasan, Xiang Gui, "Making a Case for Moving Small cells", IEEE 26th International Telecommunication Networks and Applications Conference (IEEE ITNAC), 2016, December 2016, Dunedin, New Zealand.

Chapter 3: Distributed Neighborhood Discovery. This chapter outlines our initial work towards neighborhood discovery. We have proposed a modified time-frequency frame structure that enables transmission of multiple discovery messages during a single discovery period. Comparisons between the performance of conventional and proposed frame structures have also been presented. The results demonstrate significant improvement in the probability of successful discovery due to the proposed frame structure, particularly when neighborhood density remains medium to low. Following publication [35] has contributed to this chapter.

- **Shan Jaffry**, Syed Faraz Hasan, Yaw Wen Kuo, Xiang Gui, "Distributed Device Discovery in ProSe environment", IEEE Region 10 Conference (IEEE TENCON), November 2017, Penang, Malaysia.

Chapter 4: Proximity-aware Neighborhood Discovery. In this chapter, we have presented a scheme that utilizes neighborhood density information to optimize the rate with which devices broadcast discovery messages. The adaptive scheme presented in this chapter ensures minimal time-to-discover neighbors. We have further analyzed the effect of mobility on the discovery process, which to the best of our knowledge, has not been presented in the literature before. The following publications [36, 37] have contributed to this chapter.

- **Shan Jaffry**, Syed Faraz Hasan, Xiang Gui, "Neighborhood-aware Out-of-Network D2D Discovery", IET Electronic Letters, February, 2018.

- **Shan Jaffry**, Syeda Kanwal Zaidi, Syed Tariq Shah, Syed Faraz Hasan, Xiang Gui, "D2D Neighborhood Discovery by a Mobile-Device", IEEE International Conference on Communications (IEEE ICC), May 2019, Shanghai, China.

Chapter 5: Downlink Backhaul and Access Link Resource Sharing. In this chapter, we have developed a scheme which ensures that downlink AL transmissions do not require additional frequency resources. We have proposed a scheme that enables AL's resource being shared with either backhaul link or out-of-vehicle cellular user. We have also derived expressions for success probabilities and ergodic rates for all resource sharing links. The following publications [38,39] have contributed to this chapter.

- **Shan Jaffry**, Syed Faraz Hasan, Xiang Gui, "Interference Management and Resource Sharing in Moving Networks", IET Communications, (Accepted July 2019).
- **Shan Jaffry**, Syed Faraz Hasan, Xiang Gui, "Shared Spectrum for Mobile-Cell's Backhaul and Access Link", IEEE Global Communications Conference (IEEE Globecom), December 2018, Abu-Dhabi, UAE.

Chapter 6: Sidehaul and Uplink Access Link Resource Sharing. In this chapter, we have presented two algorithms that enable resource sharing between following three links: (i) mobile-cell's sidehaul links, (ii) uplink access link, and (iii) uplink communication for out-of-vehicle users. The following publication ([40]) has contributed to this chapter

- **Shan Jaffry**, Syed Faraz Hasan, Xiang Gui, "Efficient Resource-Sharing Algorithms for Mobile-Cell's Sidehaul and Access Links", IEEE Networking Letters, February 2019.

Chapter 7: Final Discussion. This chapter concludes the whole thesis along with the discussion on some of the future directions that may originate from this research.

The bibliography is presented at the end of this thesis.

1.5 Summary of Research Outcomes

This thesis has led to the following peer-reviewed publications.

Journals Publications

- **Shan Jaffry**, Syed Faraz Hasan, Xiang Gui, "Interference Management and Resource Sharing in Moving Networks", IET Communications, (Accepted July 2019).
- **Shan Jaffry**, Syed Faraz Hasan, Xiang Gui, "Neighborhood-aware Out-of-Network D2D Discovery", IET Electronic Letters, February, 2018.
- **Shan Jaffry**, Syed Faraz Hasan, Xiang Gui, "Efficient Resource-Sharing Algorithms for Mobile-Cell's Sidehaul and Access Links", IEEE Networking Letters, February 2019.
- **Shan Jaffry**, Syed Faraz Hasan, Xiang Gui, "Mobile-Cells Assisting Future Cellular Networks", Vol. 37, Issue 5, IEEE Potentials, September 2018.

Conference Publications

- **Shan Jaffry**, Syeda Kanwal Zaidi, Syed Tariq Shah, Syed Faraz Hasan, Xiang Gui, "D2D Neighborhood Discovery by a Mobile-Device", IEEE International Conference on Communications (IEEE ICC), May 2019, Shanghai, China.
- **Shan Jaffry**, Syed Faraz Hasan, Xiang Gui, "Shared Spectrum for Mobile-Cell's Backhaul and Access Link", IEEE Global Communications Conference (IEEE Globecom), December 2018, Abu-Dhabi, UAE.
- **Shan Jaffry**, Syed Faraz Hasan, Yaw Wen Kuo, Xiang Gui, "Distributed Device Discovery in ProSe environment", IEEE Region 10 Conference (IEEE TENCON), November 2017, Penang, Malaysia.
- **Shan Jaffry**, Syed Faraz Hasan, Xiang Gui, "Making a Case for Moving Small cells", IEEE 26th International Telecommunication Networks and Applications Conference (IEEE ITNAC), 2016, December 2016, Dunedin, New Zealand.

Other Publication

- Dong-Ru Lee, **Shan Jaffry**, Syed Faraz Hasan, Yaw Wen Kuo, Xiang Gui, “Performance Evaluation of Handover Protocols in Software Defined Networking Environment”, 3rd EAI International Conference on Smart Grid and Innovative Frontiers in Telecommunications, Auckland, New Zealand, April 2018.

Chapter 2

Literature Review

The use of smartphones and tablets from public transport (such as, buses, trains, and subways etc.) is constantly on the rise [9]. However, many in-vehicle users receive low quality of service (QoS) due to vehicular penetration loss (VPL) which may degrade signal strength by as much as 23 dB [41]. As a solution to eliminate VPL, the installation of dedicated in-vehicle antenna was first proposed in [24]. Later, Third Generation Partnership Project (3GPP) introduced specifications for mobile-cell in Release 12 [42]. More recently, researchers have demonstrated that mobile-cells not only eliminate VPL, but also reduce the number of handovers, increase network performance, provide cellular services in out-of-coverage regions, and offload the core network [19, 43–48].

On the other hand, there are some challenges associated with the mobile-cells which we have briefly introduced in Chapter 1. In this chapter, we will provide the literature review to explain how researchers have addressed these issues in the past. The review is done systematically and is organized as follows. In Section 2.1 of this chapter, we review the research related to architecture of mobile-cells followed by the description of their use cases in Section 2.2. Section 2.3 and Section 2.4 discuss the relevant work related to neighborhood discovery and resource allocation, respectively, taking mobile-cells into account. The publications related to this chapter are mentioned in Section 2.5.

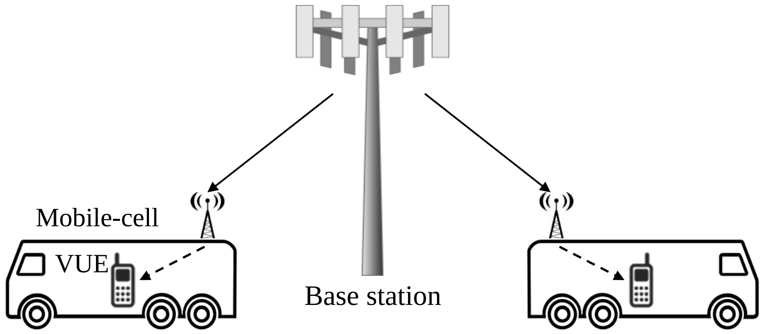

Figure 2.1: Mobile-cell with wireless backhaul link.

2.1 Mobile-Cell Architecture

The mobile-cells are connected to the cellular network through backhaul link (BL). Unlike fixed small-cells, backhaul connectivity is more challenging for mobile-cells due to their mobility. Few researchers have proposed optically backhauled mobile network (OBMN) for trains and subways [29, 49]. The authors in [29] have demonstrated that the OBMN provides high bandwidth for backhaul and stable connectivity to the on-board users. In OBMN-supported architecture, a mobile-cell is connected to the core network through autonomous base stations (ABSs). These ABSs are deployed at multiple stops (e.g. railway stations) and a fiber optic reel is attached to the roof of the mobile-cell to connect with the ABS. The on-board users get connectivity over wireless access links (AL) via in-vehicle antennas. The simulation results have demonstrated drastic load reduction for the core network. The number of handovers also scaled down drastically. However, the installation of optical fiber to cover the whole track (e.g. for connected train or subway) may incur huge deployment and maintenance cost.

On the other hand, 'wireless' backhaul has low cost of deployment and is more suitable for outdoor urban environment. Hence, many researchers have focused on wirelessly connected backhaul links for mobile-cells as shown in Figure 2.1. For example, authors in [44] have exploited coordinated multi-point (CoMP) transmission in LTE-advance (LTE-A) to improve QoS for mobile-cell's backhaul link. In LTE-A, CoMP utilizes coordination between neighboring cells to improve the QoS for the cell-edge users. The authors in [44] utilized CoMP to enable smooth handover as mobile-cells move from the coverage of a resident macro-cell to the neighboring cell. The authors have demonstrated 40% reduction in outage probability of on-board users. Similarly, [31] has demonstrated that installation

Table 2.1: A comparison of optical and wireless backhaul links.

Characteristic feature	Optical Backhaul	Wireless Backhaul
Bandwidth support	Very large (> Gbps)	Small to medium (Mbps)
Interference issues	None	Yes
Mobility support	Only deterministic	Deterministic/random
Deployment/maintenance cost	High	Low
Connectivity to cellular network	In-direct links	Direct
In-vehicle data services	Yes	Yes
In-vehicle cellular services	No	Yes

of dedicated antenna within trains increases uplink cellular coverage for on-board users by 50%. The authors have also extended the use of mobile-cell to provide services to the out-of-vehicle cellular users at the cell-edges through cooperative communication.

Many transport service providers have started offering on-board wireless Internet for the commuters [50]. Up until now, Wi-Fi has remained a prime candidate for such services as all modern devices support this technology [51, 52]. However, since Wi-Fi operates on unlicensed Industrial, Scientific, and Medical (ISM) radio bands and follows carrier sense multiple access (CSMA) medium access control (MAC) protocols, high performance cannot be guaranteed, particularly as the number of users increases. On the other hand, interference management in unlicensed bands will pose additional challenges for mobile network operators [53]. In order to solve issues such as user authentication, user billing, and providing user security, the existing Wi-Fi modules inside cellular equipment have to access the device's universal subscriber identity module (USIM). This requires changes in device's hardware and software [30]. Wi-Fi provides only data services and often users need to switch to cellular mode. More importantly, an on-board Wi-Fi cannot boost the actual capacity of cellular networks [54]. As mobile phone operators are lowering the cost of data services, it is anticipated that more users will shift to cellular mode as compared to often bandwidth-limited and less ubiquitous Wi-Fi technology [55].

The performance enhancement for in-vehicle communication using cellular

Table 2.2: A comparison of Wi-Fi vs cellular in-vehicle access links.

Characteristic feature	Wi-Fi	Cellular
Band support	2.4/5 GHz	Sub-6 GHz / mmWave
Control for cellular operators	Complicated	Easy
Deployment/maintenance cost	Low	Low
Connectivity to cellular networks	In-direct links	Direct
In-vehicle data services	Yes	Yes
In-vehicle cellular services	No	Yes

ALs has been reported by several researchers, for example [19, 30, 56–58]. The authors in [59] have proposed wireless backhaul for mobile-cell coupled with mmWave-enabled AL to mitigate interference between out-of-vehicle and in-vehicle communications. Researchers in [14] have demonstrated that 60 GHz spectrum is an ideal candidate for short range indoor AL communication.

From security point of view, researchers in [60] have proposed a mechanism to secure physical layer transmissions for in-vehicle users. The researchers have exploited differences in channel state conditions to distinguish between a legitimate user and an eavesdropper. The out-of-vehicle eavesdroppers are denied access to in-vehicle transmission exploiting VPL which severely reduces the signal quality outside mobile-cell. At this stage, it is important to mention that the considerations of security parameters are out of scope of this thesis and are only provided for the sake of completion of our discussion.

With the on going discussion on architecture for mobile-cells, several use cases have also been proposed by researchers which stem from the increasing cellular users' demand for high quality of services and ubiquitous connectivity. The next section will focus on some of these use cases.

2.2 Mobile-Cell's Use Cases

The role of mobile-cells as an intermediary relay for public safety has been presented by Shin et al. in [32]. The authors have demonstrated that using sidehaul links, a mobile-cell may extend coverage to the cellular devices in unconnected regions and link to the core network using wireless backhaul channel as shown in

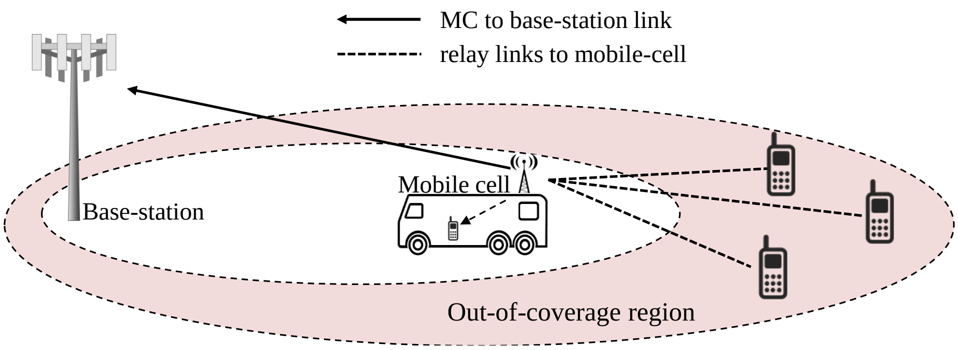

Figure 2.2: Mobile-cell assisting communication in out-of-coverage region as presented by Shin et al. [31]

Figure 2.2. In this research, the sidehaul operations share cellular uplink spectrum as specified by 3GPP, while the relaying operations utilize 700 MHz band dedicated for public safety use cases [61].

The authors in [58] have demonstrated that mobile-cell assisted communication in dense metropolitan areas will improve network connectivity for out-of-vehicle users. However, authors in [45] cautioned that inefficient deployment of mobile-cells will cause severe interference to static cellular layers. The authors have emphasized that unplanned and random mobility of mobile-cells may decrease the overall network performance. In particular, when a mobile-cell moves towards out-of-vehicle users that share the same sub-channels as in-vehicle users, high interference between the links may reduce the QoS for all resource sharing devices. On the contrary, the planned mobility of mobile-cells demonstrated significant improvement in QoS for all users, particularly at the cell-edges.

The increasing trend of using mobile data by commuting users is exerting excessive load on the cellular bandwidth. Hence, researchers have also proposed to install on-board cache mechanism [23, 25, 30]. In [30], authors demonstrated the role of a mobile-cell as a relay between in-vehicle user and the macro-cell base stations, and as a mobile cache. The authors demonstrated that in cases where mobile-cells act as relays, the main bottleneck for maintaining high QoS is the backhaul link. As a simplistic solution, the authors proposed to solve this issue by increasing the available bandwidth for the backhaul. Researchers in [31] have argued that the role of mobile-cells as relays should not be limited to providing in-vehicle services. The authors demonstrated that mobile-cells can also relay macro-cell transmission to out-of-vehicle users at the cell-edges through sidehaul cooperative communication. However, before establishing sidehaul links (with neighboring mobile-cells or out-of-vehicle users), mobile-cells must discover their neighboring devices. Hence, in the next section we will show how the researchers have addressed neighborhood discovery in the past.

2.3 Neighborhood Discovery

In a device-centric communication, each node (e.g., mobile-cell) has to maintain a neighborhood table to exchange data over its sidehaul links with neighbors [62]. For this purpose, nodes announce their presence by broadcasting *Beacon* signals periodically, as shown in Figure 2.3. A beacon payload may contain positioning information, MAC/IP address, or other relevant data. Upon successful reception of beacon messages, all interested nodes update their neighborhood tables [63]. The existing algorithms make use of this table to establish SL. There are two broad categories of neighbor discovery algorithms that have been presented in the literature. The first category includes the ALOHA-like algorithms [64], while the second category relies on schemes that are derived from LTE/LTE-A standards [65].

2.3.1 Details of Discovery Procedures

The ALOHA-like discovery procedures follow random transmission and reception of beacons [66]. Devices participating in this type of neighborhood discovery randomly select a time-slot to broadcast beacons. When in the receiving mode, interested nodes listen for beacons during the remaining time. In slotted (also called synchronous) ALOHA, as depicted in Figure 2.4, nodes can only transmit beacons at the start of the time-slot [67]. On the contrary, nodes participating in unslotted (also called asynchronous) ALOHA discovery can transmit at any time [68]. A successful discovery occurs if and only if a single node (within the discovery range of receiving node) transmits during a certain time period, called the *vulnerable period*. For example, as depicted in Figure 2.5, Node 1 (or N1) and N3 are successfully discovered by all neighbors (not shown in the figure) as no other nodes transmitted during their vulnerable period of 2τ. Examples of collision can be seen when N1, N2 collide during the first failure phase, and N2, N3 collide in the second failure phase. Due to collision, the neighbors could

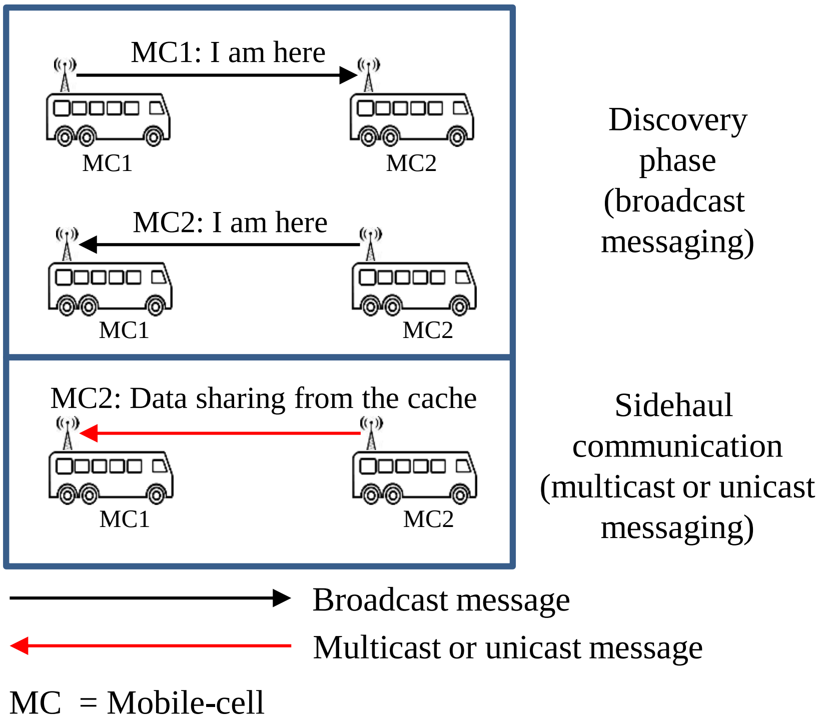

Figure 2.3: Discovery Phase and sidehaul communication between mobile-cells

not discover transmitting nodes and N2 remains undiscovered. The main drawback in ALOHA-like algorithms is the pure randomness in transmitting beacon messages which deteriorates the time-to-discovery. The slotted schemes are synchronized and may reduce the time-to-discovery, however it is very difficult to achieve synchronization in distributed ALOHA-like algorithms [67].

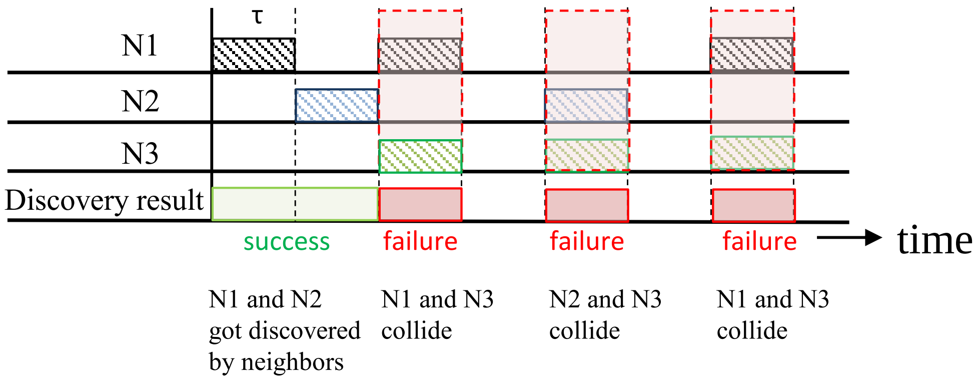

Figure 2.4: Example of one-way slotted ALOHA discovery procedure with single transmission channel.

On the other hand, several LTE-A enabled neighbor discovery schemes have been presented in the literature, [33, 69–74]. 3GPP has specified guidelines for discovery scheme in Release-12 which have been revised in Release 13 and 14. Under these guidelines, neighbor discovery can occur only during a dedicated physical sidelink discovery channel (PSDCH) [75], as shown in Figure 2.6. Each PSDCH-period contains $\mathcal{M}$ sub-frames and shares spectrum with physical uplink shared channel (PUSCH) [75]. The PSDCH-period is repeated after every $\Delta\tau_d$ milliseconds. No uplink cellular transmission takes place during PSDCH-period. Each beacon is transmitted over a Beacon Transmission Unit (BTU), where a BTU consists of two consecutive resource blocks in the time domain (i.e. two slots or a sub-frame). A BTU carries payload which contains all information related to the transmitter. A node's discovery may fail due to collision. A discovery may also fail due to half-duplex constraint [63]. The collision occurs when, for example, two nodes in close vicinity use the same BTU for beacon transmission, hence both the nodes remain undiscovered by their common neighbors. Half-duplexing occurs when multiple nodes select the same sub-frame, even with different sub-channels, and could not discover to each other [33]. This is due to the fact that a device can either transmit or listen during any given time. For example, referring back to Figure 2.6, N1, N2, and N3 are unaware of each others' existence due to half-duplex constraint. On the contrary, other neighbors can discover these nodes.

From an operational point of view, neighbor discovery procedures can be categorized as either network-assisted or autonomous discovery procedures [33].

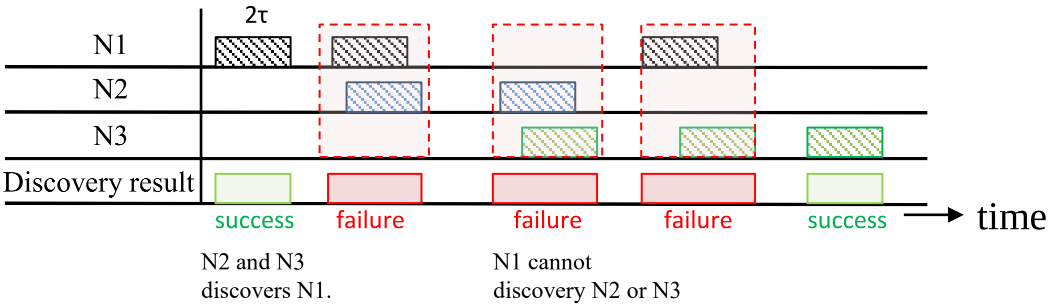

Figure 2.5: Example of one-way unslotted ALOHA discovery procedure with single transmission channel.

In network-assisted discovery, all or most aspects of transmission, such as resource allocation, power-control, etc., are controlled by a network entity such as the base station. On the other hand, nodes participating in autonomous discovery procedure select their own transmission resources and power. The literature related to these two categories is presented in the following sub-sections.

2.3.2 Network Assisted Discovery

The most important aspect of network-assisted discovery schemes is the central management of important parameters such as device synchronization [76–78], resource allocation [79, 80], and transmit power control [80–82], etc. For example, in [80], a base station divides nodes into two groups based on their respective locations. Nodes located far away from the base station are categorized as Group-1, while remaining devices are ranked as Group-2. The PSDCH-period (as shown in Fig. 2.6) is accordingly divided to manage beacon transmissions, and BTUs are assigned to each device. The base station also assigns transmission powers for beacon broadcasting to reduce interference among nodes.

In another work presented in [73], the base station measures euclidean distance between any two nodes to calculate node proximity before initiating discovery process. The base station then transmits neighbor's information to the intended devices to accomplish discovery process. In [69,74], the authors proposed LTE-A underlaid discovery models whereby resources are allocated to each node by the base station. These researches do not follow 3GPP specifications for neighborhood discovery. In [69], the authors have demonstrated that discovering devices can share spectrum with downlink cellular communication to increase the

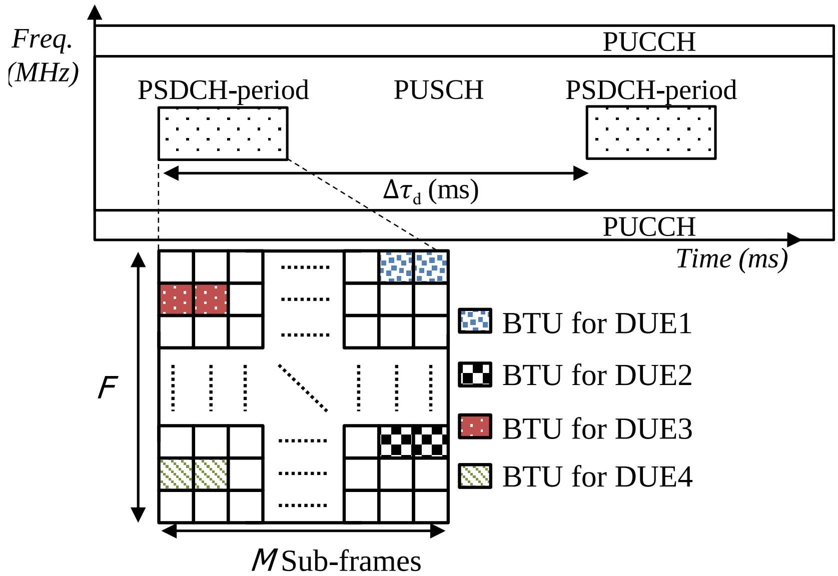

Figure 2.6: 3GPP specified neighborhood discovery frame structure.

overall sum rate of the network. However, this downlink underlaid discovery is accomplished at the expense of more transmit power for all devices. In [74], using the channel state information of each node, the base station estimates nodes' spatial locations and proximity. The base station then allocates a timing window to each device. Each node is allowed to broadcast its beacon and listen to the neighbors within this timing window. Note that the two nodes with similar CSI are assigned the timing window such that they receive each other's beacon messages with high probability of success. However, the performance of this scheme degrades as the number of devices increase. Authors in [79] have presented a base station governed interference management scheme to assist discovery procedure underlying an LTE-A system. The base station assigns resources to all participating devices to ensure the successful completion of discovery process.

In [83], the authors have proposed a network-reliant vehicular discovery mechanism in which the base station broadcasts vehicles' information in a particular geographical region. The proposed scheme extensively relies on the existing LTE-A downlink control channel to distribute the information to fast moving vehicles in a highway environment. However, such an approach will exerts additional load on the base station.

The main parameters of transmission are computed by the base station in the network-assisted discovery as reported in [69, 73, 74, 79–83]. However, with the

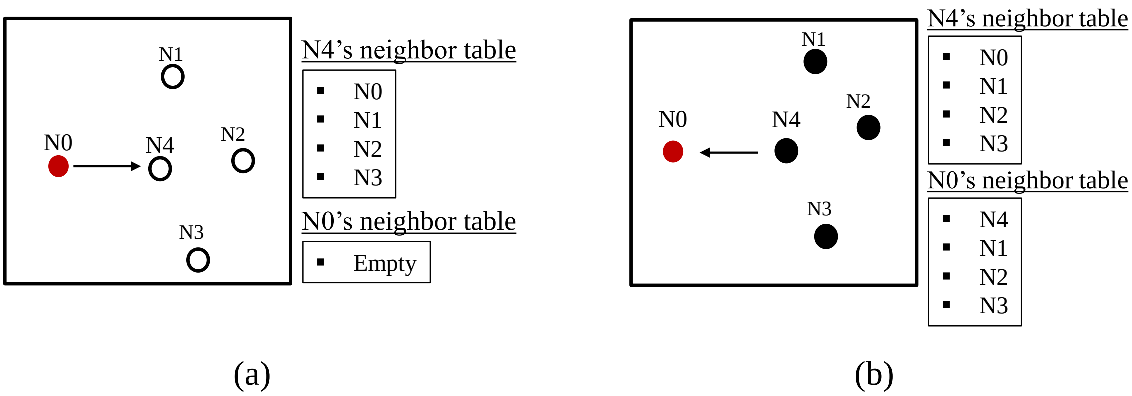

Figure 2.7: (a) Simple one-way ALOHA discovery (b) Gossip-based one-way ALOHA discovery.

large number of connected devices in the future, it is likely that the network-assisted mechanisms will consume excessive bandwidth for overhead signaling. Hence, the researchers are focusing on autonomous discovery mechanisms which can operate even in the absence of network coverage.

2.3.3 Autonomous Discovery

The autonomous discovery aims at mitigating the role of base station (or network) in discovery process and reduces overhead signaling [33]. Such schemes are also appropriate for neighbor discovery in regions where network coverage is poor or does not exist at all.

In an out-of-network scenario, Vasudevan et al. have proposed ALOHA-like neighborhood awareness scheme using "gossip-based" one-to-many approach in [84]. Using one-to-one scheme, a node only broadcasts its own details in the beacon message to its one-hop neighbors as shown in Figure 2.7(a). On the contrary, gossip-based approach enables indirect neighbor discovery by sharing the entire neighborhood table in the beacon message to enable quick discovery, as depicted in Figure 2.7(b). The Gossip algorithms drastically reduce time-to-discovery as compared to one-to-one discovery approach. In [67], the same authors have simplified the task of neighbor discovery as a Coupon Collector's problem.

In [85–88], multi-way and multi-channel ALOHA-based algorithms have been presented to ensure timely completion of the discovery process. In each of the mentioned researches, the authors have developed unique multi-way feedback-based algorithms. It was noted in [88] that with the availability of multiple channels, the nodes acheive successful discovery with low collision probabilities. The neighborhood discovery schemes presented in [67,68,84–88] are ideally suited for machine-type communication or sensor-networks, etc. where participating nodes are either static, or moving with low speed.

In [89], Chao et al. proposed a bio-inspired algorithm to simultaneously accomplish synchronization and discovery. The researchers have developed a technique that is inspired by firefly algorithm, which is suitable for any protocol. However, the time-to-convergence for such algorithms still remains too high for applications such as mobile-cell discovery. In [90], researchers have argued that beacon transmission for discovery purposes is often accompanied by background transmissions (e.g., for data exchange) made by other proximity devices. In such cases, the signal-to-interference-plus-noise ratio (SINR) gets lower and the receivers may fail to decode the beacon. Hence, the authors have proposed a novel correlation based discovery scheme whereby every device generates a Pseudo-random sequence consisting of a specific preamble and a signature. At the receiving nodes, the algorithms use cross-correlation to decode these preambles and signatures to discover the respective transmitter. The authors tested this scheme on Universal Software Radio Peripheral (USRP) hardware test-bed to demonstrate that the proposed mechanism efficiently discovers neighbors even in high interference environments.

In an LTE-A enabled scheme presented in [70], authors have developed simultaneous neighbor discovery and sidehaul channel estimation mechanism by listening to the standard uplink transmission from the peers in the vicinity. In particular, the authors have focused on sounding reference signals (SRS) and physical random access channel (PRACH) in the LTE-A. Researchers in [91] have proposed channel sensing based resource selection for beacon transmission for discovery purposes. The authors have demonstrated that channel sensing reduces the chances of beacon collisions as compared to purely random discovery.

Another out-of-coverage discovery scheme is presented in [92], in which authors have developed an adaptive wake-sleep cycle for beacon transmission and reception. The nodes remain asleep unless the probability to contact neighbors surpasses a threshold. This probability is predicted based on a stochastic

Table 2.3: Highlights of network-assisted and autonomous discovery schemes.

Characteristic feature	Network-Assisted	Autonomous
Operational domain	In-coverage	In-coverage, out-of-coverage.
Synchronization	base station	base station, independent.
Collision/half-duplex failures	None	Inevitable.
Time-to-discovery	Highly predictable	Less predictable.

model which uses node's contact history as an input parameter. However, the authors have focused on improving energy efficiency, instead of parameters like time-to-discovery, etc.

In 3GPP governed autonomous discovery (also known as mode-2 type procedures [93]), the devices select BTUs randomly from a dedicated time-frequency resource pool (See Fig. 2.6). The main reason for failures in mode-2 type are collision and half-duplexing. In [94], Hong et al. proposed to carry collision information in the BTU payloads (i.e., actual message in a beacon) to avoid failures in discovery. More recently, researchers in [71, 95] have proposed to optimize transmission probability to increase successful beacon delivery in out-of-network scenarios. The proposed schemes rely on the number of nodes in the vicinity of beacon transmitter. As an extension to [71], researchers in [96] and [97] have presented algorithms that predict optimal transmission probability based on number of discovered devices in the neighborhood table.

The algorithms proposed in this section [67, 68, 70, 71, 84–92, 94, 95], like most others in the literature, have focused on discovery procedure from the stand point of static nodes. However, many 5G-enabled nodes, such as mobile-cells, will be non-stationary [98–100]. A survey of mobility-aware neighborhood discovery for IoT applications has been presented in [66]. However, all the schemes discussed in this survey cover non-cellular protocols including 802.11, Zigbee, or Bluetooth standards, etc. On the other hand, a network-reliant vehicular discovery scheme has been presented in [83] . However, the excessive reliance on network in this scheme makes neighbor discovery impossible in regions without cellular coverage.

As part of our contribution in this thesis, we will propose a modified PS-DCH frame structure for out-of-network mode-2 type discovery in Chapter 3. We will later use a more robust approach in Chapter 4 and utilize proximity

Table 2.4: Summary of neighborhood discovery schemes.

Related Work	Type of schemes	Operational Domain
[67, 68, 84–88]	ALOHA-like discovery	In-coverage, out-of-coverage
[69, 73, 74, 79–83]	LTE/LTE-A network-assisted discovery.	In-coverage only.
[70, 89, 90, 92]	Non-3GPP distributed discovery.	In-coverage, out-of-coverage.
[71, 91, 94–97]	3GPP-enabled distributed discovery.	In-coverage, out-of-coverage

awareness to increase the probability of successful discovery. In Chapter 4, we will also an analytical model for mode-2 type neighbor discovery by a moving mobile-cell.

In the next section, we will cover the literature review for our second research objective, i.e., interference management and resource allocation for mobile-cells.

2.4 Interference Management

The envisaged heterogeneous architecture of 5G comprises of multiple tiers. The most popular layout for HetNets contains a macro-cell layer underlaid by small-cell layers as shown in Figure 2.8. The small-cells enable high spatial reuse of spectrum through deployment of several low-powered base stations [101]. The coverage of small-cells is smaller. Therefore, significant network densification is required to enhance cellular capacity [102] using small-cells. An immediate concern associated with increasing the number of small-cell transmitters is the increased level of interference. More recent generations of cellular networks, i.e., Long Term Evolution (LTE) and LTE-Advanced use orthogonal frequency-division multiple access (OFDMA) modulation scheme which successfully eliminates intra-cell interference. However, cell-edge users still suffer from co-channel interference from the neighboring cells [103].

A key to designing any interference management and resource allocation scheme for HetNet is modeling multiple cellular layers with random base station deployments. Cellular network models enable researchers to examine the effect of base-station's location and the position of cellular users, inter-layer and

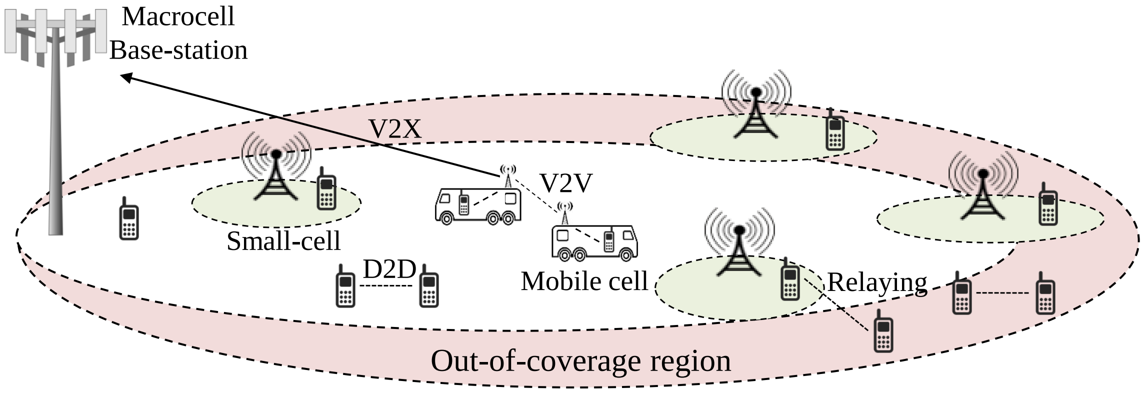

Figure 2.8: An example of 5G heterogeneous network comprising of multiple layers of communication.

intra-layer interference, and channel conditions etc. Hence, in the next section, we will review the network modeling techniques that are available in the literature.

2.4.1 Cellular Network Modeling

The coverage of cellular base stations has been traditionally examined using a hexagonal grid design (See Fig. 2.9) [104]. The hexagonal grid model is quite simplistic in terms of its coverage representation and fails to capture randomness in the modern cellular architecture. The grid model is also mathematically intractable [105]. To evaluate the performance metrics using the grid model, a complex network-level simulation is usually required. On the contrary, in the future HetNets, base stations are expected to be deployed in heterogeneous manner. Multiple layers of cells of different sizes and radio access technologies (e.g. sub 6 GHz and mmWave etc.) will transform the network into more complex form than the one represented by a simplistic hexagonal grid. Therefore, researchers have started to rely on tools of stochastic geometry to model future cellular networks with more accuracy and mathematical tractability [106–108].

From the deployment point of view, the randomness in the heterogeneous networks can be accurately captured using Point Processes (either homogeneous, non-homogeneous, or clustered point process etc.) [109]. In a pioneering research in [106], J. Andrews et. al. have developed a comprehensive analytical and tractable mathematical model for downlink cellular network using homogeneous Poisson point process (H-PPP). Extensions to this research includes designing a K-tier HetNet model [107] and uplink communication model in [108]. To validate

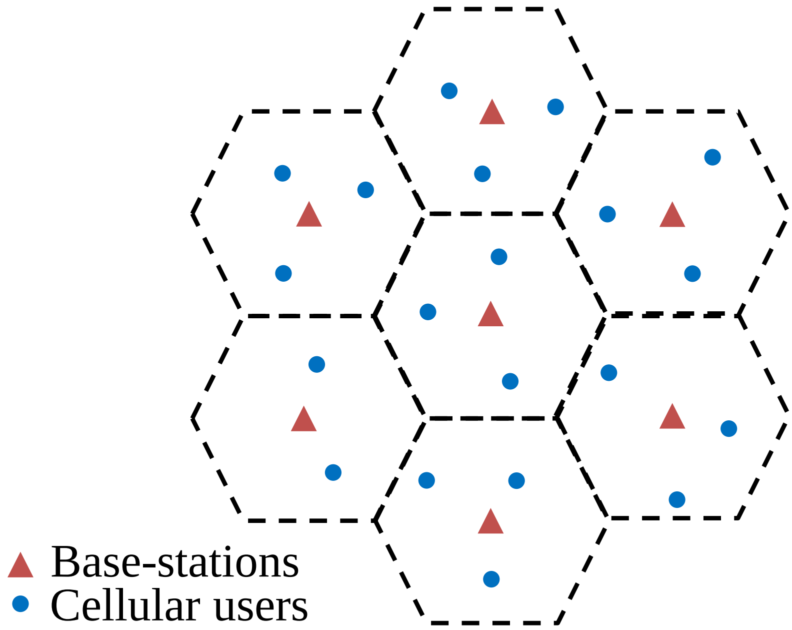

Figure 2.9: Hexagonal Grid model for cellular networks

the use of stochastic geometry tools, these researches compared the proposed models with the data available from cellular operators and hexagonal grid architectures. For example, in [106], it was observed that compared to the actual base station deployment, the proposed H-PPP model provides the lower-bound of cellular coverage (pessimistic analysis) and the grid-design provides the upper-bound of coverage (optimistic analysis). Interestingly, all three models (real-world, hexagonal, and PPP) demonstrated similar trends in terms of coverage probability.

Several researchers have utilized the findings in [106–108] to explore interesting properties of heterogeneity in networks and proposed novel mechanisms to improve network performance. For example, the researchers in [110] have presented an intelligent ON/OFF mechanism for randomly deployed small-cell base stations. The uplink analysis of dense cellular networks have been presented in [111] considering dual-slop path loss model, i.e., line-of-sight (LoS) and non line-of-sight (NLoS) transmissions. Often researchers consider only either LoS or NLoS transmission model during analysis to develop tractable mathematical model. However, the results in [111] have demonstrated that both LoS and NLoS transmissions have significant impact on the analysis performed for the coverage

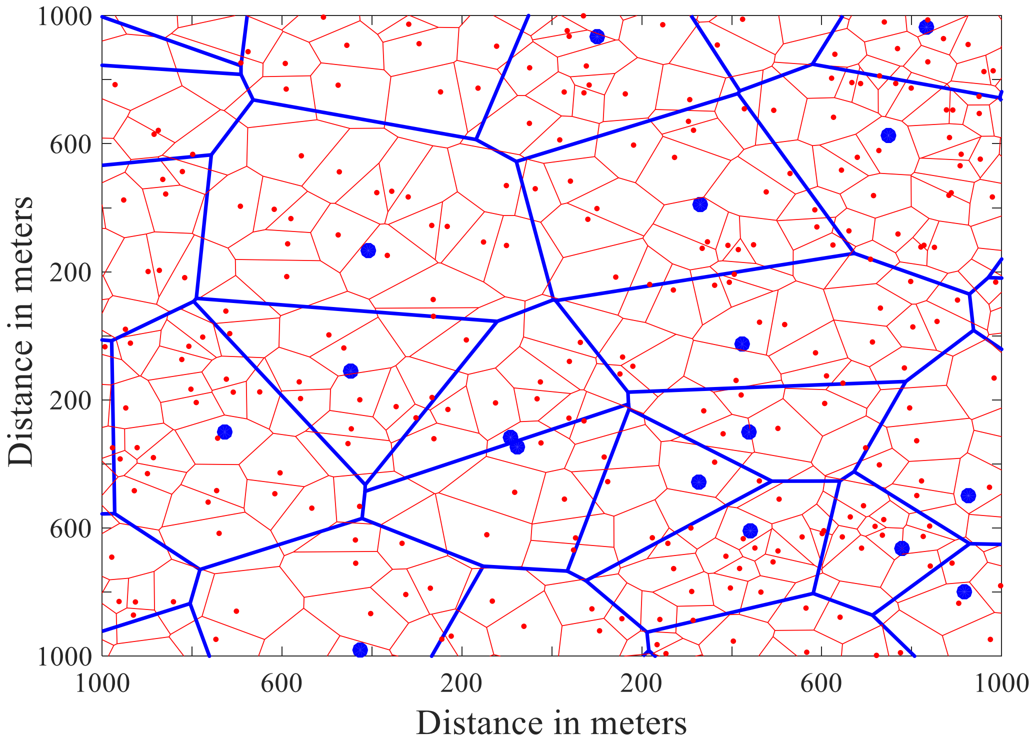

Figure 2.10: Voronoi tessellation for the H-PPP. The blue and red dots depict the macro-cell and small-cell base stations, respectively.

of dense cellular networks. The authors in [112] have proposed a stochastic distance based inter-cell interference coordination scheme for small-cell networks. Likewise, authors in [113] have used cluster-based stochastic geometry to model communication for small-cell networks.

Note that in contrast to conventional grid model, the coverage region around the base station in a PPP forms a Voronoi cell [109]. As shown in Figure 2.10, the cell boundary of a randomly deployed cell is formed by the line segments that are equidistant to the closest two sites. Hence, the cell sizes and the location of base stations are both described as random variables. Consequently, inter-cell interference also depend on, at least, two random variables that are channel gain and the distance from the interfering transmitter. This is in striking contrast to the hexagonal grid model [6] and has made the performance analysis a more complicated and non-trivial task, even for fixed small-cells.

Since there are many similarities between fixed and mobile cells, for the sake of completeness, the review in the next sub-section will focus on fixed small-cells. This review will enabled us to learn important lessons which we will utilize appropriately in this thesis.

2.4.2 Interference Mitigation in Fixed Small-Cells

The randomness associated with the distribution of fixed small-cell base stations makes coverage analysis a challenging task [18]. Analysis of user association with macro-cell and small-cell layers is another challenge in modern networks. Researchers have utilized multiple approaches to solve these challenges which we will discuss in this section.

i. Stochastic Analysis

In order to perform coverage analysis and develop user-association model for a two-tier cellular network, the authors in [114] have used stochastic method. The authors have used joint and disjoint sub-channel access schemes (JAS and DJAS, respectively) for small-cell user associations. In JAS, the whole spectrum is shared by the two layers while DJAS only allows partial spectrum for the small-cell layer. The macro-cell can use the entire spectrum in both cases. From the point of view of user association, open and closed access schemes were considered. In the closed access scheme only registered cellular users can communicate with small-cell access points (SAP). On the other hand, in the open access scheme, cellular users can communicate to any base station (either in macro- or small-cell layer) whose signal strength is above a certain threshold. The optimization of resource allocation for JAS and DJAS was performed with constraints on success probability and throughput for each layer. Intuitively, the open access user association coupled with JAS delivered optimal system throughput and coverage because the users can associate to the layer that delivers the best signal quality.

The researchers in [115] have proposed frequency reuse model for indoor small-cell network, exploiting material penetration losses (e.g., through walls, floor, or roofs) in a building. Different scenarios for the two-layered architecture were considered by the authors, each of which allowed resource-sharing between macro- and small-cell layer. In the first scenario, when reference signal received power (RSRP) is below -100 dBm, the small-cells were deployed at macro-cell's boundary. In this setting, frequency sharing provided very high throughput. The small-cell deployment extended coverage to as far as 60 meters. In the second scenario (-100 dBm $\geq RSRP \geq -10$ dBm), the small-cell coverage decreased

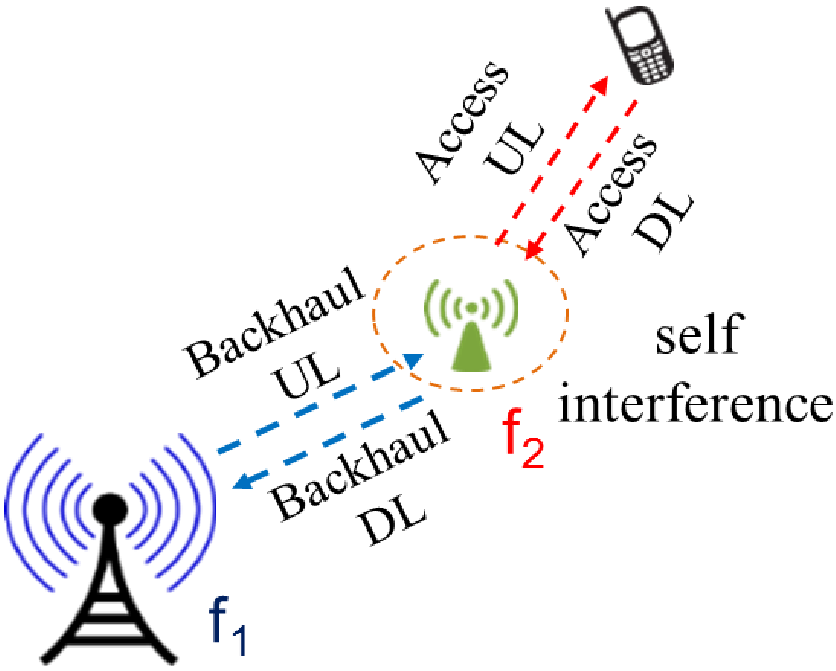

Figure 2.11: Flow diagram for the operations as presented by Chen et al. [108]

by 25% in comparison. The authors also considered small-cell clusters within a macro-cell layer to study inter-tier and intra-tier interference. In this case, the small-cell coverage reduced to 36% as compared to scenario-I. The simulations have demonstrated an average coverage gain of more than 25% using indoor small-cell deployment.

Virtual resource allocation with full-duplex self-backhauled communication has been presented by Chen et al. in [116]. The proposed network infrastructure used virtual resources (VRs) including radio spectrum, macro-cell base station (MBS), small-cell base station (SBS) and transmission time slots. The VRs were managed by an Infrastructure Provider (InP) which also owns MBSs, SBSs, and radio spectrum to offer services to different mobile virtual network operators (MVNOs). This model exploited sharing of the same physical resources and infrastructure with multiple MVNOs to fulfill network demands. Figures 2.11 and 2.12 show the overall scenario and the block diagram of the model proposed in [116], respectively.

Researchers have also used optimization tools to solve complex interference problems. This topic is covered in the next subsection.

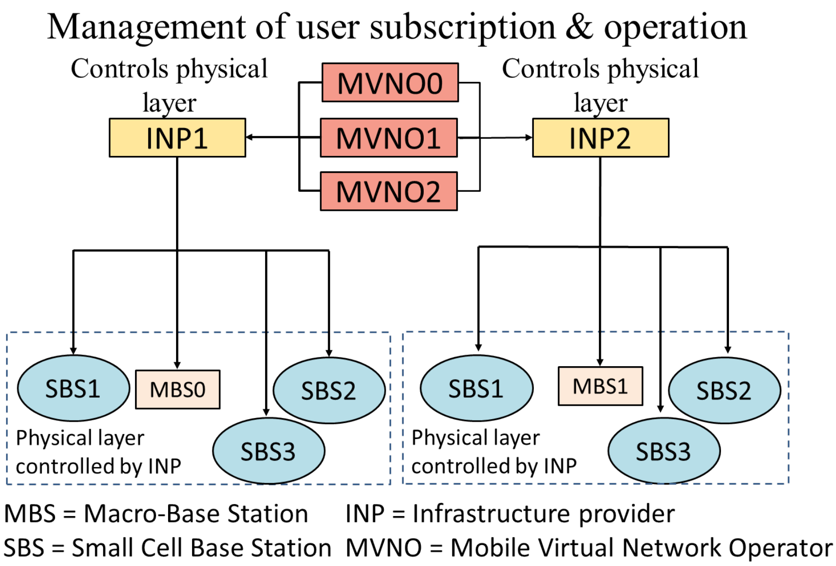

Figure 2.12: Virtualized (abstracted) layers as modeled by Chen et al. [108]

ii. Optimization based Solutions

A popular tool that researchers have used to optimize complex resource allocation problems is graph coloring. In graph coloring the adjacent vertices (i.e., transmitter-nodes) are joined with each other via edges (i.e., interference). The coloring objective is to ensure that adjacent vertices are not assigned the same color. Colors may represent a distinctive parameter such as a sub-channel. An example has been shown in Figure 2.13 in which cell-1 has cell-2 and cell-6 as neighbors. Cell-1 is colored red, while cell-2 and cell-6 are colored green and blue, respectively. Note that the difference in coloring for cell-2 and cell-6 is due to the fact that they are also neighbors. Other objective of any graph coloring scheme may be to utilize minimum number of colors (i.e., in terms of cellular networks, use minimum number of sub-channels for better spectral efficiency, etc.)

Exploiting the tools of stochastic geometry and graph coloring, Sadr et al. presented a partially distributed resource allocation method for a small-cell network [117]. The scheme comprises of cell association (step 1), load estimation at small-cell base station (step 2), channel assignment to each SBS (step 3), and resource allocation to associated users (step 4). Steps 1, 2, and 4 occur at individual SBSs to offload the core network. Each SBS calculates average data rate requirement as per its user association, and informs the network core (step 1 and

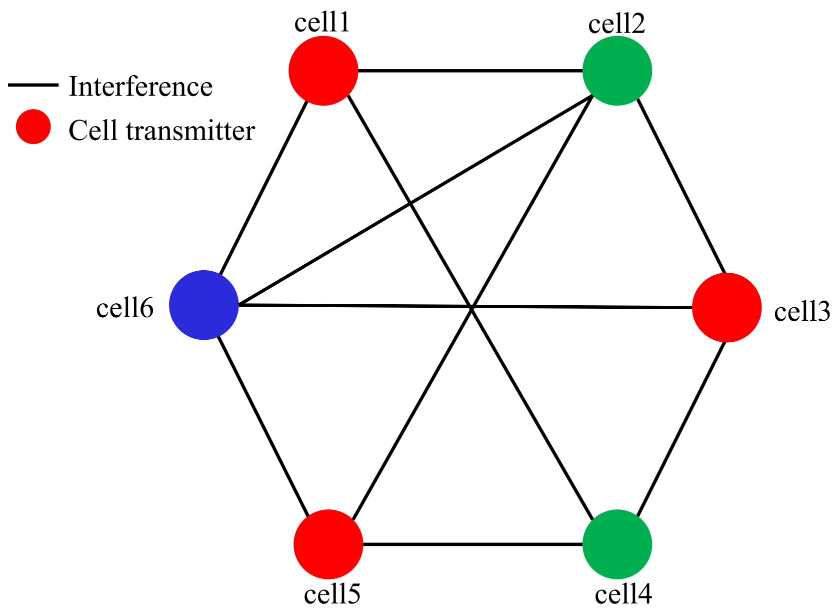

Figure 2.13: Example of graph coloring scheme for resource-sharing between neighboring cells.

2). In step 3, the network core uses graph coloring to allocate sub-channels to each of the small-cells. Finally in step-4, sub-channels are distributed by SBS to individual users. Such an scheme requires an additional backhaul communication link between small-cells and the core network.

In another two-layered network scenario, distributed resource allocation for downlink cellular communication has been presented in [118]. In the proposed scheme, the small-cell base stations maintain a strong interference table (SITable) and a weak interference table (WITable). SITable and WITable register interference levels from the neighboring cells. Two more tables, strong resource status table (SRSTable) and weak-resource-status-table (WRSTable), are maintained at each base station which record information of resource blocks (RB) assigned to the cells in SITable and WITable, respectively. The SITable records the neighbors with strong interference to the serving cell, and its associated SRSTable maintains information about the RBs being currently used in the cells within SITable. Based on the information in SRSTable and WRSTable, the base stations allocate RBs to the users. During resource allocation, priority is given to RBs that are not presented in both WRSTable and SRSTable, followed by RBs present in WRSTable. This mechanism ensures minimum inter-cell interference. The overall objective in [118] is to find the optimal resource allocation solution in

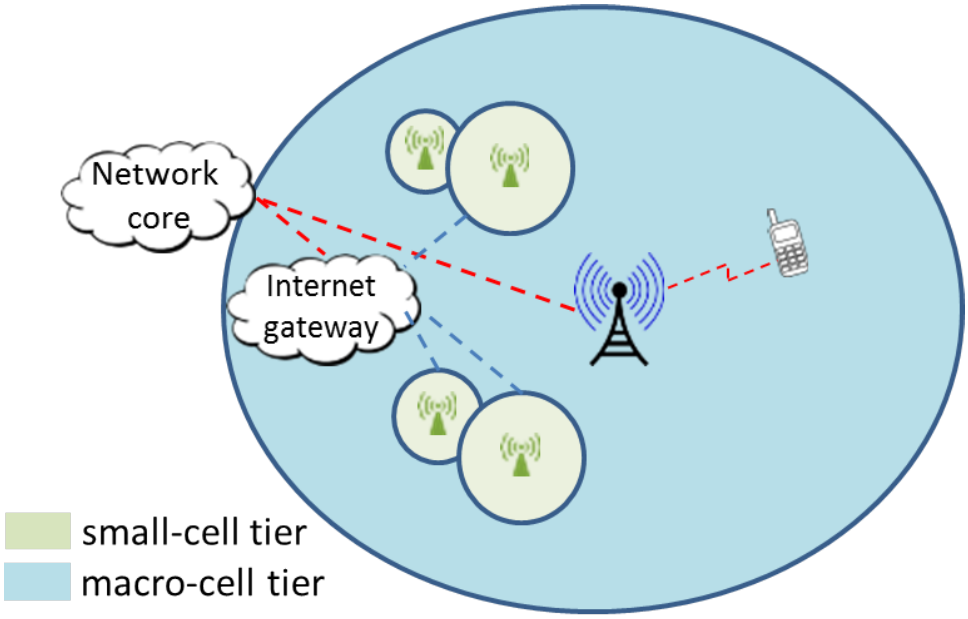

Figure 2.14: System model as presented by Abdelnasser et al.

each timeslot to maximize the average throughput of the system while satisfying the minimum data rate demand of each cellular user.

Abdelnasser et al. [119] have presented resource allocation and small-cell admission control framework in another two-layered network. The resource allocation problem for both the macro- and small-cell tiers was formulated as optimization problem. The macro-cell, being aware of the small-cells within its coverage, allocates resources to its users ensuring maximum tolerable interference. On the other hand, the small-cells aim to maximize the number of admitted users following minimum spectrum constraint (i.e., using as fewer sub-channels as possible). Macro-cell assigns sub-channels to its users and calculates maximum tolerable interference per sub-channel. On the other hand, the small-cells enable channel reuse by controlling transmit power per sub-channel. This way the inter-layer co-channel interference is minimized. Both layers are connected to the core network through wired Internet link as shown in Figure 2.14. In this iterative process, dual-decomposition method has been used to decentralize resource allocation at the small-cell level. The flowchart for [119] is shown in Figure 2.15.

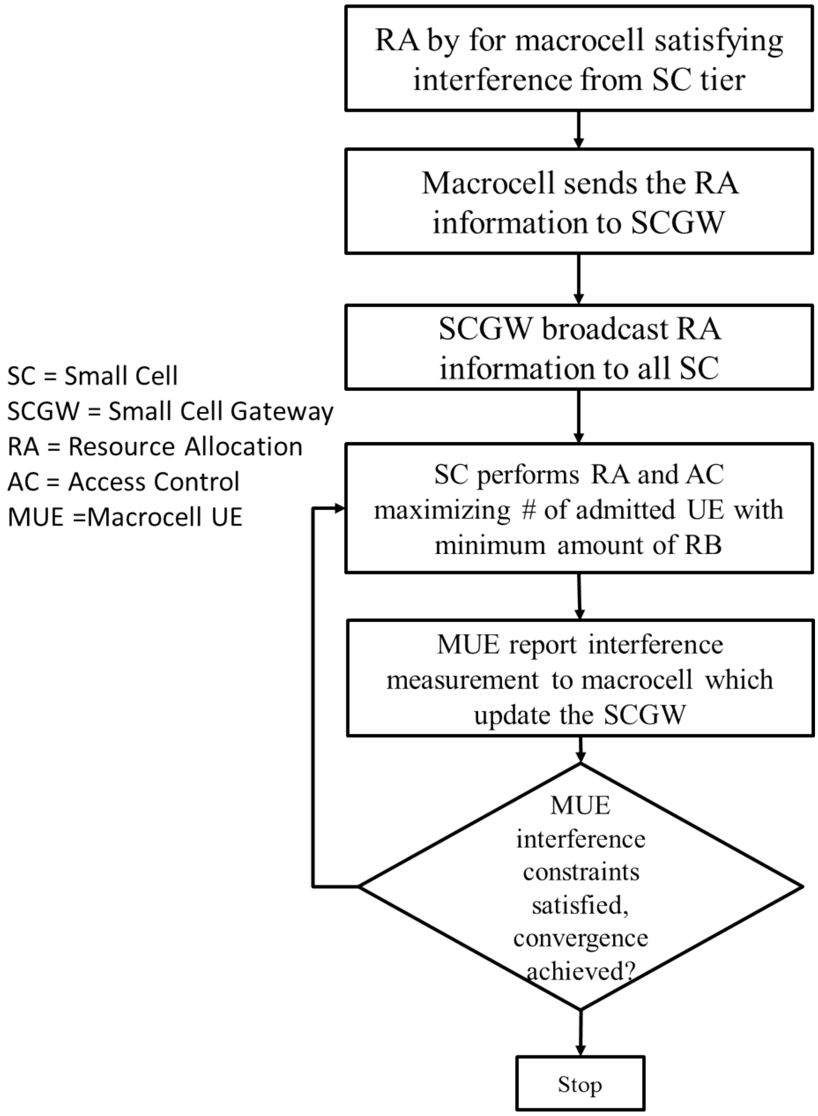

Figure 2.15: Flow diagram for the operations as presented by Abdelnasser et al.

iii. Game Theoretic Approach

Game theory is another interesting tool that researchers have used for interference mitigation. The idea behind this technique is explained by Zhang et al. in [120]. The authors considered a network with macro-cell and cognitive small-cells (CSC), such that the later share the spectrum in an opportunistic manner. The macro-cell broadcasts the so-called “interference temperature” at regular intervals to the CSC base stations. The small-cell uplink sub-channel and power allocation problem is solved using Nash’s bargaining game to alleviate the cross-tier interference. This optimization problem maximizes the rate (i.e., utility in the game) for the cognitive small-cells while adhering to QoS for the primary macro-cell users.

In [121,122], Semasinghe et al. have used evolutionary game theory to develop distributed resource allocation scheme for downlink transmissions. In this work, each small-cell base station acts as an agent interested in selecting strategy to maximize its utility. The total SINR for all users is considered as the utility of SBS. The combination of sub-carrier and power levels (referred to as transmission-alignment) helps to develop the set of strategies for the agents in the game. First, the SBSs select random transmission-alignment values. Meanwhile, the central core broadcasts the average network utility. Then the SBSs compare their utilities with the average utility of population as broadcasted by the network (i.e., small-cell network). If the SBSs’ utility remains lower than the average value, the SBSs raise their users’ power levels. When the maximum power level is reached, the SBSs randomly select another available sub-carrier and repeat the process.

Table 2.5 summarizes the research work discussed for interference management and resource allocation for HetNets with fixed small-cells. Note that the resource allocation mechanisms presented in [106–108, 110–122] observed interference management from the point of view of fixed cellular layers. On the other hand, mobile-cells rapidly change their positions and hence interference pattern varies very quickly. Furthermore, there are at least three links associated with the mobile-cells, i.e. backhaul, access, and sidehaul links. Therefore, interference management and resource allocation are more challenging for mobile-cells. In the next subsection, we will provide a review of how the researchers have addressed these challenges in the past.

Table 2.5: Summary for resource allocation and interference mitigation in HetNet with fixed cells.

Proposal	Core Technique	Resource allocation type
[119]	MINLP Optimization for tier aware RB and power allocation	Resource allocation and admission control
[116]	Full duplex self-backhaul, virtual resource allocation	-
[106–108, 110, 111, 113]	Stochastic Geometry	sub-channel allocation
[112]	Stochastic Geometry	Distance based inter-cell interference coordination
[114]	Stochastic Analysis and optimization	Resource allocation and admission control
[115]	Stochastic Analysis, System-level simulation	Resource Allocation and interference management
[117]	(4-step) Graph coloring partial distribution	Channel allocation
[118]	Using Neighbor relation table to decide orthogonal RB distribution to UE in small-cells	Sub-channel and power allocation
[120]	Cognitive Small-cell based two-tier network, distribution based on Nash Bargaining Game	Sub-channel and power allocation
[121, 122]	Evolutionary Game Theory	Sub-carrier and power allocation

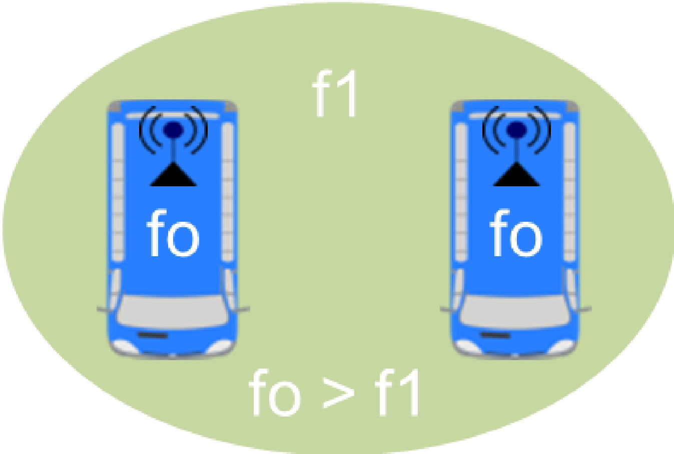

Figure 2.16: Dual spectrum resource allocation for in-vehicle and out-of-vehicle users in a mobile-cell environment as proposed by Chae et al. [115]

2.4.3 Resource Allocation in Mobile-Cells

Several researches, have demonstrated the performance enhancement of networks with mobile-cell integration [19,26,30,43–46]. In [25], the researchers have empirically demonstrated that a cache mechanism installed within mobile-cells can significantly reduce bandwidth consumption for the network. Intuitively, a mobile-cell with caching capability will not frequently access the core network. To achieve optimal benefits from mobile-caching, [26] has proposed a radio resource management scheme. The authors focused on downloading the data from macro-cell base station to the mobile-cell. Based on content's popularity, macro-cell base station uses either broadcast or multicast mode. For example, if similar requests are made by several mobile-cells, then the broadcast mode is used. The multicast mode is used only if each mobile-cell requests unique contents. The popular contents can also be requested from the neighboring mobile-cell over SLs. System level simulations have demonstrated that optimal selection of transmission mode (i.e., either multicast or broadcast) based on popular web content increased the overall network performance. The network throughput improved with the rise in content popularity and the number of mobile-cells. Furthermore, the mutual sharing of contents among mobile-cells over SLs released the backhaul resources for the conventional cellular users.

The mobile-cell may also act as relay for commuting users to increase the QoS

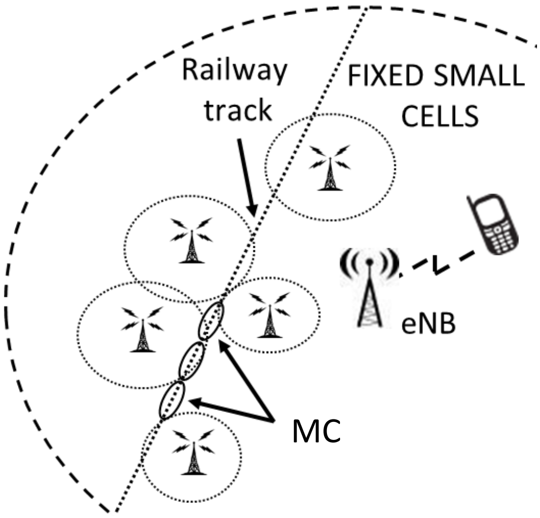

Figure 2.17: System model as presented by Jangsher et al. for deterministic mobility [48, 117].

by eliminating VPL [43]. In [19], authors have presented sub-channel utilization for backhaul and access links in half-duplex decode-and-forward relays (HDFR) within mobile-cells. The authors have used the same sub-channel for both links in orthogonal time slots to increase the SINR for downlink transmission to in-vehicle users. The researchers in [31] have demonstrated that HDFR may increase uplink coverage for in-vehicular users by 50%. By using cooperative communication, HDFR can also provide services to out-of-vehicle cellular users at the cell-edges.

The work in [45] has demonstrated the challenges associated with the additional interference that mobile-cells' links may add to the network. Therefore it is essential to devise dynamic resource allocation schemes for mobile-cells so that interference to the fixed cellular layer is minimized. To eliminate the interference between in-vehicle and out-of-vehicle cellular users, Chae et al. [123] have proposed to use separate frequency bands as shown in Figure 2.16. By isolating two operating bands ($f_o, f_1 \; \forall f_o > f_1$), this scheme eliminates intra-tier interference, but, at the cost of poor spectral efficiency. Since frequency spectrum is an expensive commodity, such a scheme is not a viable solution for mobile network operators. In contrast, optimization based resource allocation methodologies for mobile-cells have been developed by Jangsher et al. in [56,124–126]. The authors have combined graph theory and mixed integer non-linear programming (MINLP) to optimize resource allocation in networks containing mobile-cells. In [124], the

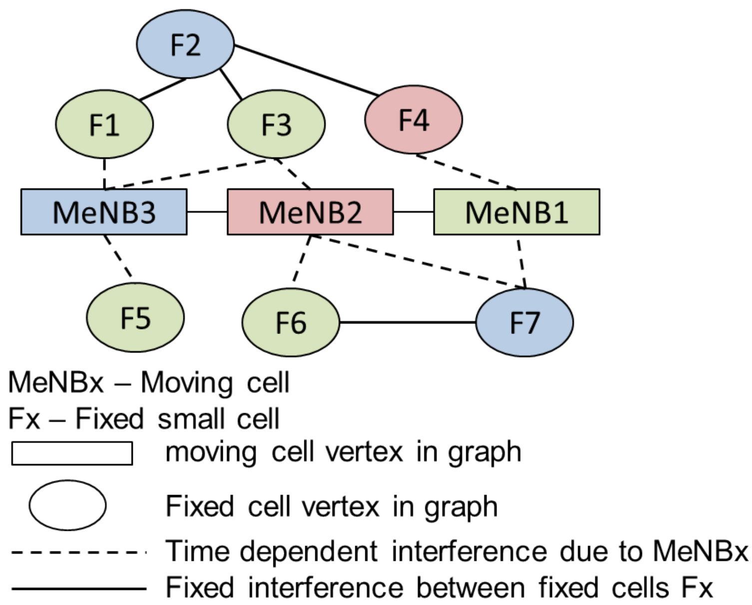

Figure 2.18: Graph coloring as presented by Jangsher et al. for deterministic mobility [481, 117].

authors have proposed probabilistic resource allocation for mobile-cell considering the public transport mobility model presented in [127]. The proposed probabilistic resource allocation utilizes the fact that buses often follow nondeterministic route and timing. For vehicles that have deterministic mobility, such as for trains, resource allocation algorithms have been presented by the same authors in [56] and [125].

In [56, 124–126], the allocation of resources (i.e., sub-channel and transmit-power) is formulated as an MINLP problem. In the proposed scheme, a centralized controller (e.g., base station) calculates the interference pattern for a fixed timeslot. Because of its motion, mobile-cells interfere with adjacent cells as they travel through their routes. Hence, the central core calculates the interference patterns for different timeslots. Note that for each timeslot, several subslots are formed based on the consequent interference patterns. Hence a single time interval dependent interference (TIDI) graph is formed for each subslot. The number of TIDI graphs depends on the speed and direction of vehicles. The core then solves the optimization problem for sub-channels and power distribution for uplink transmission for each TIDI graph for a single timeslot. In summary, the centralized core has the following functions: (i) formation of graph for a time frame, (ii) solving the joint optimization problem for sub-channels and power allocation, and (iii) resource distribution using graph coloring. Figure 2.17 shows the system model and Figure 2.18 shows graph formation. The solid lines in Figure 2.18 shows the permanent interference between two cells, e.g., between the neighboring fixed cells or the mobile-cells. The dotted lines indicate varying interference between the cells for a given time period. Intuitively, fine tuning for timeslots is required to achieve accuracy which exerts additional load on the base station in terms of computational complexity. In [126], the same authors have presented resource allocation for BL using separated spectrum for in-vehicle and out-of vehicle link.

In [30], Shah et al. have demonstrated that mobile-cell can be simultaneously used either as relay between macro-cell base station and the commuting users, or as a dedicated on-board cache for online content delivery. The authors have demonstrated that multiple links of mobile-cells share resources with fixed macro-cell layer. For example, access link for mobile-cell and the macro-cell users share the same 2.0 GHz spectrum. On the other hand, uplink backhaul links of mobile-cell shares spectrum with its sidehaul links on 3.5 GHz spectrum. Through system level simulations, the authors demonstrated significant improvement in the capacity of cellular network.

The solutions presented in [19, 30, 31, 56, 57, 123–126] have assigned either dedicated frequency resources to mobile-cell's individual link, or utilized separate bands for in-vehicle and out-of-vehicle users. However, these schemes lower the spectral efficiency of cellular network. On the other hand, in our research, we have proposed resource sharing between mobile-cell's links and out-of-vehicle users. Our schemes not only guarantee QoS for each user, but also improve spectral efficiency. We present resource sharing between downlink access link with backhaul link and out-of-vehicle users in Chapter 5. The dense resource sharing between uplink access link and out-of-vehicle users, along with sidehaul links is presented in Chapter 6. Note that mobile-cells need to discover their neighboring nodes before establishing sidehaul links. The neighborhood discovery constitutes our first research contribution in this thesis, which we will present in the next chapter.

2.5 Related Publications

- **Shan Jaffry**, Syed Faraz Hasan, Xiang Gui, "Mobile-cells Assisting Future Cellular Networks", Vol. 37, Issue 5, IEEE Potentials, September 2018.

- **Shan Jaffry**, Syed Faraz Hasan, Xiang Gui, "Making a Case for Moving Small Cells", IEEE 26th International Telecommunication Networks and Applications Conference (IEEE ITNAC), December 2016, Dunedin, New Zealand.

Chapter 3

Distributed Neighborhood Discovery

3.1 Introduction

A mobile-cell may communicate with neighboring mobile-cells and out-of-vehicle cellular users over sidehaul links to exchange data or to extend coverage of cellular networks [23, 30–32]. The network-independent sidehaul communication requires a mobile-cell to discover its neighbors during the 'neighborhood discovery phase'. The Third Generation Partnership Project (3GPP) has specified a basic frame structure for physical sidelink discovery channel (PSDCH) to facilitate neighborhood discovery [93]. The PSDCH will eliminate the interference to/from conventional cellular communication. The 3GPP specifications are meant to facilitate neighborhood discovery for any device, not particularly mobile-cells. Therefore in this discussion, we refer to any node seeking to discover neighbors as a discovering user equipment (DUE), keeping in view that the proposed schemes and their performance evaluations apply directly to mobile-cells. Regardless of the type of device involved in the process, successful neighborhood discovery is limited by two main factors: collision and half-duplexing. In this chapter, we propose a modified discovery frame structure to mitigate these constraints. First, we present the fundamentals of neighborhood discovery procedure. Later, our contribution towards achieving successful discovery to initiate sidehaul communication is presented.

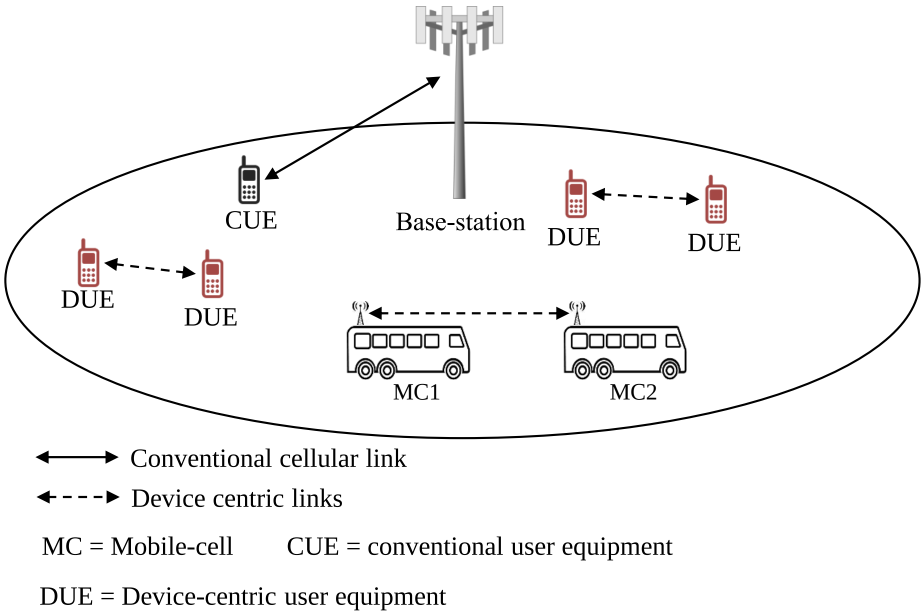

Figure 3.1: A cellular environment with conventional communication and device-to-device communication.

3.1.1 Overview of Neighborhood Discovery

According to 3GPP specifications, devices can only transmit and receive discovery beacons during the PSDCH-period as shown in Figure 3.2 which is periodically repeated after $\Delta\mathcal{T}_d$ milli-seconds. The DUEs can initiate discovery by autonomously selecting transmission resources from PSCDH-period. This network-independent mode of discovery, also known as mode-2, supports out-of-network autonomous neighborhood discovery. However, mode-2 type discovery often suffers from failures due to the effects of collision and half-duplexing, which are the consequences of random selection of beacon transmission resources.

As discussed earlier in Chapter 2, collision between two (or more) devices occurs if both (or all) of them select exactly the same resource for beacon-transmission. In this case, rest of the neighboring devices are unable to detect either (or all) of the colliding devices. On the other hand, half-duplexing occurs if more than one neighboring devices select different transmission resources (i.e. different sub-channel) in the same sub-frame. Consequently each device fails to discover one another.

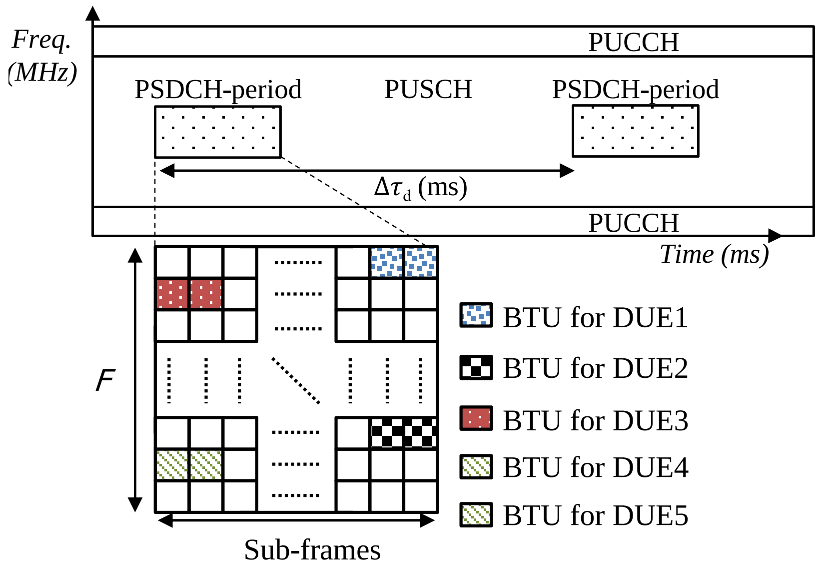

Figure 3.2: 3GPP standardized Physical Sidelink Discovery Channel and frame structure.

Following 3GPP guidelines, researchers in [71, 94, 95] have proposed mechanisms to avoid failures under mode-2 type discovery. Authors in [92] have presented a probabilistic wake-sleep process according to which nodes wake up to transmit beacon messages following a stochastic process that exploits device's communication history. However, the authors has focused more on energy conservation of the devices than reducing collision or half-duplexing effects.

3.1.2 Research Contribution

To mitigate the effects of collision and half-duplexing, we have proposed a modified frame structure for neighborhood discovery. We have split the PSDCH-period into two sub-periods. The participating devices will transmit beacon messages in both sub-periods. If the transmission fails during the first sub-period, devices will attempt to successfully transmit beacons in the subsequent sub-period. The frame splitting will enhance the probability that the devices may get discovered in either of the two sub-periods.

3.1.3 Chapter Organization

The rest of the chapter is organized as following. In Section 3.2, we present the system model. Section 3.3 explains our proposed discovery frame structure. The

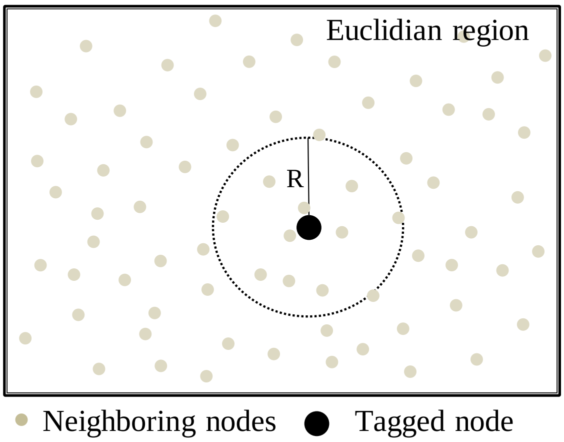

Figure 3.3: Node distribution in homogeneous Poisson point process.

analytical and simulation results are presented in Section 3.4. We conclude this chapter in Section 3.5. The publication related to this chapter is presented in Section 3.6.

3.2 System Model

We have considered that DUEs are distributed uniformly and randomly forming a homogeneous Poisson point process (H-PPP) Φ with density λ (per m^2) on the euclidean plane. Each interested DUE has equal opportunity to participate in the discovery process, that is, they can independently select any resource from the available PSDCH time-frequency resource pool.

Each DUE can discover only those neighbors that are within its discovery range $\mathcal{R}$ (in meters) as shown in Figure 3.3. **With slight abuse of terminology, the expected number of neighbors around any receiving DUE may be considered as a binomial point process (BPP)** $\Phi_{\mathcal{D}}$ with $\mathcal{D}$ points [Section 2.2.2, [128]]. For the sake of clarity, each point in a BPP refers to a neighboring node. The discovery range $\mathcal{R}$ is same for all devices. Within the discovery range of a DUE, there are an average of $\mathcal{D} = \lambda\pi\mathcal{R}^2 - 1$ possible neighbors. All DUEs (including mobile-cells and out-of-vehicle users) are static at this stage. Mobility shall be considered in Chapter 4.

Neighborhood discovery can take place only during the dedicated PSDCH-period which shares the spectrum with physical uplink shared channel (PUSCH). Note that according to 3GPP Release-12, physical uplink control channel (PUCCH) operates normally for transmitting uplink control signals from cellular user to the base station, even during the PSDCH-period. The PSDCH-period is repeated after every $\Delta\mathcal{T}_d$ milliseconds and consists of $|\mathcal{M}|$ sub-frames such that each sub-frame has a duration of 1 ms. A total of $|\mathcal{F}|$ sub-channels are available per sub-frame. Interested DUEs select resources, called the beacon transmission unit (BTU), during PSDCH-period (see Fig. 3.2) to transmit discovery beacons. A BTU consists of two consecutive slots in time (also called a sub-frame) at a given frequency. All nodes are assumed to be synchronized in time and frequency following the 3GPP standards [76]. No cellular communication takes place during PSDCH-period [Section 5.10.7 [78]]. This frame structure is same for both frequency-division duplexing (FDD) and time-division duplexing (TDD). We have used FDD mode in this work. However, our modifications can be used with TDD mode equally well.

The sub-frames and sub-channels form the set $\mathcal{M}$ and $\mathcal{F}$, respectively. The individual sub-frames are denoted as m, such that $m \in \mathcal{M} = \{1, 2, 3....|M|\}$, where $|.|$ shows the cardinality of the set. Similarly, the sub-channels are denoted as $f \in \mathcal{F} = \{1, 2, 3...|F|\}$. Note that a sub-frame contains $|\mathcal{F}|$ sub-channels as shown in Figure 3.2. In total $|\mathcal{M} \times \mathcal{F}|$ BTUs are available during a single PSDCH-period and a BTU is represented as $\{(m, f) \mid m \in \mathcal{M} \text{ and } f \in \mathcal{F}\}$. Each interested device randomly selects one BTU for beacon transmission. We have considered collision based discovery at this stage to acheive tractability in the analysis. Considerations of signal-to-interference-plus-noise ratio (SINR) will be presented in Section 3.3.1.

DUE j may successfully discover the DUE i if both DUEs do not select the same sub-frame and other devices do not select the same BTU as i. Mathematically, the successful discovery probability ($\delta_{i,j}$) can be written as:

$$\delta_{i,j} = \binom{\mathcal{MF}}{1}\Big(\frac{1}{\mathcal{MF}}\Big)\Big(\frac{\mathcal{MF}-\mathcal{F}}{\mathcal{MF}}\Big)\Big(1-\frac{1}{\mathcal{MF}}\Big)^{\mathcal{D}-2}. \tag{3.1}$$

Since $\delta_{i,j}$ can be generalized for any transmitter-receiver pair i and j, we will remove the subscripts in the remaining discussion. The probability that any particular DUE is discovered by a receiver after n PSDCH-periods is:

$$P_{\mathcal{D},i} = 1 - (1-\delta)^n. \tag{3.2}$$

Given that there are $\mathcal{D}-1$ neighbors within the coverage range of an arbitrary receiver, the expected number of DUEs that can be discovered is given as:

$$\mathbb{E}[\mathcal{N}_{\mathcal{D}}] = (\mathcal{D}-1) \times P_{\mathcal{D},i}. \tag{3.3}$$

In the next section we will propose a modified frame structure. Intuitively, this modification should lead to higher successful discovery probability as each device will transmit at least twice.

3.3 Multiple Beacon Transmission

The main modification in the proposed structure is that each PSDCH-period of length $|\mathcal{M}|$ sub-frames and duration of t_p (milli-seconds) is equally divided into sub-period 1 and sub-period 2, with t_{p_1} and t_{p_2} milli-seconds, respectively. Each sub-period now comprises of $|\mathcal{M}|/2$ sub-frames. The devices will transmit a beacon in one of the randomly chosen sub-frames, and will listen to the other devices in the remaining t_{p_1}. During t_{p_2}, the devices will again randomly choose a BTU for beacon transmission. Even if two (or more) nodes select BTUs in the same sub-frame during t_{p_1}, they may choose BTUs in a different sub-frame during t_{p_2}. The modified frame structure for the PSDCH-period is shown in Figure 3.4. The frequency-time grid is similar to that shown in Fig 3.2 so it is not included in the figure.

As the PSDCH-period is divided into two sub-periods, i.e., sub-period 1 and sub-period 2, the discovery probabilities are respectively denoted as δ_1 and δ_2. These probabilities are calculated in the same way as Eq. (3.1). The total discovery probability for a given PSDCH-period becomes:

$$\delta_{T_2} = \delta_1 \cup \delta_2 - \delta_1 \cap \delta_2. \tag{3.4}$$

where $\delta_1 = \delta_2 = \delta$ due to homogeneity of the point process.

For a homogeneous binomial point process, Eq. (3.4) can be written as:

$$\delta_{T_2} = 2\delta - \delta^2. \tag{3.5}$$

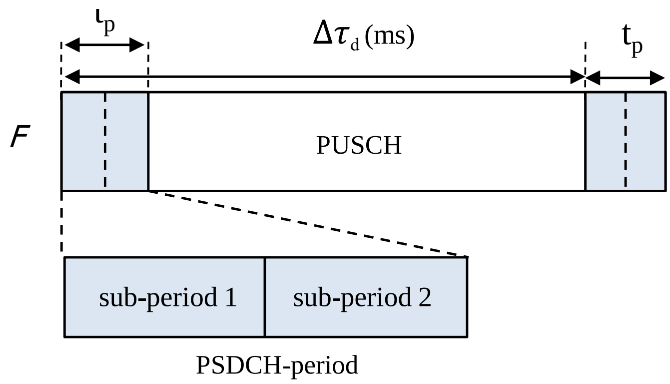

Figure 3.4: Proposed frame structure for PSDCH-period following 3GPP guidelines. © 2019 IEEE [35].

For the sake of completion of our analysis, we have also calculated the case when PSDCH-period is divided into three (equally sized) sub-periods. In this case, and following homogeneity of point process, the probability that a particular neighbor is discovered by a receiving DUE is:

$$\delta_{T_3} = 3\delta - 3\delta^2 + \delta^3. \tag{3.6}$$

In Section 3.4, we will compare the performance difference when we divide PSDCH-period into two sub-periods, versus when PSDCH-period is divided into three sub-periods.

3.3.1 Modeling Noise and Interference

In a noise and interference limited environment, SINR plays an important role. During any discovery process, a DUE is discovered if the transmitted message on a BTU-payload is decoded successfully by the receiving DUE. The success in decoding beacon information is possible only if the SINR at the receiver is greater than a threshold value [94]. The SINR of beacon transmitted by DUE i and observed by receiver j is calculated as:

$$\gamma_{i,j} = \frac{P_i r_{i,j}^{-\alpha} \zeta |h_{i,j}|^2}{\sum\limits_{k \in \Phi_D, k \neq i,j} P_k r_{k,j}^{-\alpha} \zeta |h_{k,j}|^2 + \sigma^2} \tag{3.7}$$

where P_{t_x} is the transmit power of transmitter t_x, $|h_{t_x,t_r}|^2$ is exponentially distributed power for a Rayleigh fading channel between $t_x \to t_r$, and r_{t_x,t_r} is

Table 3.1: Parameters for Monte-Carlo simulation.

Parameter	Values
Range of discovery	500 m
Number of discovering devices in a cell	50 to 1000
Beacon transmit Power	23 dBm (-7 dB)
Channel Bandwidth	10 MHz
Number of sub-channels per sub-frame	44
Total Number of sub-frames	64
pathloss-exponent (α)	4
AWGN (σ^2)	-121 dBm
SINR threshold (γ_{thr})	3 dB
Log-normal shadowing (ζ)	6 dB standard deviation

the distance between $t_x \to t_r$. The symbols ζ, α denote the log-normal shadowing and pathloss exponent, respectively. The aggregate interference from the other transmitters in Φ_D excluding transmitter i and receiver j is denoted as $\sum\limits_{k \in \Phi_D, k \neq i,j} P_k r_{k,j}^{-\alpha} h_{k,j}$. The Additive White Gaussian Noise (AWGN) is referred to as σ^2.

The node discovery under a noise and interference limited environment is calculated using a detection parameter $\beta_{i,j} \in \{0, 1\}$. For a given DUE receiver j, $\beta_{i,j} = 1$ when the SINR of the received beacon from i_{th} DUE is above the threshold (γ_{thr}). If the beacon from i is received with a lower SINR, then $\beta_{i,j} = 0$. Mathematically, we can express this binary parameter as:

$$\beta_{i,j} = \begin{cases} 1, & \gamma_{i,j} \geq \gamma_{\text{thr}} \\ 0, & \gamma_{i,j} < \gamma_{thr} \end{cases}. \tag{3.8}$$

We define ξ_j as the ratio of all DUEs discovered by receiver $j \in \Phi$ to the total number of DUEs in $\Phi_{\mathcal{D}}$ which are within the discovery range of DUE j:

$$\xi_j = \frac{1}{\mathcal{D} - 1} \sum_{i=1, i \neq j}^{\mathcal{D}} \beta_{i,j}. \tag{3.9}$$

3.4 Results and Discussion

To demonstrate the accuracy of our model and analysis, we will first focus on the collision based model which does not include SINR decoding. In a collision based

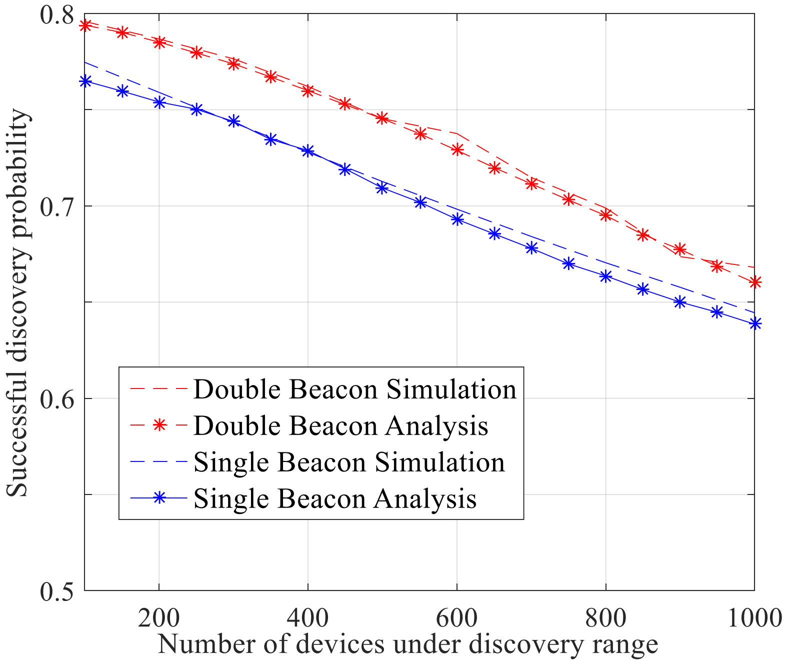

Figure 3.5: Analytical and simulation results per single discovery period for various number of devices. © 2019 IEEE [35].

model, if two (or more) devices select the same resource, they are not discovered by their neighbors. On the other hand, in the SINR-based model, the device with high signal strength gets successfully discovered if their SINR is above a certain threshold. Hence, collision based model gives the pessimistic assessment of successful discovery. In our simulations, we have run 500 iterations for each case and then averaged the outcomes. The simulation observations were found to be matching closely with the analytical results. The relevant parameters for simulations are presented in Table 3.1.

Figure 3.5 shows the comparison of the successful discovery probability achieved using the proposed and the conventional discovery frame structure. It can be seen that the successful neighbor discovery probability per PSDCH-period decreases linearly as the number of devices increases. However, the proposed scheme discovers more neighbors compared to the conventional scheme.

For very large number of neighbors, the proposed scheme slightly underperforms as compared to conventional discovery mechanism. In fact, for the chosen

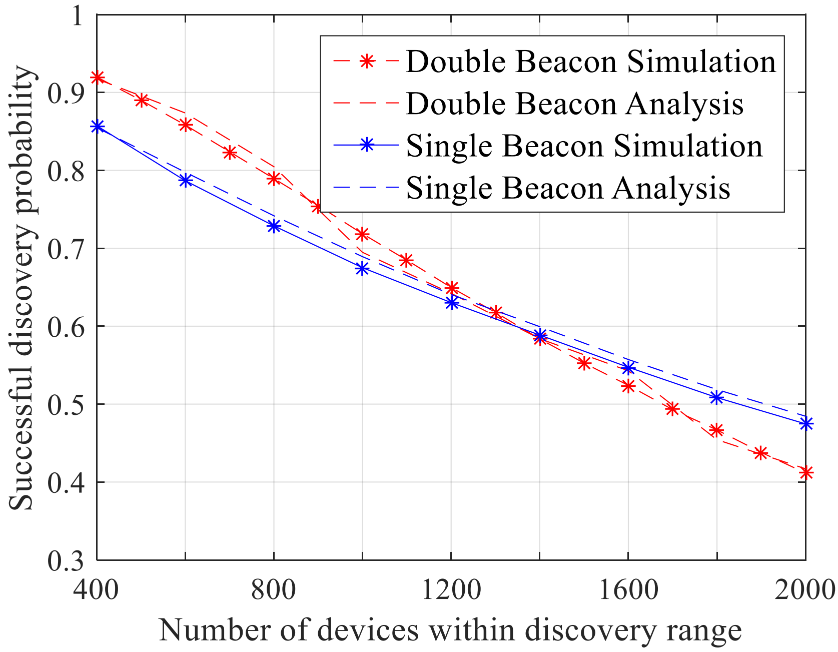

Figure 3.6: Performance comparison of the proposed vs conventional schemes for very large number of devices. © 2019 IEEE [35].

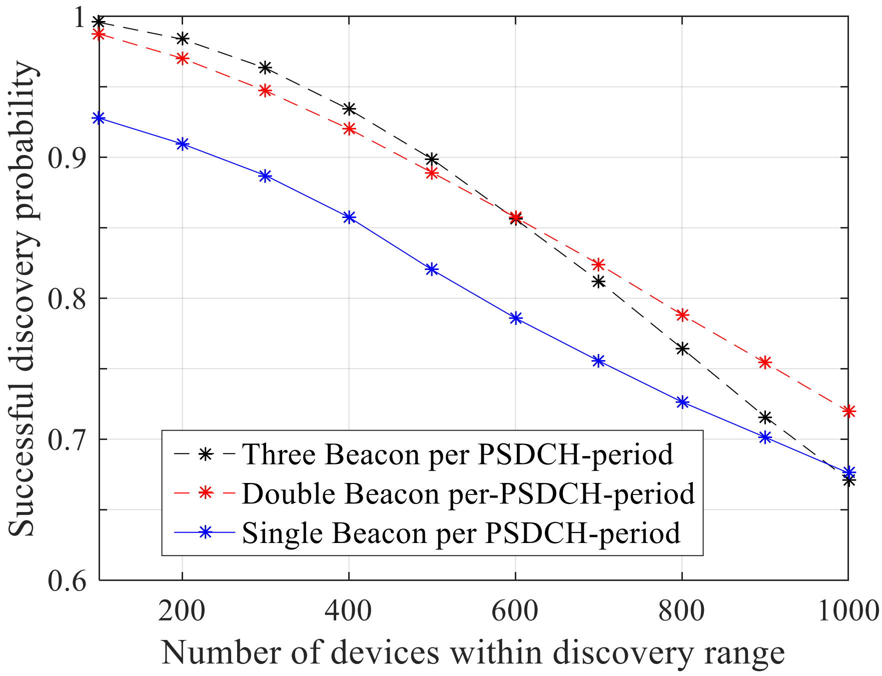

Figure 3.7: Performance comparison between single, two, and three beacons per PSDCH-period.

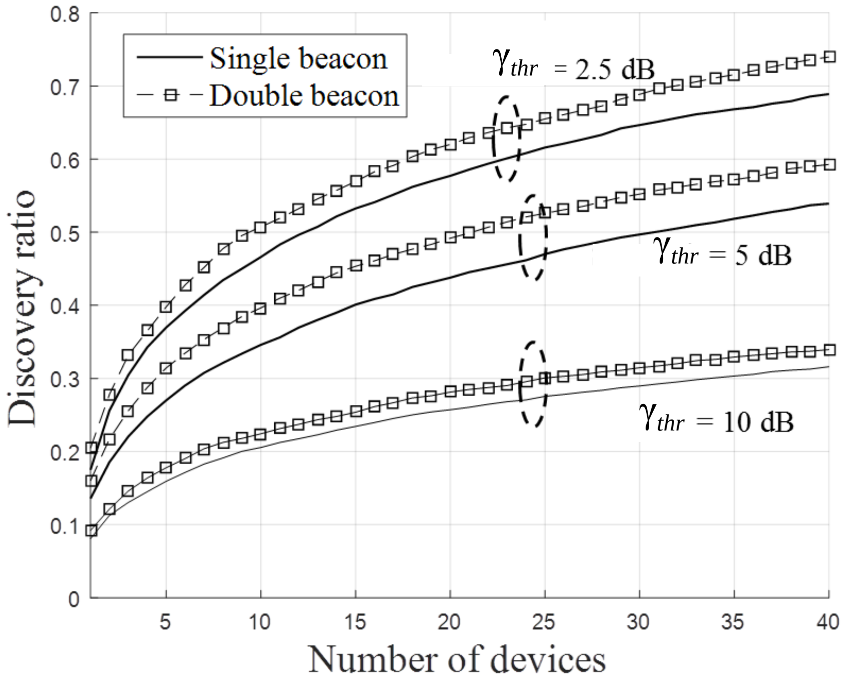

Figure 3.8: Discovery results for different SINR thresholds (γ_{thr}). © 2019 IEEE [35].

parameters of $\mathcal{M}$ and $\mathcal{F}$, the discovery ratio decreases even below the conventional scheme for very high density of devices in the neighborhood. This is shown in Figure 3.6. Note that the reduction in successful discovery is due to the fact that as the number of devices increase, the failure in discovery will also increase as more devices will select the same BTU and the sub-frame.

For the sake of completeness of our analysis, Figure 3.7 shows the comparison of successful discovery probability when the PSDCH-period is divided into three sub-periods. It can be observed that the difference in the discovery success ratio with two or three sub-periods per PSDCH-period is only marginal. It can be further observed that when PSDCH-period is sliced into three sub-periods, the discovery probability starts to decrease sharply when participating devices gets larger than 600. This is again due to the increased number of collisions and half-duplexing when number of participating neighbors gets higher.

In Figure 3.8 and Figure 3.9, we present the simulation results introducing noise and interference. If two (or more) DUEs select the same BTU, then the DUE with SINR exceeding threshold level at the receiver gets successfully discovered. We assumed the same communication range for all DUEs. Again, it

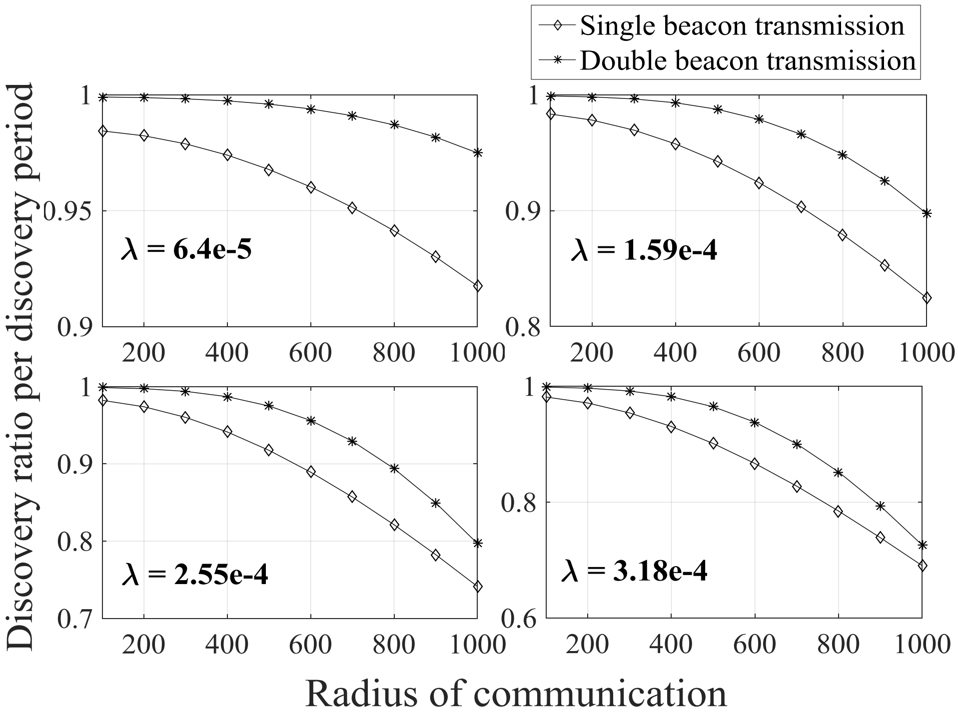

Figure 3.9: Discovery results with different discovery ranges and varying DUE distribution rate (λ). © 2019 IEEE [35].

can be observed from Figure 3.8 that there is increase in the discovery ratio with the proposed scheme as compared to conventional single beacon transmission. However, this increase is lower than our initial expectations.

Figure 3.9 compares the proposed scheme against conventional single beacon transmission model for different densities of neighboring nodes in a noise and interference limited environment. It can be observed that for low density of nodes, we achieve comparatively higher discovery ratio. This is especially true for larger radius of communication for all DUEs. On the contrary, as the density of nodes increase, the difference between the two schemes gets marginal.

3.5 Conclusion

In this chapter, we have presented our initial work to mitigate the effects of collision and half-duplexing in mode-2 type neighborhood discovery. All the nodes are considered static in this chapter. We have proposed to split the PSDCH-period into multiple sub-periods. We have observed that if the PSDCH-period is sliced into two sub-periods, a comparatively higher probability of successful discovery is achieved. Splitting the PSDCH-period into three sub-periods does not provide any significant improvements. The gains achieved through the proposed scheme depends upon the density of nodes in the neighborhood. For example, as the number of neighbors gets very high, the proposed scheme tends to underperform as compared to the conventional scheme. This is because as number of participating devices gets higher, the collision between devices also increases which result in discovery failure.

In the next chapter, we will propose a dynamic discovery scheme which will utilize the neighborhood information to transmit beacon messages. We will demonstrate how this dynamic scheme will enhance the probability of successful discovery using the knowledge of neighborhood density. We will also formulate a mathematical model for the discovery by the moving device, such as a mobile-cell.

3.6 Related Publication

- **Shan Jaffry**, Syed Faraz Hasan, Yaw Wen Kuo, Xiang Gui, "Distributed Device Discovery in ProSe environment", IEEE Region 10 Conference (IEEE TENCON), November 2017, Penang, Malaysia.

Chapter 4

Proximity-aware Neighborhood Discovery

4.1 Introduction

3GPP has specified mode-2 type neighborhood discovery so that devices may know their neighbors without network assistance [129]. The devices may then establish sidehaul communication with their neighbors. For example, a mobile-cell may communicate with neighboring mobile-cells [23] or with out-of-vehicle users [32, 57]. Following the convention used in Chapter 3, we will use the term discovery user equipment (DUE) to refer to all static devices that participate in discovery process, including mobile-cells and out-of-vehicle users.

The inherent randomness of mode-2 type procedures may prolong the successful discovery of neighbors due to collisions and half-duplexing effects as earlier explained in Section 3.1.1. In the previous chapter, we have proposed a basic modification to the PSDCH-period to mitigate these effects and expedite the discovery process. We observed that our proposed scheme underperformed as the density of neighboring devices increases. In this chapter, following the modifications by 3GPP in Release 14 (R-14), we will develop a scheme which adapts according to the neighborhood density to increase successful discovery probability. We will also develop a mathematical model to study the effect of mobility on the neighborhood discovery by a mobile cell which, to the best of our knowledge, has not been presented in the past literature. First, we will briefly explain the modification related to neighborhood discovery in 3GPP R-14 in the next section.

4.1.1 Overview of 3GPP Modifications

The 3GPP R-14 has introduced a transmission probability parameter *txProbability* (Tx_P) to control the beacon broadcast rate by DUEs. Each discovery beacon is carried by a fundamental resource called beacon transmission unit (BTU) (See Fig. 3.2). According to 3GPP, if a DUE wants to participate in the discovery process, it selects a random variable, say p_1, such that $p_1 \in (0, 1]$. This is an internal process within each device. The DUE will only broadcast its BTU if and only if $p_1 < Tx_p$ [130], where Tx_P is the threshold transmission probability which can take only 4 values: $\{0.25, 0.50, 0.75, 1.0\}$. In case $p1 \geq Tx_p$, the DUE will buffer its message and make another attempt to broadcast in the next PSDCH-period using the same protocol. This mechanism has been introduced by 3GPP to avoid redundant beacon transmission in regions where DUE density is very high (Sec 6.3.8, [129]). If DUE density is very high and $Tx_p = 1$, excessive collisions may occur leading to decrease in successful discovery probability. On the other hand, if Tx_p is reduced to lower values, then the number of transmitting devices during a given PSDCH-period will reduce. Consequently, the number of failed attempts during the discovery phase will also decrease.

In the presence of network infrastructure, the base station broadcasts the value for Tx_P. In a base station free environment, the DUEs select the predefined value of Tx_P to begin beacon transmission. However, the selection of Tx_P value without the awareness of the number of neighbors in the proximity of transmitting device may lead to failure in discovery.

4.1.2 Research Contribution

The contribution of this chapter is the development of a proximity-aware mode-2 type neighborhood discovery scheme for network-independent scenarios. To this end, we will first numerically formulate the effect of neighborhood density on the successful discovery probability. We will propose a mechanism which will enable a DUE to select optimal value of Tx_p based on neighborhood density. Devices will broadcast beacons using this Tx_p value. Later, we will develop an analytical model for the neighborhood discovery by a mobile DUE (mDUE), such as mobile-cell. To the best of our knowledge, the mode-2 type discovery for mDUE has never been studied in the literature before.

4.1.3 Chapter Organization

The rest of this chapter is organized as follows. In Section 4.2, we present our optimized beacon transmission scheme. Neighbor discovery by a mDUE is presented in Section 4.3. We will conclude this Chapter in Section 4.5. The publication related to this chapter is presented in Section 4.6.

4.2 Adaptive Out-of-Coverage Discovery

4.2.1 System Model

In our system model, DUEs are distributed on the euclidean plane as a homogeneous Poisson point process (H-PPP) Φ with density λ. We consider that there are $\mathcal{D}-1$ DUEs around DUE $i \in \Phi$ that participate in the discovery process, where $\mathcal{D} = \lambda\pi\mathcal{R}^2$. With slight abuse of terminology, we can say that $\mathcal{D}$ forms a binomial point process with $|\mathcal{D}|$ points [Sec. 2.2.2, [128]], and $|.|$ shows the cardinality of the set. Note that all devices have a discovery range of $\mathcal{R}$ (meters) within which they can discover neighbors by listening to their beacons.

The PSDCH-period has $|\mathcal{M}|$ sub-frames and $|\mathcal{F}|$ sub-channels which make a total of $|\mathcal{M} \times \mathcal{F}|$ available BTUs. Each DUE can select any BTU with equal probability. We have considered a collision-based discovery model, i.e., if two devices select the same BTU, their discovery messages will be lost due to collision. All devices are assumed to be synchronized in time and frequency (Section 5.10.7 of [129]).

DUE i will successfully receive a beacon from DUE $j \in \mathcal{D}-1$ if the latter does not collide with any other transmitting DUE, and i and j do not select the same sub-frame for their respective BTUs. If Ψ is the probability of an event when $p_1 < Tx_p$, then probability that i discovers j is:

$$p_{j\to i} = \Psi\left(1-\frac{\Psi}{\mathcal{M}}\right)\left(1-\frac{\Psi}{M\mathcal{F}}\right)^{\mathcal{D}-2} \tag{4.1}$$

The probability to discover j after n PSDCH-periods is:

$$\rho = 1-(1-p_{j\to i})^n \tag{4.2}$$

DUE i successfully discovers DUE j in ε_{ij} PSDCH-periods which forms a

Geometric Distribution given by parameter $p_{j\to i}$, where $\varepsilon_{ij} = \dfrac{1}{p_{j\to i}}$. For all $\mathcal{D}$ DUEs, the successful discovery ratio is given by $P = \mathcal{D}\rho$. Finally, for all static DUEs within the discovery range, the expected number of discovered neighbors after the discovery period $\mathcal{T}_d$ can be found by using Exclusion-Inclusion principle [131] as:

$$\mathbb{D}_{\mathcal{T}_d} = \mathcal{D}\sum_{n=1}^{\mathcal{T}_d}(-1)^{n+1}\binom{\mathcal{T}_d}{n}p_{j\to i}^{n}. \tag{4.3}$$

It is evident from Eq. (4.1) that successful discovery probability $p_{j\to i}$ depends on the factors such as $\Psi, \mathcal{M}, \mathcal{F}$, and $\mathcal{D}$. Hence, with a prior knowledge of these parameters, we can increase the discovery probability. Note that in case of network coverage, the eNB decides the value of Ψ (or Tx_p) based on network traffic conditions, etc. On the contrary, in case of network unavailability, Ψ will be a pre-set constant [71]. We propose that DUEs can adaptively control Ψ to increase the discovery probability, even in out-of-network environments. In the next section, we will first formulate the optimal value of Ψ in terms of parameters like $\mathcal{M}, \mathcal{D}$, etc. We will then present an adaptive out-of-network discovery scheme. A complete list of important variables are presented in Table 4.1.

4.2.2 Optimal Transmission Probability

The expression of successful discovery probability given in Eq. (4.1) shows that we can control $p_{j\to i}$ by changing parameters such as $\Psi, \mathcal{M}$, and $\mathcal{F}$. This section will evaluate the effects of these parameters on discovery probability, given the awareness of the neighboring devices (i.e., information of $\mathcal{D}$). To find the optimal number of sub-frames required to increase discovery probability, we take partial derivative of Eq. (4.1) with respect to $\mathcal{M}$ to get:

$$\frac{\partial p_{j\to i}}{\partial \mathcal{M}} = p'_{j\to i(\mathcal{M})} = \frac{\Psi^2\left(1-\frac{\Psi}{\mathcal{F}\mathcal{M}}\right)^{\mathcal{D}-2}}{\mathcal{M}^2} + \frac{(\mathcal{D}-2)\,\Psi^2\left(1-\frac{\Psi}{\mathcal{M}}\right)\left(1-\frac{x}{\mathcal{F}\mathcal{M}}\right)^{\mathcal{D}-3}}{\mathcal{F}\mathcal{M}^2} \tag{4.4}$$

Letting $p'_{j\to i(\mathcal{M})} = 0$, we get $\mathcal{M}^* = \dfrac{\Psi(\mathcal{D}-1)}{\mathcal{D}+\mathcal{F}-2}$. After second partial derivative of $p'_{j\to i(\mathcal{M})}$ and inserting $\mathcal{M}^*$ in Eq. (4.4), we get:

Table 4.1: System model parameters

Symbol	Definition
Φ	Homogeneous Poisson Point Process.
λ	Density of H-PPP points.
$\mathcal{M}, \mathcal{F}$	Number of sub-frames, number of sub-channels.
$\mathcal{R}$	Discovery range of a DUE.
$\mathcal{D}$	Number of points (DUEs) in a binomial point process within a circle of radius $\mathcal{R}$.
$p_{j\to i}$	Probability that DUE i successfully receive a beacon from DUE j.
ρ	The probability to discover j after n PSDCH-periods.
p_1	A random variable selected by DUE within the range $(0, 1]$.
Tx_p	Threshold value for Transmission Probability.
Ψ	Probability of an event when $p_1 < Tx_p$.
Ψ^*	Optimal value of Ψ.

$$\frac{\partial'' p_{j\to i}}{\partial \mathcal{M}''} = p''_{j\to i(\mathcal{M})} = \frac{(\mathcal{D}+\mathcal{F}-2)^4}{\Psi(\mathcal{D}-2)(\mathcal{F}-1)(\mathcal{D}-1)^2}\left(\frac{(\mathcal{D}-2)(\mathcal{F}-1)}{\mathcal{F}(\mathcal{D}-1)}\right) \tag{4.5}$$

Since $\mathcal{D} \gg 1$ and $\mathcal{F} > 1$, Eq. (4.5) will always yield a non-negative result, because $p''_{j\to i(\mathcal{M})} > 0$. This means that we will get the minima of $p_{j\to i}$ at $\mathcal{M}^*$. Thus $p_{j\to i}$ cannot be optimized with respect to the number of sub-frame per PSDCH-period. On the contrary, we can get the maxima of $p_{j\to i}$ by differentiating Eq. (4.1) with respect to Ψ as [71]:

$$\frac{\partial p_{j\to i}}{\partial \Psi} = p'_{j\to i(\Psi)} = \left(1-\frac{\Psi}{\mathcal{M}}\right)\left(1-\frac{\Psi}{\mathcal{M}\mathcal{F}}\right)^{\mathcal{D}-2} - \frac{\Psi\left(1-\frac{\Psi}{\mathcal{M}\mathcal{F}}\right)^{\mathcal{D}-2}}{\mathcal{M}} - \frac{(\mathcal{D}-2)\,\Psi\left(1-\frac{\Psi}{\mathcal{M}}\right)\left(1-\frac{\Psi}{\mathcal{M}\mathcal{F}}\right)^{\mathcal{D}-3}}{\mathcal{M}\mathcal{F}} \tag{4.6}$$

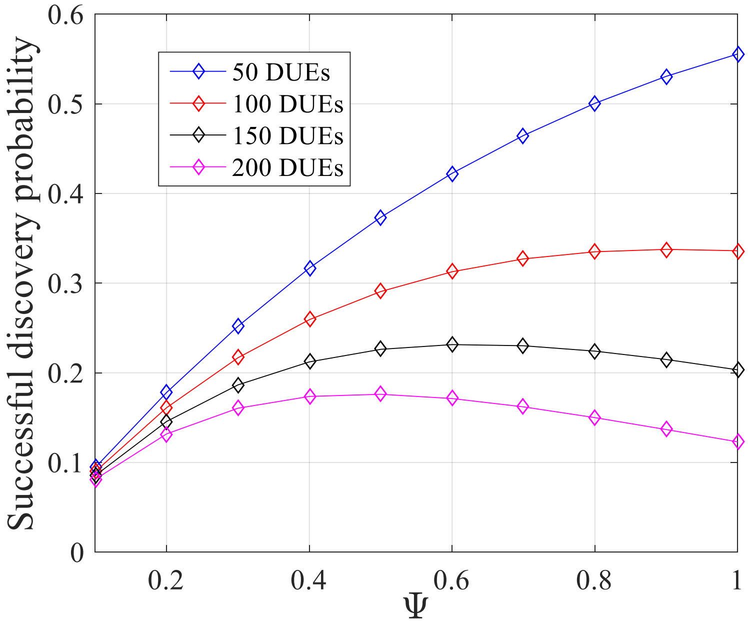

Figure 4.1: Discovery probability per PSDCH-period versus Ψ, $\mathcal{M} = \mathcal{F} = 10$. © 2018 IET.

Letting $p'_{j \to i(\Psi)} = 0$, we get the roots for Eq. (4.6) as $\Psi_1 = \frac{\sqrt{4\mathcal{F}^2 - 4\mathcal{F} + \mathcal{D}^2 - 2\mathcal{D} + 1}\mathcal{M} + (2\mathcal{F} + \mathcal{D} - 1)\mathcal{M}}{2\mathcal{D}}$ and $\Psi_2 = -\frac{\sqrt{4\mathcal{F}^2 - 4\mathcal{F} + \mathcal{D}^2 - 2\mathcal{D} + 1}\mathcal{M} - (2\mathcal{F} + \mathcal{D} - 1)\mathcal{M}}{2\mathcal{D}}$. The second order partial derivative for $p_{j \to i}$ is a negative quantity, because $\frac{\partial'' p_{j \to i}}{\partial \Psi''} < 0, \forall\ \Psi \leq 1$. This suffices the condition for finding optimal Ψ.

Note that $\Psi_1 >> 1$ since $\mathcal{M}, \mathcal{F} > 1$, and $\mathcal{D} >> 1$. We already know that $0 < \Psi \leq 1$. Hence, Ψ_1 cannot be the optimal Ψ. On the contrary, Ψ_2 will yield an optimal value (Ψ^*), such that $\Psi^* = \Psi_2$. However, this optimality is only valid under for the following conditions:

$$\mathcal{A} \leq \mathcal{B}^2 - \frac{4\mathcal{B}\mathcal{D}}{\mathcal{M}} + \frac{4\mathcal{D}^2}{\mathcal{M}^2} \tag{4.7}$$

where $\mathcal{A} = 4\mathcal{F}^2 - 4\mathcal{F} + \mathcal{D}^2 - 2\mathcal{D} + 1$ and $\mathcal{B} = 2\mathcal{F} + \mathcal{D} - 1$. In case when this condition does not suffice, we notice that $\Psi_2 > 1$. Hence, in that case, we consider $\Psi^* = \Psi_2 = 1$ (i.e., we round off to 1 following 3GPP guidelines).

Following the discussion above, we now know that the optimal transmission

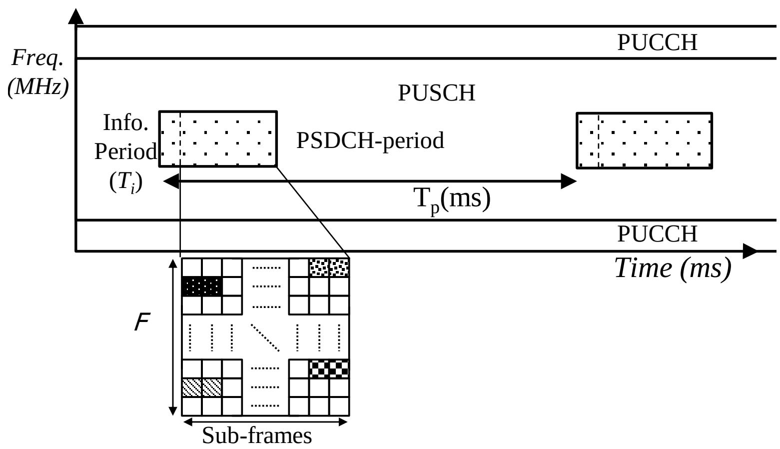

Figure 4.2: The frame structure for adaptive neighborhood discovery in out-of-coverage scenario. © 2018 IET.

probability for the discovery of DUE j by a DUE i is:

$$\Psi^* = \frac{\mathcal{M}}{2\mathcal{D}}\Big(2\mathcal{F} + (\mathcal{D}-1) - \sqrt{4\mathcal{F}^2 - 4\mathcal{F} + \mathcal{D}^2 - 2\mathcal{D} + 1}\Big) \qquad (4.8)$$

From Eq. (4.8), it can be deduced that the knowledge of parameters like $\mathcal{D}$ will increase $p_{j\rightarrow i}$. Figure 4.1 plots successful discovery probability as a function of Ψ which demonstrate that Eq. (4.1) is an upward convex function with respect to Ψ. The maxima for Eq. (4.1) is different for various values of $\mathcal{D}$. For example, for greater number of devices, the optimal point of the function is achieved for lower values of Ψ. This is because for lower value of Ψ, fewer devices transmit leading to smaller number of collisions. On the other hand, when $\mathcal{D}$ is a small, optimal point of Eq. (4.1) occurs at higher values of Ψ. This is due to the fact that the lower number of devices tend to cause less number of collisions, even for $\Psi = 1$. Since only four Tx_p values can be set according to 3GPP guidelines, i.e., $Tx_p \in \{0.25, 0.50, 0.75, 1.0\}$, we round-off Ψ^* to the nearest value within Tx_p.

4.2.3 Adaptive Beacon Transmission

We have shown in Section 4.2.2 that optimal transmission probability for neighbor discovery can be predicted with prior information about the number of devices in the neighborhood. However, in the absence of any central entity (such as base station) in out-of-coverage scenarios, this information is not readily available to the

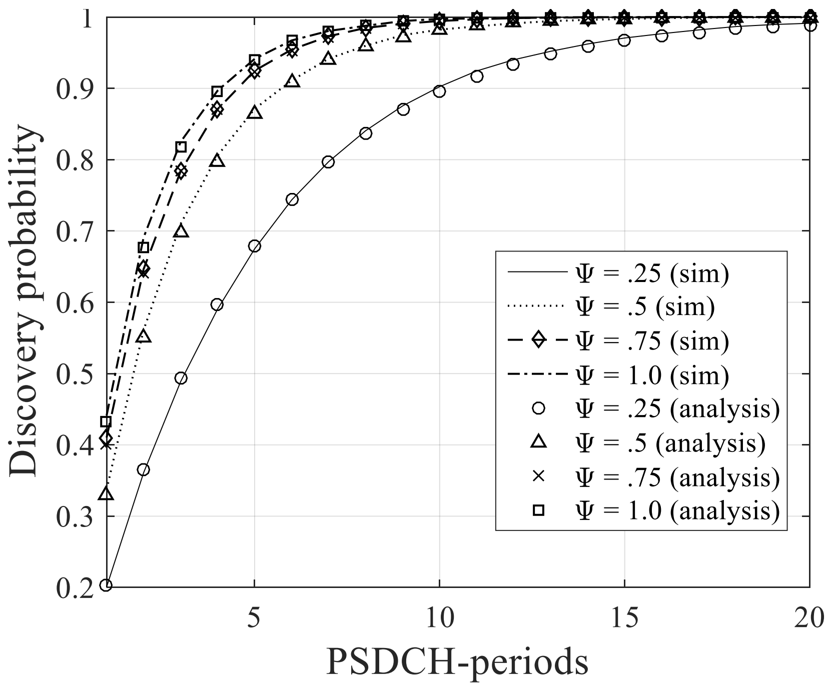

Figure 4.3: Relationship between discovery probability and Ψ ($\mathcal{M} = 10, \mathcal{F} = 10, \lambda = 1.9 \times 10^{-4}$). © 2018 IET.

transmitting devices. We propose a short sub-period which we call Information-period (T_i). The Information-period is reserved for neighborhood awareness only and always initiates before PSDCH-period as shown in Figure 4.2. If we consider M' sub-frames during T_i, then there are total of $M' \times \mathcal{F}$ resources available for information transmission. T_i is very short period and consumes small spectral resources but enables more successful discoveries as we will demonstrate in Section 4.2.4. No neighborhood discovery or uplink cellular communication takes place during this period.

During the Information-period, proximity information like neighborhood density, etc. is broadcasted to the DUEs by the dedicated devices. We call these devices as cluster-heads (CH). In a typical out-of-network scenario, the device transmitting the synchronization signals (e.g., physical sidelink synchronization signal) to the neighboring DUEs may assume the role of cluster-heads [132]. Several other techniques and algorithms have been presented in the literature [133–135] for cluster-head selection which is not the focus of our study. We assume that a sufficient number of cluster-heads are always present to provide information to the available DUEs. In the worst-case scenario, if no cluster-head is present, the

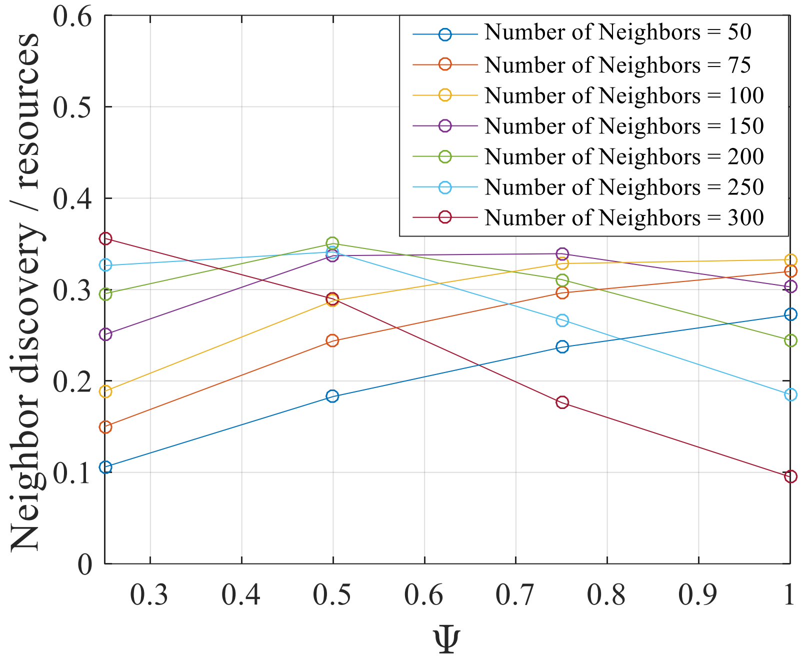

Figure 4.4: Neighbor discovery per available resources for different values of Ψ $(\mathcal{M}, \mathcal{F} = 10)$

devices will select the pre-set values as specified by 3GPP [71].

To understand the process of information broadcast by cluster-heads, consider that CH C_1 wants to transmit information about DUE-density (λ_1) in period T_i. There is a risk that C_1's broadcast may collide with other CHs' transmission on the same sub-channel. In order to avoid collision, each CH selects a random variable $\chi \in \{k\}$, where k is a positive integer and $1 \leq k \leq \mathcal{F}$, and the CH selects sub-channel $\mathcal{F} = \chi$. This mechanism will ensure successful transmission of information during T_i with probability $P_{succ} = \left(1 - \frac{1}{\mathcal{M}'\mathcal{F}}\right)^{\mathcal{C}-1}$, where $\mathcal{C}$ is total number of CHs within DUE communication range. For example, given that $\mathcal{M}' = 4$ and $\mathcal{F}' = 10$, if 10 CHs participate in information transmission, then 80% of messages will be delivered successfully to the participating DUEs. In other words, 8 out of 10 cluster-heads will successfully transmit their information. For a required P_{succ} , $\mathcal{M}'$, is calculated as:

$$\mathcal{M}' \simeq \left\lfloor \frac{1}{\mathcal{F}} \left(\frac{1}{1 - \sqrt[\mathcal{C}-1]{P_{succ}}} \right) \right\rfloor. \tag{4.9}$$

where $\lfloor . \rfloor$ denotes the floor value.

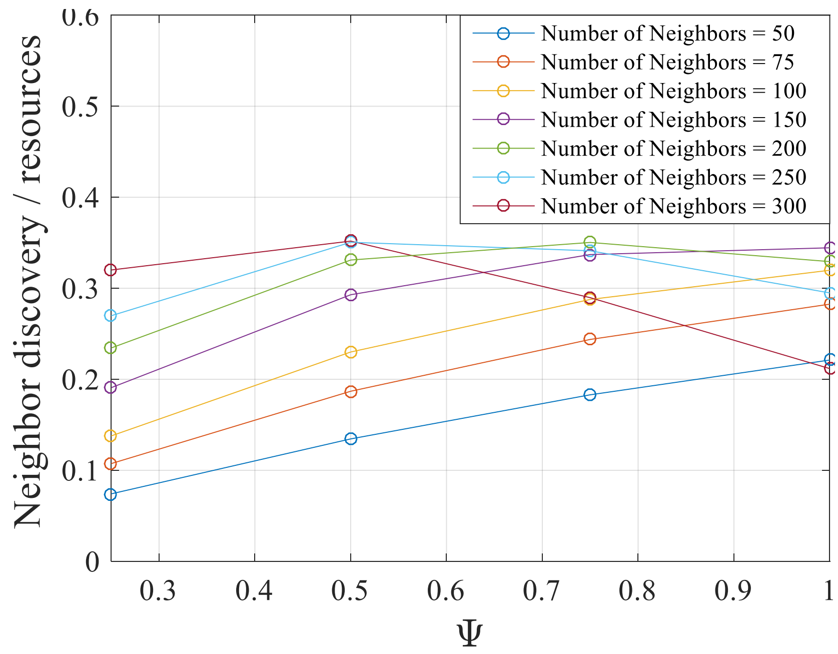

Figure 4.5: Neighbor discovery per available resources for different values of Ψ ($\mathcal{M} = 15,\ \mathcal{F} = 10$)

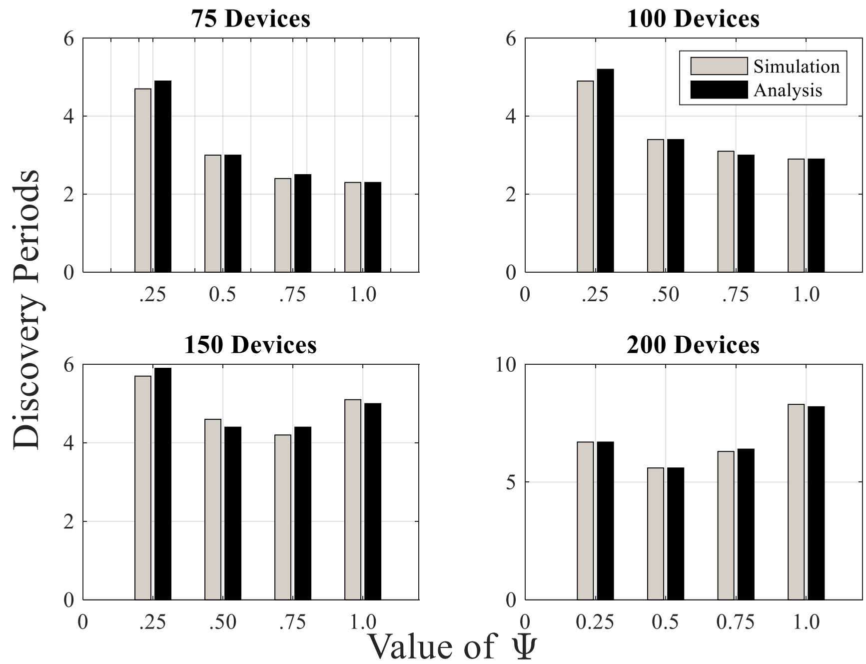

Figure 4.6: Estimated PSDCH-periods to discover single DUE based on different Ψ ($\mathcal{M} = 10,\ \mathcal{F} = 10$).

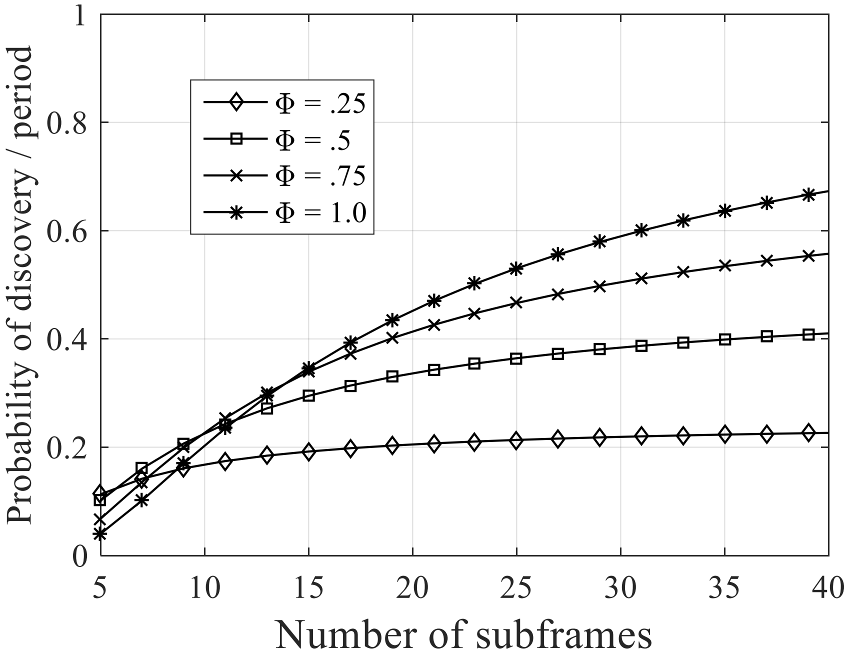

Figure 4.7: Probability of success per PSDCH-period versus subframes ($N_f = 10$, DUEs = 150). © 2019 IET [36].

4.2.4 Performance Evaluation

In this section, we evaluate the performance of the proposed adaptive discovery scheme. For this purpose, we have performed Monte-Carlo simulations with 100 runs per simulation and averaged the results for all devices.

Figure 4.3 compares the discovery probability to different values of Ψ. It can be seen that with $\lambda = 1.9 \times 10^{-4}$ (150 neighbors when $\mathcal{R} = 500$m radius) discovery probability is highest when $\Psi = 1.0$. On the other hand, for $\Psi = 0.25$, the discovery probability is significantly low. In this case, out of all the devices that participate in the discovery process, only those that have $p1 < 0.25$ are allowed to transmit discovery beacons. Figure 4.4 and Figure 4.5 show the effect of Ψ on the ratio of neighbors discovered to the available resources (BTUs). We consider $\mathcal{M} = \mathcal{F} = 10$ in Figure 4.4 and $\mathcal{M} = 15, \mathcal{F} = 10$ in Figure 4.5. Both these figures demonstrate that for lower number of devices in the proximity, the ratio of discovered neighbors per resources will linearly increase with the increase in the value of Ψ. On the contrary, if number of neighbors gets very high (for example, > 250), then the ratio decreases with an increase in Ψ.

Figure 4.6 shows the results for the expected number of PSDCH-periods required for a DUE to successfully discover an individual neighbor. It is evident from the figure that if we use a fixed value of Ψ, optimal performance during the discovery process cannot be guaranteed. As an example, it can be observed from Figure 4.6 that for scenarios with sparse density of DUEs, the higher values of Ψ will enable a DUE to discover its neighbor in fewer PSDCH-periods. For instance, if there exist 75 DUEs in the vicinity, an estimated number of 2 PSDCH-periods are required to discover an individual neighbor when $\Psi = 1.0$. Keeping all other variables unchanged, setting $\Psi = 0.25$ will require roughly 5 PSDCH-periods to discover a neighbor. In more densely populated regions, where $\mathcal{D} > 100$, neither $\Psi = 0.25$ nor $\Psi = 1.0$ gives optimal discovery results. This is because when Ψ is very small, the devices miss the opportunity for successful discovery. On the other hand, if Ψ is very high ($\Psi = 1.0$), there may be more collisions resulting in lowering of successful discovery probability. In such a case, $\Psi = 0.5,\ 0.75$ are optimal values as shown in Figure 4.6.

Figure 4.7 demonstrates the impact of varying $\mathcal{M}$ with different values of Ψ. It can be observed that as $\mathcal{M}$ gets higher, the successful discovery probability per PSDCH-period improves. However, it is intuitive that varying $\mathcal{M}$ is not desirable since larger values of $\mathcal{M}$ mean more spectral resources are required for the PSDCH-period. Consequently, these resources will have to be borrowed from PUSCH, which is not recommended as it will affect the cellular uplink communication.

4.2.5 Percentage Error in Neighborhood Information

There may be difference in the actual number of neighbors and the estimated neighbors calculated by each device during the Information-period. We will formulate this difference as percentage error E_r. The information transmission by the cluster-heads depends on the available sub-frames ($\mathcal{M}'$) reserved for the Information-period. The expected neighborhood density around a DUE is λ', where $\lambda' = \sum_{c=1}^{\bar{\mathcal{C}}} \lambda_c/\bar{\mathcal{C}}$ and $\bar{\mathcal{C}} = \mathcal{C} \times P_{succ}$ is the expected number of CHs within DUE's range whose messages successfully arrive at DUE and $\mathcal{C}$ is the actual number of CHs. The estimated number of neighboring DUEs are $\mathcal{D}^* = \lambda'\pi\mathcal{R}^2$. If λ is the actual DUE density, then the estimated percentage error E_r in evaluating neighboring DUEs is:

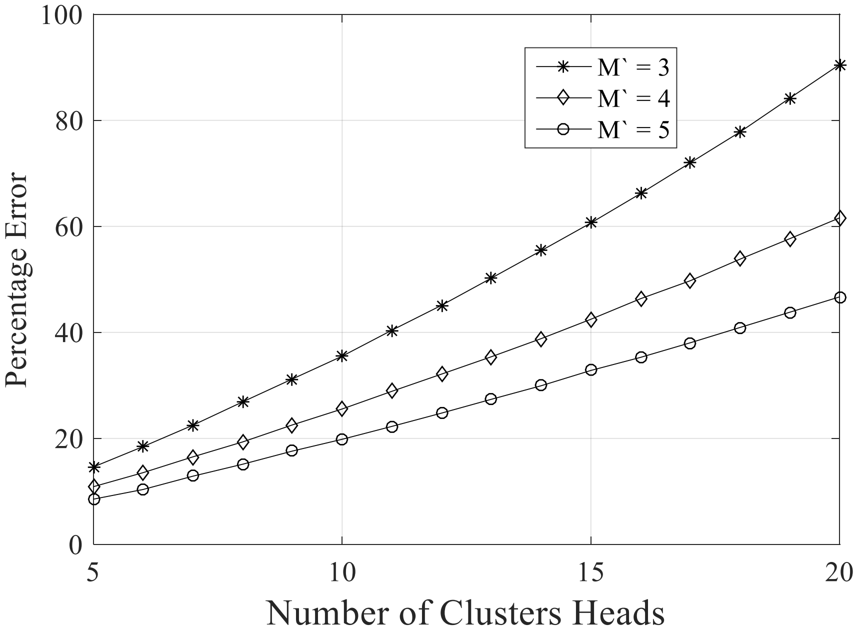

Figure 4.8: Percentage error in approximating neighborhood with different T_i ($\mathcal{F} = 10, \lambda = 1.9 \times 10^{-4}$). © 2019 IET [36].

$$E_r = \left| \frac{\lambda\pi\mathcal{R}^2 - \frac{\pi\mathcal{R}^2}{N}\sum_{c=1}^{\bar{\mathcal{C}}}\lambda_c}{\lambda\pi\mathcal{R}^2} \right| \times 100 \tag{4.10}$$

$$E_r = \left| 1 - \frac{1}{\lambda\mathcal{C}}\left(\frac{\mathcal{M}\mathcal{F}}{\mathcal{M}\mathcal{F}-1}\right)^{\mathcal{C}-1}\sum_{c=1}^{\bar{\mathcal{C}}}\lambda_c \right| \times 100 \tag{4.11}$$

Figure 4.8 demonstrates the percentage error with respect to the number of CHs and the size of Information-period. It can be observed that as the duration of Information-period increases, the percentage error decreases. On the other hand, as the number of cluster-heads increases, percentage error also rises as a consequence of increased collisions.

To this end, we have shown that our proposed scheme chooses the optimized value of Tx_p to expedite the neighborhood discovery. In the next section, we will analyze the performance of the proposed scheme for a mobile-cell.

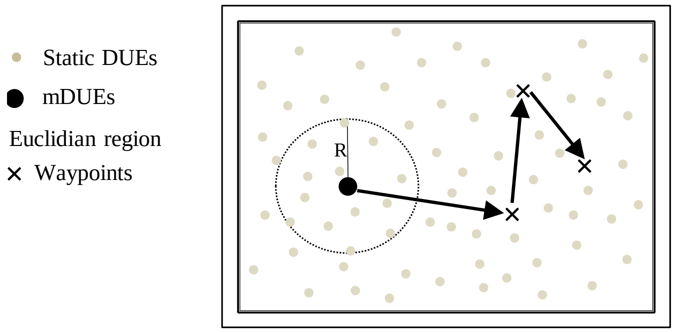

Figure 4.9: Mobility Scenario for mDUE and H-PPP distribution of static DUEs

4.3 Neighborhood Discovery by Mobile-Cell

Most of the existing works that have discussed mode-2 type discovery [71, 92, 94–97] (also references therein) have only focused on the static DUEs. In case DUEs are moving, such as mobile-cells, it is essential to consider mobility while investigating discovery process. Authors in [100] have discussed resource assignment for sidehaul links between mobile DUEs. The authors in [99] have noted that the mDUEs inside moving vehicles can share popular contents using sidehaul links. However, the researchers in [99, 100] have assumed that mDUEs are aware of their neighboring devices. It is important to note that factors such as time-to-discover-neighbor, etc., are crucial for mDUEs and need an in-depth analysis to fully realize a completely autonomous and mobile sidehaul communication. In [66], the authors have presented a survey of non-cellular neighborhood discovery schemes for mobile-devices, particularly for IoT-based applications. On the contrary, in [83] the LTE-A base station broadcasts neighborhood information to mobile vehicles. However, the scheme proposed in [83] fails when the network availability is poor. To the best of our knowledge, the analysis provided in the following sections for mode-2 type autonomous discovery for a mDUE has never been presented in the literature. We start this discussion by first explaining the system model.

4.3.1 System Model for Mobility

The main system model remains the same as described in Section 4.2.1. In order to incorporate mobility we have considered an mDUE which seeks to discover the neighboring DUEs while on the move [99]. For sake of simplicity only single mDUE is mobile in our analysis. The to-be-discovered DUEs remain static at all times and are distributed as homogeneous Poisson point process with density λ $(1/m^2)$ on 2D plane (see Fig. 4.9). This scenario can be best described when a mobile-cell tries to discover out-of-vehicle devices while on the move to provide sidehaul connectivity, for example, in regions with poor network coverage [32, 136]. This model enables analytical tractability which can further be extended to scenarios when multiple DUEs are mobile. We use the combinatorial technique to develop an analytical model for 3GPP-based mode-2 type discovery for mDUE. The probability that mDUE discovers any neighbor is similar to Eq. (4.1). However, since static devices are distributed as a homogeneous point process, the probability of discovering any randomly selected neighbor is the same. Therefore, we omit the subscript $(j \to i)$ from $p_{j \to i}$ in Eq. (4.1) and denote this probability simply as p:

$$p = \Psi \left(1 - \frac{\Psi}{\mathcal{M}}\right) \left(1 - \frac{\Psi}{M\mathcal{F}}\right)^{\mathcal{D}-2} \tag{4.12}$$

where $\mathcal{M}, \mathcal{F},$ and $\mathcal{D}, \Psi$ have been described in Section 4.2.1.

To model the motion of mDUE, we have used random way-point (RWP) mobility in 2D euclidean plane [137]. However, the analysis presented below can be easily extended to other mobility models as well. In context of wireless networks, RWP is frequently used stochastic model to study the mobility behaviors of mobile devices. In RWP, the destination points for a mobile device are called way-points. A device randomly chooses it's destination point and moves in a straight line towards that point with a constant velocity as depicted in Figure 4.9. After choosing a certain pause time, the device selects another way-point and resumes its motion in the way-point's direction with the chosen velocity [138].

In our analysis, the way-points are identically and independently distributed (i.i.d.) [139]. At first, mDUE starts from $\mathcal{X}(\bar{t})$ at time $\bar{t}$ and moves in a straight line to a randomly selected location $\mathcal{X}(\bar{t}+1)$ at time $\bar{t}+1$ with velocity $v(t)$ following velocity distribution $f_V(v)$. The transition time between two way-points is denoted as T_t. Without the loss of generality, we can select any two adjacent way-points $\mathcal{X}(\bar{t})$ and $\mathcal{X}(\bar{t}+1)$ to analyze the discovery process.

4.3.2 Transition Lengths and Durations

We consider the movement of mDUE in a square shaped 2D space with $L \times L$ area, where L is the maximum length of the region along both x- and y- axes. Hence, the expected transition length between $\mathcal{X}(t)$ and $\mathcal{X}(t+1)$ is $\mathbb{E}[l] = 0.5214\ L$ [139]. In the similar manner, the expected lengths for other shapes (such as rectangular and circular regions) are already derived in the existing literature [140–142]. Assuming that the mDUE moves with a fixed velocity (v_{const}), the transition time (T_t) is measured as $\mathbb{E}[T_t] = \dfrac{\mathbb{E}[L]}{v_{const}}$. Considering that an mDUE chooses its speed from a distribution $f_V(v)$, then $\mathbb{E}[T_t]$ is:

$$\mathbb{E}[T_t] = \mathbb{E}[L] \int_{v_{low}}^{v_{high}} \frac{1}{v} f_V(v) dv, \tag{4.13}$$

If $f_V(v)$ follows uniform distribution between $[v_{low}, v_{high}]$, then the expected transition time is [139]:

$$\mathbb{E}[T_t] = \frac{\ln(v_{high}/v_{low})}{v_{high} - v_{low}} \mathbb{E}[L]. \tag{4.14}$$

Here, we define η as the rate of PSDCH-period (i.e., number of PSDCH-periods per second). Then, an mDUE will experience $\mathbb{E}[\mathcal{T}_d] = \lceil \eta \mathbb{E}[T_t] \rceil$ PSDCH-periods from $\mathcal{X}(\bar{t})$ to $\mathcal{X}(\bar{t}+1)$, where $\lceil . \rceil$ is the ceiling function.

4.4 Performance Evaluation

If an mDUE travels with a velocity v towards a way-point, the distance traveled during the time duration $\Delta\mathcal{T}_d$ between any two PSDCH-periods is $w_{\Delta\mathcal{T}_d} = v \times \Delta\mathcal{T}_d$. Hence there exist $\mathcal{D}_{t_d+1}$ new stationary DUEs in the mDUE's discovery range $\mathcal{R}$. As the DUEs follow H-PPP, $\mathcal{D}_{t_d+1} = \lambda(\pi\mathcal{R}^2 - A(w_{\Delta\mathcal{T}_d}, \mathcal{R}))$, where $A(w_{\Delta\mathcal{T}_d}, \mathcal{R})$ is the overlapping area ODEF (See Fig. 4.10), $A(w_{\Delta\mathcal{T}_d}, \mathcal{R})$ can be found as:

$$A(w_{\Delta\mathcal{T}_d}, \mathcal{R}) = \pi\mathcal{R}^2 - (2A_{\text{sector } DEF} - 2A_{\triangle DEF}), \tag{4.15}$$

The Eq. (4.15) is true because $A_{\text{sector } DEF} = A_{\text{sector} DOF}$ (See Fig. 4.10). Therefore, the corresponding triangles are also equal i.e., $A_{\triangle DEF} = A_{\triangle DOF}$. The

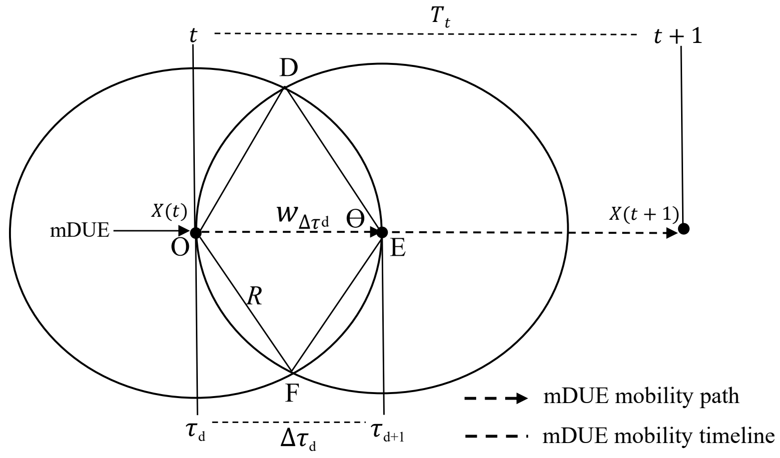

Figure 4.10: Depiction of mDUE mobility between two way-points. © 2019 IEEE [37]..

sector and triangles formed in Figure 4.10 has the area of $A_{\text{sector}DEF} = \frac{1}{2}\mathcal{R}^2\Theta$ and $A_{\triangle DEF} = \frac{1}{2}\mathcal{R}^2 \sin\Theta$, respectively, where Θ is the angle in radians. The region ODEF in Figure 4.10 has the area of:

$$A(w_{\Delta\mathcal{T}_d}, \mathcal{R}) = \mathcal{R}^2(\pi - \Theta + \sin\Theta), \tag{4.16}$$

where $\Theta = \cos^{-1}\left(1 - \frac{c^2}{2\mathcal{R}^2}\right)$ and $c = 2\mathcal{R}^2 - \frac{w^2_{\Delta\mathcal{T}_d}}{2}$. The expression for $A(w_{\Delta\mathcal{T}_d}, \mathcal{R})$ becomes:

$$A(w_{\Delta\mathcal{T}_d}, \mathcal{R}) = \mathcal{R}^2[\pi - \cos^{-1}\left(1 - \frac{c^2}{2\mathcal{R}^2}\right) + \sin\left(\cos^{-1}\left(1 - \frac{c^2}{2\mathcal{R}^2}\right)\right)], \tag{4.17}$$

We use forward-inverse trigonometric function $\sin(\cos^{-1}(\phi)) = \sqrt{1-\phi^2}$ [131] to simplify $A(w_{\Delta\mathcal{T}_d}, \mathcal{R})$ as:

$$A(w_{\Delta\mathcal{T}_d}, \mathcal{R}) = \mathcal{R}^2\left[\pi - \cos^{-1}\left\{1 - \frac{c^2}{2\mathcal{R}^2}\right\} + \sqrt{\frac{4\mathcal{R}^2 - w^2_{\Delta\mathcal{T}_d}}{2\mathcal{R}^2}}\right]. \tag{4.18}$$

$$A(w_{\Delta\mathcal{T}_d}, \mathcal{R}) = \mathcal{R}^2\left[\pi - \cos^{-1}(1 - \frac{2}{\mathcal{R}^2}(\mathcal{R}^2 - w^2_{\Delta\mathcal{T}_d})^2) + \sqrt{\frac{4\mathcal{R}^2 - w^2_{\Delta\mathcal{T}_d}}{2\mathcal{R}^2}}\right]. \tag{4.19}$$

We will use $A(w_{\Delta\mathcal{T}_d}, \mathcal{R})$ to find the expected number of neighbors that a mDUE discovers during its transition between two way-points. The number of neighbors discovered are presented as Theorem 4.1 below.

Theorem 4.1

The expected number of static neighbors discovered by an mDUE traveling in a straight line for $\mathcal{T}_d$ discovery periods is given as:

$$\mathbb{D}(\mathcal{T}_d) = \mathcal{T}_d \mathcal{D} p + \sum_{n=2}^{\mathcal{T}_d} (-1)^{n+1} p^n \left[\sum_{\Delta x = n-1}^{\mathcal{T}_d - 1} \Gamma_{\Delta x} X_{\Delta x} \right]. \tag{4.20}$$

where $\Delta x \in \mathbb{N}$ and $X_{\Delta x} = \mathcal{D}_{\mathcal{T}_o + \Delta x}$ and $\mathbb{N}$ shows the set of natural numbers. $\mathcal{T}_o$ is the initial PSDCH-period. $\Gamma_{\Delta x}$ is the coefficient given as:

$$\Gamma_{\Delta x} = (\mathcal{T}_d - \Delta x) \binom{\Delta x - 1}{n - 2}. \tag{4.21}$$

Proof

For any mobile device initiating discovery for the first time, the expected number of DUEs discovered during a single PSDCH-period are:

$$\mathbb{D}(\mathcal{T}_d = 1) = \mathcal{D}_1 p_1. \tag{4.22}$$

where $\mathcal{D}_1$ denotes the neighboring DUEs in the mDUE's discovery range at $\mathcal{T}_d = 1$.

The expected number of discovered DUEs when $\mathcal{T}_d = 2$ are:

$$\mathbb{D}(\mathcal{T}_d = 2) = \mathcal{D}_1 p_1 + \mathcal{D}_2 p_2 - \mathcal{D}_{1,2} p_1 p_2, \tag{4.23}$$

where $\mathcal{D}_{1,2}$ represents the neighboring DUEs that exist in the common geometrical area for sector ODEF when mDUE is located at $\mathcal{X}(\mathcal{T}_d = 1)$ and $\mathcal{X}(\mathcal{T}_d = 2)$, respectively (See Figure 4.10).

As the DUEs are distributed following H-PPP, without the loss of generality, we can write $p = p_1 = p_2$. As the discovery range for an mDUE is fixed, we can say that $\mathcal{D} = \mathcal{D}_1 \approx \mathcal{D}_2$. Therefore, we can write the expression for $\mathbb{D}(\mathcal{T}_d = 2)$ as:

$$\mathbb{D}(\mathcal{T}_d = 2) = 2\mathcal{D}p - \mathcal{D}_{1,2}p^2. \tag{4.24}$$

For the third PSDCH-period, the expected number of devices are:

$$\mathbb{D}(\mathcal{T}_d = 3) = 3\mathcal{D}p - [\mathcal{D}_{1,2} + \mathcal{D}_{1,3} + \mathcal{D}_{2,3}]p^2 + p^3\mathcal{D}_{1,2,3}, \tag{4.25}$$

where $\mathcal{D}_{1,2,3}$ denotes the DUEs that are common within the discovery range of an mDUE during $\mathcal{T}_d = 1, 2, 3$, respectively. Due to the property of H-PPP, $\mathcal{D}_{1,2} \equiv \mathcal{D}_{2,3} = \mathcal{D}_{\mathcal{T}_o,\mathcal{T}_{o+1}} = \lambda A(w_{\Delta\mathcal{T}_d}, \mathcal{R})$, where $\mathcal{T}_o$ is the initial PSDCH-period.

Note that during $\mathcal{T}_d = 1 \rightarrow 3$, the DUEs distributed in the mutual geometrical region within the mDUE's range $\mathcal{R}$ are essentially only those DUEs that exist in the overlapping area for $\mathcal{T}_d = \{1, 3\}$. The proof for this statement is trivial which is explained in the following.

Note that only those DUEs are considered in the common geometrical area that exist for all discovery periods $\mathcal{T}_d = \{1, 2, 3\}$. It follows that we are looking at only those DUEs that must appear within mDUE's range $\mathcal{R}$ during $\mathcal{T}_d = 1$ and $\mathcal{T}_d = 3$. Hence, we are not concerned about the DUEs appearing in common between intermediary periods. So we can write $\mathcal{D}_{1,2,3} \equiv \mathcal{D}_{1,3} = \mathcal{D}_{\mathcal{T}_o,\mathcal{T}_{o+2}} = \lambda A(2 \times w_{\Delta\mathcal{T}_d}, \mathcal{R})$. The expressions in Eq. (4.25) for $\mathbb{D}(\mathcal{T}_d = 3)$ can be written as:

$$\mathbb{D}(\mathcal{T}_d = 3) = 3\mathcal{D}p - p^2[2\mathcal{D}_{\mathcal{T}_o,\mathcal{T}_{o+1}} + \mathcal{D}_{\mathcal{T}_o,\mathcal{T}_{o+2}}] + p^3\mathcal{D}_{\mathcal{T}_o,\mathcal{T}_{o+2}}. \tag{4.26}$$

The expression for the expected number of discovered neighbors by an mDUE after $\mathcal{T}_d = \{1, 2, ..., 7, 8\}$ when mDUE is traveling in a straight line is expressed as Eq. (4.27).

$$
\mathbb{D}(\mathcal{T}_d) = \begin{cases}
\mathcal{D}p & \mathcal{T}_d{=}1. \\
2\mathcal{D}p - p^2\mathcal{D}_{\mathcal{T}_o+1} & \mathcal{T}_d{=}2. \\
3\mathcal{D}p - p^2[2\mathcal{D}_{\mathcal{T}_o+1} + \mathcal{D}_{\mathcal{T}_o+2}] + p^3\mathcal{D}_{\mathcal{T}_o+2} & \mathcal{T}_d{=}3 \\
4\mathcal{D} - p^2[3\mathcal{D}_{\mathcal{T}_o+1} + 2\mathcal{D}_{\mathcal{T}_o+2} + \mathcal{D}_{\mathcal{T}_o+3}] + p^3[2\mathcal{D}_{\mathcal{T}_o,\mathcal{T}_o+2} + 2\mathcal{D}_{\mathcal{T}_o+3}]- & \\
p^4\mathcal{D}_{\mathcal{T}_o+3} & \mathcal{T}_d{=}4 \\
5\mathcal{D}p - p^2[4\mathcal{D}_{\mathcal{T}_o+1} + 3\mathcal{D}_{\mathcal{T}_o+2} + 2\mathcal{D}_{\mathcal{T}_o+3} + \mathcal{D}_{\mathcal{T}_o+4}]+ & \\
p^3[3\mathcal{D}_{\mathcal{T}_o+2} + 4\mathcal{D}_{\mathcal{T}_o+3} + 3\mathcal{D}_{\mathcal{T}_o+4}] - p^4[2\mathcal{D}_{\mathcal{T}_o+3} + 2\mathcal{D}_{\mathcal{T}_o+4}] + p^5\mathcal{D}_{\mathcal{T}_o+4} & \mathcal{T}_d{=}5 \\
6\mathcal{D}p - p^2[5\mathcal{D}_{\mathcal{T}_o+1} + 4\mathcal{D}_{\mathcal{T}_o+2} + 3\mathcal{D}_{\mathcal{T}_o+3} + 2\mathcal{D}_{\mathcal{T}_o+4} + \mathcal{D}_{\mathcal{T}_o+5}]+ & \\
p^3[4\mathcal{D}_{\mathcal{T}_o+2} + 6\mathcal{D}_{\mathcal{T}_o+3} + 6\mathcal{D}_{\mathcal{T}_o+4} + 4\mathcal{D}_{\mathcal{T}_o+5}]- & \\
p^4[3\mathcal{D}_{\mathcal{T}_o+3} + 6\mathcal{D}_{\mathcal{T}_o+4} + 6\mathcal{D}_{\mathcal{T}_o+5}]+ & \\
p^5[2\mathcal{D}_{\mathcal{T}_o+4} + 4\mathcal{D}_{\mathcal{T}_o+5}] - p^6\mathcal{D}_{\mathcal{T}_o+5} & \mathcal{T}_d{=}6 \\
7\mathcal{D}p - p^2[6\mathcal{D}_{\mathcal{T}_o+1} + 5\mathcal{D}_{\mathcal{T}_o+2} + 4\mathcal{D}_{\mathcal{T}_o+3} + 3\mathcal{D}_{\mathcal{T}_o+4} + 2\mathcal{D}_{\mathcal{T}_o+5} + \mathcal{D}_{\mathcal{T}_o+6}]+ & \\
p^3[5\mathcal{D}_{\mathcal{T}_o+2} + 8\mathcal{D}_{\mathcal{T}_o+3} + 9\mathcal{D}_{\mathcal{T}_o+4} + 8\mathcal{D}_{\mathcal{T}_o+5} + 5\mathcal{D}_{\mathcal{T}_o+6}]- & \\
p^4[4\mathcal{D}_{\mathcal{T}_o+3} + 9\mathcal{D}_{\mathcal{T}_o+4} + 12\mathcal{D}_{\mathcal{T}_o+5} + 10\mathcal{D}_{\mathcal{T}_o+6}]+ & \\
p^5[3\mathcal{D}_{\mathcal{T}_o+4} + 8\mathcal{D}_{\mathcal{T}_o+5} + 10\mathcal{D}_{\mathcal{T}_o+6}]- & \\
p^6[2\mathcal{D}_{\mathcal{T}_o+5} + 5\mathcal{D}_{\mathcal{T}_o+6}] + p^7\mathcal{D}_{\mathcal{T}_o+6} & \mathcal{T}_d{=}7 \\
8\mathcal{D}p - p^2[7\mathcal{D}_{\mathcal{T}_o+1} + 6\mathcal{D}_{\mathcal{T}_o+2} + 5\mathcal{D}_{\mathcal{T}_o+3} + 4\mathcal{D}_{\mathcal{T}_o+4} + 3\mathcal{D}_{\mathcal{T}_o+5} + 2\mathcal{D}_{\mathcal{T}_o+6}+ & \\
\mathcal{D}_{\mathcal{T}_o+7}] + p^3[6\mathcal{D}_{\mathcal{T}_o+2} + 10\mathcal{D}_{\mathcal{T}_o+3} + 12\mathcal{D}_{\mathcal{T}_o+4} + 12\mathcal{D}_{\mathcal{T}_o+5+10\mathcal{D}_{\mathcal{T}_o+6}}]- & \\
p^4[5\mathcal{D}_{\mathcal{T}_o+3} + 12\mathcal{D}_{\mathcal{T}_o+4} + 18\mathcal{D}_{\mathcal{T}_o+5} + 20\mathcal{D}_{\mathcal{T}_o+6} + 15\mathcal{D}_{\mathcal{T}_o+7}]+ & \\
p^5[4\mathcal{D}_{\mathcal{T}_o+4} + 12\mathcal{D}_{\mathcal{T}_o+5} + 20\mathcal{D}_{\mathcal{T}_o+6} + 20\mathcal{D}_{\mathcal{T}_o+7}]- & \\
p^6[3\mathcal{D}_{\mathcal{T}_o+5} + 10\mathcal{D}_{\mathcal{T}_o+6} + 15\mathcal{D}_{\mathcal{T}_o+7}]+ & \\
p^7[2\mathcal{D}_{\mathcal{T}_o+6} + 6\mathcal{D}_{\mathcal{T}_o+7}] - p^8 & \mathcal{T}_d{=}8 \\
\ldots
\end{cases} . \tag{4.27}
$$

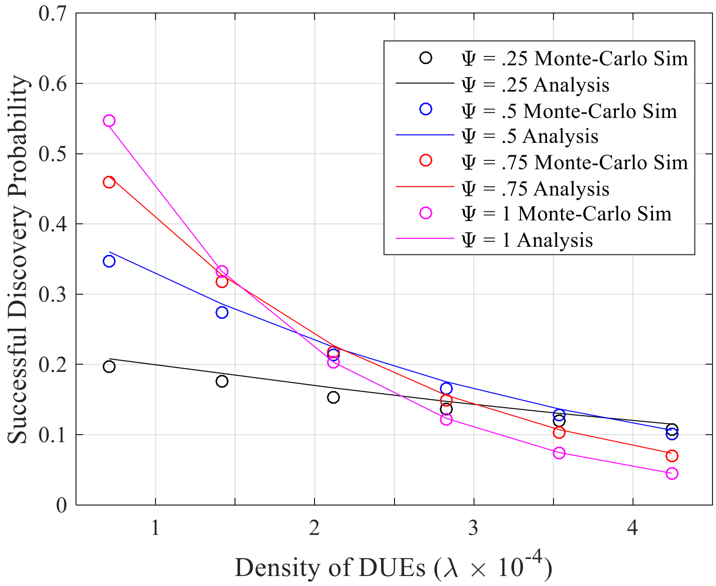

Figure 4.11: Discovery probability at first point of contact mDUE and static DUE. © 2019 IEEE [37]..

Let $X_i \equiv \mathcal{D}_{\mathcal{T}_o+i}$, where $\mathcal{D}_{\mathcal{T}_o+i}$ denotes the devices discovered between initial period $\mathcal{T}_o$ and any period i. Therefore the expected number of discovered neighbors after $\mathcal{T}_d$ PSDCH-period(s) are:

$$\mathbb{D}(\mathcal{T}_d) = \mathcal{T}_d\mathcal{D}p - p^2[X_1 + ...X_{\binom{\mathcal{T}_d}{2}}] + p^3[X_1 + ...X_{\binom{\mathcal{T}_d}{3}}] \\ - p^4[X_1 + ...X_{\binom{\mathcal{T}_d}{4}}] + ...(-1)^{\mathcal{T}_d+1}p^{\mathcal{T}_d}[X_{\mathcal{T}_d}], \quad (4.28)$$

$$\mathbb{D}(\mathcal{T}_d) = \mathcal{T}_d\mathcal{D}p + \sum_{n=2}^{\mathcal{T}_d}(-1)^{n+1}p^n[X_1 + ...X_{\binom{\mathcal{T}_d}{n}}]. \quad (4.29)$$

If $\bar{X} = \{X_1, X_2, ...X_{\binom{\mathcal{T}_d}{n}}\}$, then $|\bar{X}| = \binom{\mathcal{T}_d}{n}$ and $|.|$ shows the cardinality of set. Any combination $X_i \in \bar{X}$ is an n-element subset of $\mathcal{S} = \{1, 2, 3, ...\mathcal{T}_d\}$ such that $X_i = \{x_1, x_2..., x_n\}$ where $x_1 < x_2... < x_n \in \mathcal{S}$. Δx is the width of set X_i,and is given as, $\Delta x = \max(X_i) - \min(X_i)\ \forall\ X_i$. For $X_i \in \bar{X}$, iff $\Delta x = \max(X_i) - \min(X_i)$, $X_i \implies X_{\Delta x}$, where $\Delta x \in \mathbb{N}$ (see Eq. (4.27)). We simplify the expression for the expected number of discovered DUEs to arrive at Eq. (4.20).

This completes the proof ■

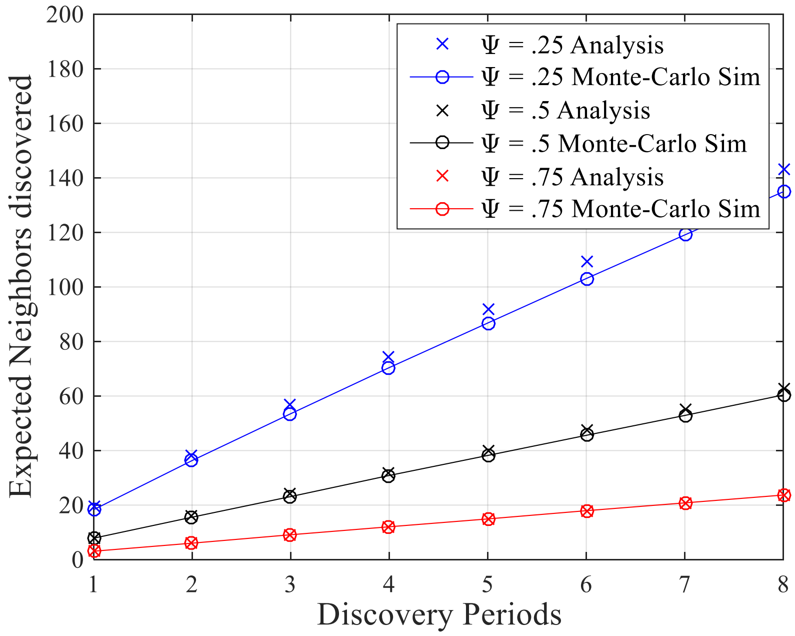

Figure 4.12: Expected discovery of devices by mDUE with different values of Ψ ($\mathcal{R} = 150$). © 2019 IEEE [37]..

4.4.1 Results and Discussion

To validate the accuracy of our analysis, we have performed Monte-Carlo simulations. The DUEs are distributed randomly and uniformly following H-PPP with density λ. A single mDUE moves in a linear direction between any two way-points following RWP mobility. The speed between two way-points is constant in RWP [139]. So we normalized speed to $v = 1$. We further consider $\mathcal{M} = 10$, $\mathcal{F} = 10$. The discovery range for all devices is $\mathcal{R} = 150$ m, unless otherwise stated. During simulation, we averaged the results of 500 iterations for each case.

Figure 4.11 shows the probability when a particular DUE is discovered by mDUE during first PSDCH-period. This result can also be interpreted as the probability of discovery at the first point of contact between the mDUE and the static DUE. The role of Ψ can be seen in Figure 4.11. It is obvious that for low density of neighboring devices (e.g. $\lambda = 1 \times 10^{-4}$), $\Psi = 1.0$ enables highest successful discovery probability and $\Psi = 0.25$ yields the lowest discovery probability. For highly dense environment, the lower values of Ψ are more suitable as compared to the higher values of Ψ. The slight difference between analytical and simulation results is likely due to the inherent addition and subtraction of

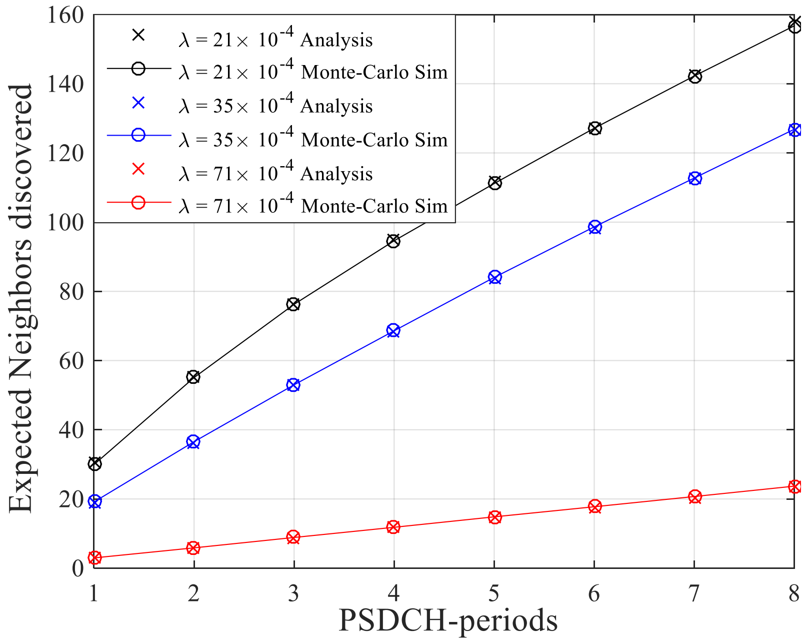

Figure 4.13: Expected discovery of devices by mDUE with different DUE density ($\Psi = 1, \mathcal{R} = 150$). © 2019 IEEE [37]..

overlapping DUEs in the analysis using the Exclusion-Inclusion principle (See Eq. (4.20)). However, this difference remains well below 6% in all cases.

Figure 4.12 shows the expected number of neighbors discovered when mDUE is on the move. It can be observed that the number of devices discovered when $\Psi = 0.5$ are considerably larger than that when $\Psi = 0.75$. In Figure 4.13, we have fixed Ψ to the maximum limit of 1.0 and observe the effect of DUE density as the mDUE moves in a straight line. It is quite evident that as the density of DUEs increases, the expected number of discovered devices decreases drastically. This is due to the increased number of collisions as all the participating devices can potentially transmit their beacon messages simultaneously.

Figure 4.14 shows the relationship between the discovery rate (i.e., neighbor discovery per PSDCH-period) with λ and Ψ. Note that incorrect value of Ψ may lead to poor discovery performance. For example, in scenarios where DUEs are densely deployed, lower values of Ψ enable high discovery-rates. We can observe that for $\lambda = 35 \times 10^{-4}$ and $\lambda = 71 \times 10^{-4}$, the value of Ψ can have significant impact on the discovery rate. On the other hand, when $\lambda = 21 \times 10^{-4}$, the difference in the discovery rate is very small in case when $\Psi = 0.5$ versus the cases when $\Psi = 1.0$.

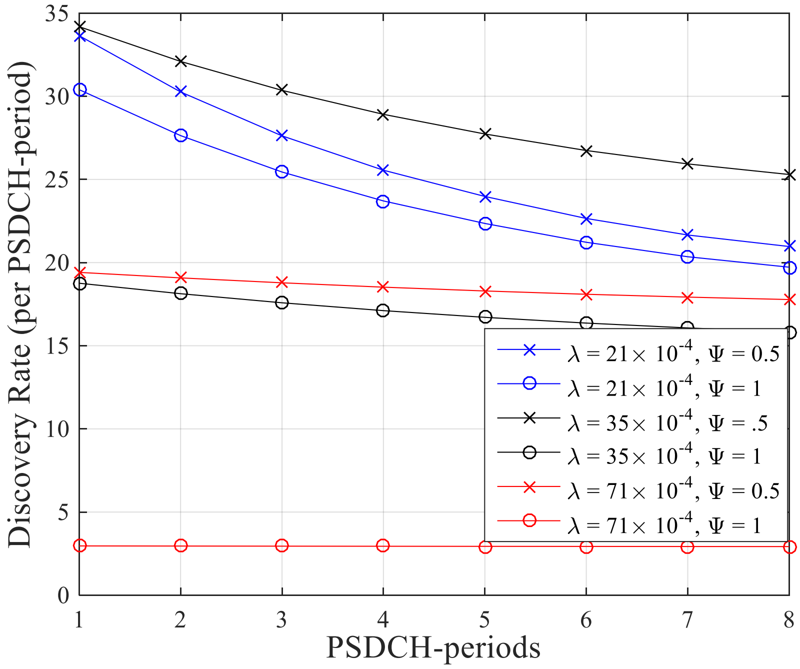

Figure 4.14: Effect of Ψ, λ on discovery-rates (DUEs discovered / PSDCH-period). © 2019 IEEE [37]..

4.5 Conclusion

In this chapter, we have proposed an adaptive scheme for autonomous neighborhood discovery with proximity awareness. First, in Section 4.2, we have demonstrated that the probability of successful discovery can be increased by calculating the optimal transmission probability parameter Ψ. We have found that in order to transmit beacon messages with optimal Ψ, each device needs to know parameters such as $\mathcal{M}, \mathcal{F},$ and, $\mathcal{D}$. While $\mathcal{M}$ and $\mathcal{F}$ are known to a device as they are constants, it is impossible for the DUEs to know $\mathcal{D}$ in the absence of network-coverage. Therefore in Section 4.2.3, we have proposed a scheme to acquire neighborhood-awareness so that each DUE can successfully choose optimal Ψ. We have also shown that the proposed adaptive scheme also enables high successful discovery probability even when the discovering device is mobile, such as a mobile-cell. An analytical model has been developed in Section 4.3 based on device's mobility between two way-points following the random way-point model. Our analysis can also be used for other types of mobility models. The results have demonstrated that the neighborhood awareness significantly improves the performance of mode-2 type autonomous neighborhood discovery.

As part of the future extension to this research, an interesting direction can be the development of discovery model when multiple devices are moving. In such a scenario, the biggest challenge will be the intermittent connectivity between the mobile devices. In the next chapter, we will present our first contribution to the second research objective of this thesis which is interference management and resource allocation for mobile-cells with key emphasis on spectral efficiency.

4.6 Related Publications

- **Shan Jaffry**, Syed Faraz Hasan, Xiang Gui, "Neighborhood-aware Out-of-Network D2D Discovery", IET Electronic Letters, February, 2018.
- **Shan Jaffry**, Syeda Kanwal Zaidi, Syed Tariq Shah, Syed Faraz Hasan, Xiang Gui, "D2D Neighborhood Discovery by a Mobile-Device", IEEE International Conference on Communications (IEEE ICC), May 2019, Shanghai, China.

Chapter 5

Downlink Backhaul and Access Link Resource Sharing

5.1 Introduction

Mobile-cells will increase the quality of service (QoS) for commuters inside public transport (such as buses and trains, etc.) by bringing the communication antenna closer to them [143]. However, the enhancement in QoS will be achieved at the expense of additional wireless links. The commuters inside mobile-cell will be linked to the in-vehicle antenna over the access link (AL). The AL-antenna will be mounted under the roof of the vehicle as shown in Figure 5.1. The out-of-vehicle antennas (usually attached to the top of vehicle) will be responsible for mobile-cell's communication with the core network over backhaul link (BL), and with neighboring mobile-cells over sidehaul links (SLs). The wireless links associated with the mobile-cell may cause severe interference to the cellular users outside the vehicle [45]. The works that have addressed interference management for mobile-cells have focused on assigning dedicated resources to the individual links [19, 43, 45, 56, 124–126, 144]. However, as frequency spectrum is an expensive and increasingly scarce commodity, assigning a sub-channel exclusively to individual links is not a spectrally efficient solution. Therefore in this chapter we have proposed spectrally efficient resource sharing scheme for mobile-cells. Our research contribution is presented in the following.

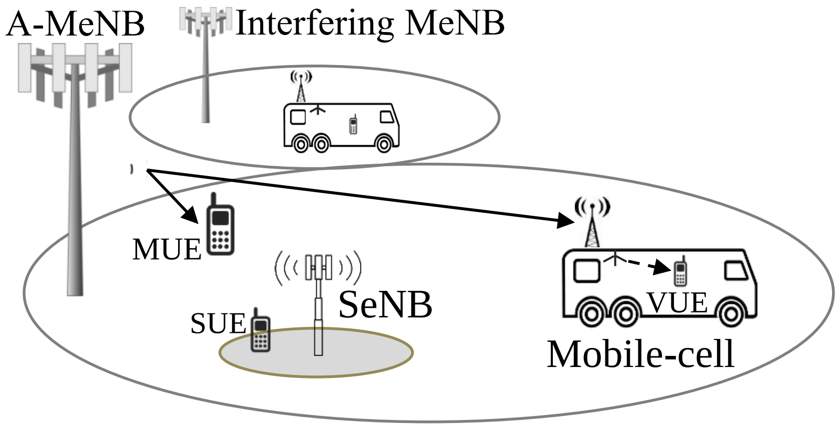

Figure 5.1: Mobile-cells with active backhaul and access link communication. © 2019 IET [39].

5.1.1 Research Contribution

The main contribution of this chapter is the development of a resource sharing scheme to ensure that additional resources are not required when mobile-cells are integrated into future cellular network. In the proposed scheme, the AL shares the sub-channel with mobile-cell's BL. However, when there is no transmission on the BL from the base station, AL shares the sub-channel with the out-of-vehicle macrocell user. When BL and AL share the sub-channels, the transceivers placed in each others' close proximity will experience high interference. We have used successive interference cancellation (SIC) [145] to enhance the signal-to-interference ratio (SIR) for the weaker BL signals, thus enabling effective resource sharing. We have derived expressions for success probabilities and ergodic rates for all resource sharing links. We have presented two algorithms which ensure that the proposed sub-channel sharing enable high success probability and ergodic rate for each link. We have also proposed a power control scheme for AL-antenna so that AL's interference to the BL can be minimized. The AL power control does not deteriorate the QoS of in-vehicle users.

5.1.2 Chapter Organization

The rest of this chapter is organized as follows. Section 5.2 presents the system model that will be used in this chapter. The analysis for resource sharing between backhaul and access links is presented in Section 5.3. The resource sharing with out-of-vehicle macro-cell users is presented in Section 5.4. The ergodic rates and sub-channel reuse parameter are discussed in Section 5.5. Results are presented in Section 5.6 followed by conclusion in Section 5.7. The publications related to this Chapter are mentioned in Section 5.8.

5.2 System Model

5.2.1 Network and Transmission Model

We have considered a heterogeneous network with macro-cell eNB (MeNB) and fixed small-cell eNB (SeNB) distributed as homogeneous Poisson point processes (H-PPP) $\Phi_{\mathcal{M}}$ and $\Phi_{\mathcal{S}}$, with density $\lambda_{\mathcal{M}}$ and $\lambda_{\mathcal{S}}$, respectively. The mobile-cells also form a H-PPP $\Phi_{\mathtt{m}}$ with density $\lambda_{\mathtt{m}}$. Mobile-cells are assumed to be static for very short time instances (for example, in scale of milli-seconds) [125, 146]. The macro-cell user equipment (MUE) are also dispersed as H-PPP Φ_m with density λ_m, where m is an individual MUE. We assume that each node (e.g., MUE or mobile-cell) can determine its position very accurately [147] . The nodes transmit their location information to MeNB periodically over the control channels.

The distance (d) between MeNB and its associated receiver (i.e., mobile-cell or out-of-vehicle user) is described in terms of probability density function (PDF) as [106]:

$$f_{\mathcal{D}}(d) = 2\pi\lambda_{\mathcal{M}} d e^{-\lambda_{\mathcal{M}}\pi d^2} \tag{5.1}$$

Without the loss of generality, we have considered a single small-cell user equipment (SUE, s) under the coverage of a SeNB. The serving radius of SeNB is $R_{\mathcal{S}}$ within which SUE is randomly deployed. Hence, the PDF of the distance (r_s) of SeNB to its SUE is:

$$f_{\mathcal{R}}(r_s) = \mathbb{P}[\mathcal{R} = r_s | \mathcal{R} \leq R_{\mathcal{S}}] = \frac{2\pi\lambda_{\mathcal{S}} r_s e^{-\pi\lambda_{\mathcal{S}} r_s^2}}{1 - e^{-\pi R_{\mathcal{S}}^2 \lambda_{\mathcal{S}}}} \tag{5.2}$$

Again, without loss of generality, a single active in-vehicle user equipment (VUE, v) is considered within each mobile-cell. As we are focusing on sharing a single sub-channel across multiple wireless links, we have considered one active SUE and VUE within the fixed small-cells and mobile-cells, respectively. However, this scheme can be generalized to any number of sub-channels or users.

We focus on the downlink communication of all links. These include four

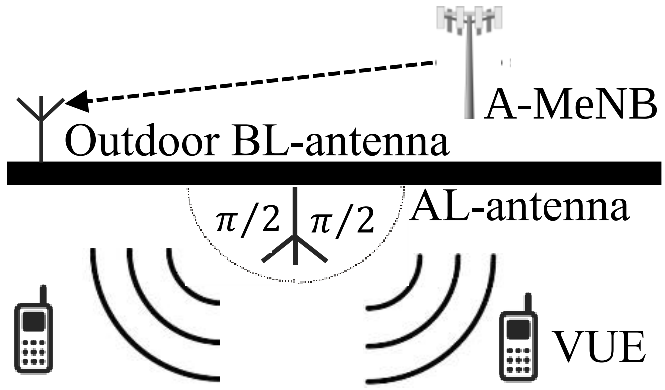

Figure 5.2: AL-antenna mounted under roof inside mobile-cell. © 2019 IET [39].

links: A-MeNB to MUE, SeNB to SUE, A-MeNB to mobile-cell's backhaul, and mobile-cell AL-antenna to VUE. Mobile-cells only communicate with macro-cell layer and do not interact with SeNB because "mobile-cell to SeNB" backhaul link will incur a large number of handovers due to smaller coverage of SeNBs [148].

Each mobile-cell is equipped with the out-of-vehicle isotropic BL-antenna with unit antenna gain. The AL-antenna is mounted under the vehicle's roof. The AL-antenna ($\tilde{a}$) is highly directional and enable strong line-of-sight (LoS) link to the in-vehicle users [149]. The orientation of AL-antenna, as shown in Figure 5.2, also reduces the effect of AL transmission on the BL. The AL-antenna and BL-antenna are connected through wired links which are managed by common communication control unit (CCU) [145]. The CCU also manages the transmissions (and receptions) for mobile-cell's backhaul and access links [145]. We employ SIC at the BL-antenna to enhance SIR for BL by subtracting the interfering AL signal.

The channel gain is taken as the product of the small-scale and large-scale fading, along with antenna gains for all links. Standard pathloss model is followed for large scale attenuation, i.e., $d^{-\alpha}$, where α is the general pathloss exponent. In particular, we have used α_i and α_o as the non-LoS and LoS exponents, respectively, where $\alpha_i > \alpha_o$. As for small-scale fading, all the links to the mobile-cell's BL-antenna and out-of-vehicle users, including all interfering links, follow quasi-static Rayleigh fading with exponentially distributed fading power $h^{\omega}_{t_x,t_r} \sim \exp(1)$ between transmitter (t_x) and receiver (t_r). Due to the presence of strong LoS component, AL follows Rician fading with K-factor determining the strength of the

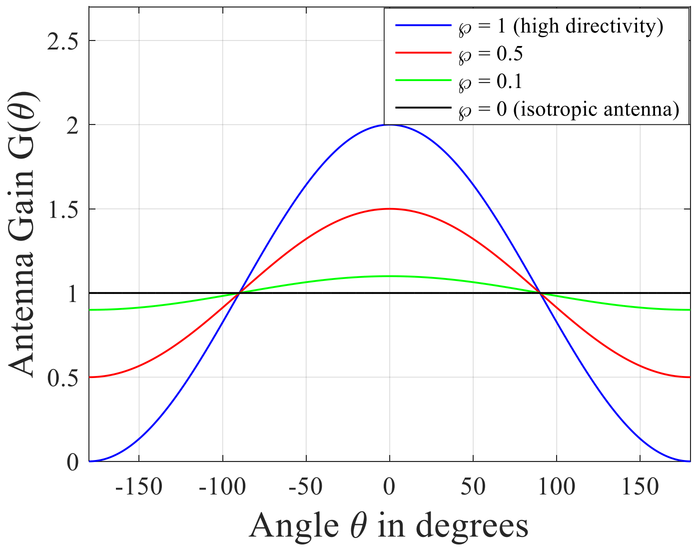

Figure 5.3: Antenna gains in terms of directivity and angle θ ($\jmath = 1$) depicting Eq. (5.4) [143].

LoS signal [150]. The antenna gains are represented as $G_{t_x}(\theta)$ for transmitter t_x, and $\bar{G}_{t_r}(\theta)$ for receiver t_r in direction θ. If P_{t_x} is the transmit power for transmitter t_x, the received power P_{t_r} at receiver t_r is:

$$P_{t_r} = P_{t_x} d^{-\alpha} G_{t_x}(\theta) \bar{G}_{t_r}(\theta) h^{\omega}_{t_x,t_r}. \tag{5.3}$$

For mathematical tractability, we ignore the side and back lobes for AL-antenna [151, 152]. The gain function is then given as [151]:

$$G(\theta) = 1 + \wp \cos(\jmath\theta), \quad 0 \leq \wp \leq 1, \quad \jmath \in \mathbb{N}. \tag{5.4}$$

The gain function determines the power transmitted (or received) in the direction θ compared to the power transmitted (or received) by an isotropic antenna. $\wp \in [0, 1]$ determines the directivity such that $\wp = 0$ for an isotropic antenna. For $\wp > 0$, AL-antenna has $\jmath$ radiation directions, where $\jmath = \{1, 2, ...\}$ determines the number of main lobes. We have considered $\jmath = 1$. The average antenna gain in all directions is $\mu_G = \frac{1}{2\pi}\int_0^{2\pi} G(\theta) d\theta = 1$. Figure 5.3 shows the gains with respect to the direction of antenna. It can be seen that for $\wp = 0$, the gain is 1 which is the basic gain for an isotropic antenna. For a highly directional antenna with single lobe, i.e., when $\wp = 1$, the highest gain can be observed at the center of the main lobe at $\theta = 0°$. For notational convenience, we will omit θ from the gain variables G and $\bar{G}$ in the rest of this chapter.

The mobile-cell's AL shares sub-channel $\omega \in \mathcal{W}$ with either BL or the out-of-vehicle cellular user. The sub-channel sharing is formally explained in Algorithm-1 in Section 5.3. We further define $\kappa \in [0, 1]$ as the indicator of transmission over sub-channel ω in the fixed small-cell layer [114]. The case when $\kappa = 1$ represents a scenario when all SeNBs utilize ω. This will be the worst case scenario when user population within small-cells is very high and all SeNBs are forced to transmit over ω. On the contrary, $\kappa = 0$ indicates a scenario when no small-cell uses ω.

The links that share the same resources are often characterized by SIR, as explained in the next section. We have summarized all the variables used in this chapter in Table 5.1.

5.2.2 Representing Signal-to-Interference Ratio

We have considered an interference limited environment due the presence of large number of cellular transmitters. In such an environment, noise effect is negligible in comparison to the interference from neighboring transmitters [106, 114]. Therefore we only consider SIR for each link.

In case BL shares sub-channel ω with mobile-cell's AL, we can find SIR as:

$$\Upsilon_1(\omega, \mathcal{M} \to \mathfrak{m}) = \frac{P_{\mathcal{M}} G_{\mathcal{M}} \bar{G}_{\mathfrak{m}} r_{\mathfrak{m}}^{-\alpha_i} h_{\mathcal{M},\mathfrak{m}}^{\omega}}{I_{\mathcal{M}} + I_{\mathcal{S}} + I_{\tilde{a}} \gamma \epsilon + I'_{\tilde{a}} \epsilon}, \tag{5.5}$$

where $r_{\mathfrak{m}}$ is the distance from A-MeNB to mobile-cell $\mathfrak{m}$. $I_{\mathcal{M}} = \sum_{\mathcal{M}' \in \Phi_{\mathcal{M}} \setminus \{\mathcal{M}\}} P_{\mathcal{M}'} G_{\mathcal{M}'} \bar{G}_{\mathfrak{m}} r_{\mathcal{M}'}^{-\alpha_i} h_{\mathcal{M}',\mathfrak{m}}^{\omega}$ is the cumulative interference from neighboring MeNBs using the same sub-channel. $I_{\mathcal{S}} = \sum_{S \in \Phi_{\mathcal{S}}} P_{\mathcal{S}} G_{\mathcal{S}} \bar{G}_{\mathfrak{m}} r_{\mathcal{S}}^{-\alpha_i} h_{S,\mathfrak{m}}^{\omega}$ is the interference from SeNBs. The symbols $r_{\mathcal{M}'}$, $r_{\mathcal{S}}$ denotes the mobile-cell's distances from interfering MeNB and SeNBs, respectively. The interference from AL-antenna of mobile-cell $\mathfrak{m}$ is denoted as $I_{\tilde{a}} = P_{\tilde{a}} G_{\tilde{a}} \bar{G}_{\mathfrak{m}} r_{\tilde{a}\mathfrak{m}}^{-\alpha_i} h_{\tilde{a},\mathfrak{m}}^{\omega}$, where $r_{\tilde{a}\mathfrak{m}}$ is the distance between AL-antenna and BL-antenna. The VPL effect is represented by ϵ ($0 < \epsilon \leq 1$), which determines the quality of isolation between in-vehicle and out-of-vehicle communication. The higher values of ϵ show poor isolation between the two (in-vehicle and out-of-vehicle) links. γ denotes the SIC factor, such that $0 < \gamma \leq 1$. SIC is applied at BL-antenna as the CCU cancels out the dominant AL interference to enhance SIR Υ_1 [145].

Note that in Orthogonal Frequency-Division Multiple Access (OFDMA) a

Table 5.1: System model parameters

Symbol	Definition
$\mathcal{M}, \mathcal{S}, \tilde{a}$	Transmitter for MeNB, SeNB, and AL-antenna.
$\Phi_{\mathcal{M}}, \Phi_{\mathcal{S}}$	H-PPP MeNBs, SeNBs.
$\Phi_m, \Phi_{\mathfrak{m}}$	H-PPP MUEs, MCs.
$\lambda_{\mathcal{M}}, \lambda_{\mathcal{S}}$	Density of MUEs, and MCs.
$\lambda_m, \lambda_{\mathfrak{m}}$	Density of MUEs, and MCs.
$\mathfrak{m}, m, v, s$	Mobile-cell, macro-cell user, in-vehicle user, and fixed small-cell user.
$r_{\mathfrak{m}}$	Distance from A-MeNB to mobile-cell $\mathfrak{m}$.
$r_{\tilde{a}v}$	Max. distance between AL-antenna and VUE.
$r_{\tilde{a}\mathfrak{m}}$	Distance between AL-antenna and BL-antenna.
$r_{\mathcal{S}}$	Distance of $\mathfrak{m}$ from interfering SeNBs.
$r_{_{\mathcal{M}'}}$	$\mathfrak{m}$ to interfering MeNB distance (excluding A-MeNB).
ω	Sub-channel.
κ	Small-cell transmission indicator.
$P_{\mathcal{M}}$, $P_{\mathcal{S}}$, $P_{\tilde{a}}$	Transmit Power of MeNB, SeNB, AL-antenna.
$h^{\omega}_{t_x,t_r}$	Exponentially distributed fading power of channel between $t_x - t_r$ pair for ω.
α_i, α_o	non-LoS and LoS pathloss exponents, respectively.
ϵ, γ	VPE, SIC factor $(0 < \epsilon \leq 1)$ $(0 \leq \gamma \leq 1)$.
$G_{t_x}(\theta), \bar{G}_{t_r}(\theta)$	Transmit, receive antenna gains in direction θ

single resource is assigned only to one user under the coverage of a cell. Therefore, no other mobile-cell $\mathfrak{m}' \in \Phi_{\mathfrak{m}}, \mathfrak{m}' \neq \mathfrak{m}$ under the coverage of A-MeNB will use the same sub-channel as that used by mobile-cell $\mathfrak{m} \in \Phi_{\mathfrak{m}}$. The interference from the ALs of mobile-cells residing in neighboring macro-cells is negligible due to low transmit power of AL-antennas and VPL, hence $I'_{\tilde{a}}\epsilon \approx 0$. Therefore, Eq. (5.5) becomes:

$$\Upsilon_1(\omega, \mathcal{M} \rightarrow \mathfrak{m}) = \frac{P_{\mathcal{M}} G_{\mathcal{M}} \bar{G}_{\mathfrak{m}} r_{\mathfrak{m}}^{-\alpha_i} h^{\omega}_{\mathcal{M},\mathfrak{m}}}{I_{\mathcal{M}} + I_{\mathcal{S}} + I_{\tilde{a}}\gamma\epsilon}. \tag{5.6}$$

The SIR for MUE m that receives transmission over sub-channel ω is:

$$\Upsilon_2(\omega, \mathcal{M} \to m) = \frac{P_{\mathcal{M}} G_{\mathcal{M}} \bar{G}_m r_m^{-\alpha_i} h^{\omega}_{\mathcal{M},m}}{I_{\mathcal{M}'} + I_{\mathcal{S}'} + I'_{\tilde{a}}\epsilon}. \tag{5.7}$$

where r_m is the distance between MUE m and A-MeNB. The symbols $I_{\mathcal{M}'}$ and $I_{\mathcal{S}'}$ denote the respective interference from the neighboring macor-cells and small-cells as $\Phi_{\mathcal{M}}$ and $\Phi_{\mathcal{S}}$. The interference from access link of mobile-cell $\mathfrak{m}$ is $I'_{\tilde{a}}$ where $I'_{\tilde{a}} = P_{\tilde{a}} G_{\tilde{a}} h^{\omega}_{\tilde{a},m} r_{\mathfrak{m}m}^{-\alpha_i}$ and $r_{\mathfrak{m}m}$ is the distance from $\mathfrak{m}$ to m.

The SIR for the link between AL-antenna $\tilde{a}$ and VUE v on sub-channel ω is Υ_3, which is written as:

$$\Upsilon_3(\omega, \tilde{a} \to v) = \frac{P_{\tilde{a}} G_{\tilde{a}} \bar{G}_v r_{\tilde{a}v}^{-\alpha_o} h^{\omega}_{\tilde{a},v}}{I_C\epsilon + I'_{\tilde{a}}\epsilon^2}, \tag{5.8}$$

where $I_C = \sum_{\mathcal{M}\in\Phi_{\mathcal{M}}} I_{\mathcal{M}} + \sum_{\mathcal{S}\in\Phi_{\mathcal{S}}} I_{\mathcal{S}}$ is the interference from all cellular transmitters including MeNBs and SeNBs. The distance between AL-antenna and VUE v is $r_{\tilde{a}v}$. The interference from neighboring mobile-cells' ALs experiences VPL effect at least twice and can be neglected. Mathematically, $I'_{\tilde{a}}\epsilon^2 \approx 0$. Hence, $I'_{\tilde{a}}$ factor can be neglected in Eq. (5.8) and the new form of Υ_3 becomes:

$$\Upsilon_3(\omega, \tilde{a} \to v) = \frac{P_{\tilde{a}} G_{\tilde{a}} \bar{G}_v r_{\tilde{a}v}^{-\alpha_o} h^{\omega}_{\tilde{a},v}}{I_C\epsilon}. \tag{5.9}$$

Finally, for SUE s, SIR is given as:

$$\Upsilon_4(\omega, S \to s) = \frac{P_{\mathcal{S}} G_{\mathcal{S}} \bar{G}_s r_{Ss}^{-\alpha_i} h^{\omega}_{S,s}}{I_C + I_{\tilde{a}}\epsilon}. \tag{5.10}$$

where $I_{\tilde{a}}$ is the interference from mobile-cells.

Using the expressions of SIR for all respective links that we have formulated in this section, we will present the analysis for resource sharing scheme in the coming sections.

5.3 Resource Sharing: Backhaul and Access Links

We propose that mobile-cell's AL shares the sub-channel with BL or out-of-vehicle macro-cell user's transmission. As mentioned earlier, all links follow downlink

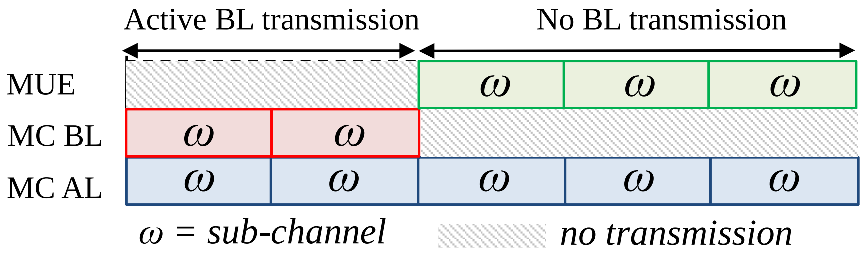

Figure 5.4: Sub-channel sharing (excluding small-cell layer). © 2019 IET [39].

Algorithm 1 Resource Sharing Algorithm

A-MeNB : Associated MeNB.
ω : Sub-channel.
$\bar{t}$: Unit of time.
for all $\bar{t} > 0$ **do**
  if there exists transmission for backhaul link **then**
    A-MeNB assigns ω to mobile-cell's BL.
    mobile-cell's AL shares ω with BL.
  else
    A-MeNB assigns ω to MUE following Algorithm-2
    mobile-cell's AL shares ω with MUE
  end if
end for

transmission. The Algorithm 1 outlines the resource sharing scheme which is also shown in Figure 5.4. If there is an active transmission from A-MeNB to mobile-cell $\mathfrak{m}$, the AL shares resources with the BL. On the other hand, if there is no transmission from A-MeNB, AL shares ω with the MUE m. The criteria to choose MUE m will be explained in Section 5.4.

We will now analyze the performance of the backhaul and access links with specific regard to QoS. The parameter of interest is the success probability (p), which depends on the SIR for each link. For successful signal reception, the SIR of a signal at the receiver should be greater than a threshold level $\mho$. Numerically, for a link between t_x and t_r over sub-channel ω, success probability (which is also called coverage probability) can be expressed as $p = \mathbb{P}[\Upsilon(\omega, t_x \to t_r) > \mho]$, where $\mathbb{P}[.]$ shows the probability. The success probabilities of each individual link of a mobile-cell are derived in the following.

5.3.1 Backhaul Success Probability

Theorem 5.1: Success Probability for backhaul link

The success probability for BL is calculated for the following two cases:

When $\kappa \neq 0$

$$p_{BL} = \int_0^1 \frac{1}{\varpi^2} \exp\Big\{ - \Big(\frac{1}{\varpi} - 1\Big) \mathcal{Z}_1 \Big\} \times \frac{1}{1 + \mathcal{Y}_1 (\frac{1}{\varpi} - 1)^2} d\varpi. \quad (5.11)$$

where $\mathcal{Z}_1 = \sqrt{\mho}(\frac{\pi}{2} - \arctan(\frac{1}{\sqrt{\mho}})) + \frac{\lambda_{\mathcal{S}}}{\lambda_{\mathcal{M}}} \frac{\pi}{2} \sqrt{\frac{P_{\mathcal{S}} G_{\mathcal{S}}}{P_{\mathcal{M}} G_{\mathcal{M}}} \mho + 1}$, and

$$\mathcal{Y}_1 = \frac{\gamma \epsilon \mho P_{\tilde{a}} G_{\tilde{a}}}{P_{\mathcal{M}} G_{\mathcal{M}} \pi^2 \lambda_{\mathcal{M}}^2 r_{\tilde{a}\mathfrak{m}}^4}. \quad (5.12)$$

When $\kappa = 0$

$$p_{BL} = 2\pi\lambda_{\mathcal{M}} \int_0^1 \frac{1}{z^2} (\frac{1}{z} - 1) \frac{\exp\{ - \mathcal{Z}_2 (\frac{1}{z} - 1)^2 \}}{1 + \mathcal{Y}_2 (\frac{1}{z} - 1)^4} dz. \quad (5.13)$$

where $\mathcal{Z}_2 = \pi\lambda_{\mathcal{M}}[\ 1 + \sqrt{\mho}(\pi/2 - \tan^{-1}(1/\sqrt{\mho}))\ ]$, and

$$\mathcal{Y}_2 = \frac{\gamma \epsilon \mho P_{\tilde{a}} G_{\tilde{a}}}{P_{\mathcal{M}} G_{\mathcal{M}} r_{\tilde{a}\mathfrak{m}}^4}. \quad (5.14)$$

Note that Eqs. (5.11) and (5.13) are not exact closed-form expressions and are difficult to solve analytically. Hence, they are evaluated numerically [106] and the results are presented in Section 5.6.

Proof

We denote success probability for backhaul link as p_{BL} which is averaged over the euclidean plane. Mathematically p_{BL} is denoted as:

$$p_{BL} = \mathbb{E}_{r_{\mathfrak{m}}} \Big[\mathbb{P}[\Upsilon_1(\omega, M \to \mathfrak{m}) > \mho \mid r_{\mathfrak{m}}] \Big], \quad (5.15)$$

The expectation $\mathbb{E}[.]$ is with respect to the random position of the mobile-cells and A-MeNB.

$$p_{BL} = \int_{r_{\mathfrak{m}} > 0} \mathbb{P}[\Upsilon_1(\omega, M \to \mathfrak{m}) > \mho \mid r_{\mathfrak{m}}]\ f_{\mathcal{M}}(r_{\mathfrak{m}}) dr_{\mathfrak{m}}, \quad (5.16)$$

Since $h^{\omega}_{M,\mathfrak{m}} \sim \exp(1)$, we use the complimentary cumulative distribution (CCDF) of $h^{\omega}_{M,\mathfrak{m}}$ and re-write Eq. (5.16) as:

$$p_{BL} = \mathbb{E}\Big[\int_{r_{\mathfrak{m}}>0} \exp\big(\frac{-\mho r_{\mathfrak{m}}^{\alpha_i}}{P_{\mathcal{M}}G_{\mathcal{M}}\bar{G}_{\mathfrak{m}}}(I_{\mathcal{M}}+I_{\mathcal{S}}+\gamma I_{\tilde{a}}\epsilon)\big)2\pi\lambda_{\mathcal{M}}r_{\mathfrak{m}}e^{-\pi\lambda_{\mathcal{M}}r_{\mathfrak{m}}^2}dr_{\mathfrak{m}}\Big], \tag{5.17}$$

The expectation is with respect to the total interference from neighboring transmitters (i.e., MeNB, SeNB, and mobile-cells). Applying the property of Laplace transform for random variable i.e., $\mathcal{L}_X(\mathfrak{s}) = \mathbb{E}[e^{-\mathfrak{s}X}]$, and using the fact that $I_{\mathcal{M}}$, $I_{\mathcal{S}}$, and $I_{\tilde{a}}$ are identical and independent (i.i.d.) random variables, p_{BL} becomes:

$$p_{BL} = \int_0^{\infty} \mathcal{L}_{I_{\mathcal{M}}}(\delta)\mathcal{L}_{I_{\mathcal{S}}}(\delta)\mathcal{L}_{I_{\tilde{a}}}(\delta\gamma\epsilon)2\pi\lambda_{\mathcal{M}}r_{\mathfrak{m}}e^{-\pi\lambda_{\mathcal{M}}r_{\mathfrak{m}}^2}dr_{\mathfrak{m}}, \tag{5.18}$$

where $\delta = \dfrac{\mho r_{\mathfrak{m}}^{\alpha_i}}{P_{\mathcal{M}}G_{\mathcal{M}}\bar{G}_{\mathfrak{m}}}$.

Keeping in view the conditions when small-cells transmit on the same sub-channel as shared by the AL, we have following two cases.

Backhaul Success Probability when $\kappa \neq 0$

In case, the fixed small-cells also transmit on the sub-channel shared by access link, we will resume from Eq. (5.18) to calculate $\mathcal{L}_{I_{\mathcal{M}}}(\mathfrak{s})$ as [106]:

$$\mathcal{L}_{I_{\mathcal{M}}}(\delta) = \exp(-\pi r_{\mathfrak{m}}^2\lambda_{\mathcal{M}}\rho(\mho,\alpha_i)), \tag{5.19}$$

where $\rho(\mho,\alpha_i) = \mho^{2/\alpha_i}\int\limits_{\mho^{-2/\alpha_i}}^{\infty} \frac{1}{1+\Lambda^{\alpha_n/2}}d\Lambda$.

Then, we find $\mathcal{L}_{I_{\mathcal{S}}}(\delta)$ as:

$$\mathcal{L}_{I_{\mathcal{S}}}(\delta) = \mathbb{E}_{I_{\mathcal{S}}}\big[\exp\big\{-\lambda_{\mathcal{S}}\pi r_{\mathfrak{m}}^2\beta(\alpha_i)\big(\frac{P_{\mathcal{S}}G_{\mathcal{S}}\bar{G}_{\mathfrak{m}}\mho}{P_{\mathcal{M}}G_{\mathcal{M}}\bar{G}_{\mathfrak{m}}}\big)^{2/\alpha_i}\big\}\big], \tag{5.20}$$

where

$$\beta(\alpha) = \Gamma(\alpha/2)\Gamma(1-\alpha/2) = \frac{(2\pi/\alpha)}{\sin(2\pi/\alpha)} \tag{5.21}$$

and $\Gamma(.)$ is the Gamma function.

$$\mathcal{L}_{I_{\mathcal{S}}}(\delta) = \mathbb{E}_{I_{\mathcal{S}}}[\exp\{-\lambda_{\mathcal{S}}\pi r_{\mathfrak{m}}^2 \beta(\alpha_i)(\frac{P_{\mathcal{S}}G_{\mathcal{S}}\mho}{P_{\mathcal{M}}G_{\mathcal{M}}})^{2/\alpha_i}\}], \tag{5.22}$$

Let $\mathfrak{s} = \gamma\epsilon\mho(r_{\mathfrak{m}}/r_{\tilde{a}\mathfrak{m}})^{\alpha_i}\frac{P_{\tilde{a}}G_{\tilde{a}}}{P_{\mathcal{M}}G_{\mathcal{M}}}$. Using the property that $\mathcal{L}_h(\mathfrak{s}) = \frac{1}{1+\mathfrak{s}}$ for exponential random variable $h \sim \exp(1)$, we find $\mathcal{L}_{I_{\tilde{a}}}(\mathfrak{s})$ for Eq. (5.18) as:

$$\mathcal{L}_{I_{\tilde{a}}}(\mathfrak{s}) = \frac{1}{1+\gamma\epsilon\mho(\frac{r_{\mathfrak{m}}}{r_{\tilde{a}\mathfrak{m}}})^{\alpha_i}\frac{P_{\tilde{a}}G_{\tilde{a}}}{P_{\mathcal{M}}G_{\mathcal{M}}}}, \tag{5.23}$$

Hence, p_{BL} becomes:

$$p_{BL} = \int_{r_{\mathfrak{m}}=0}^{\infty} \mathcal{L}_{I_{\tilde{a}}}(\mathfrak{s})\mathcal{L}_{I_{\mathcal{M}}}(\mathfrak{s})\mathcal{L}_{I_{\mathcal{S}}}(\mathfrak{s})e^{-\lambda_{\mathcal{M}}\pi r_{\mathfrak{m}}^2} 2\lambda_{\mathcal{M}}\pi r_{\mathfrak{m}} \tag{5.24}$$

$$p_{BL} = \int_0^{\infty} \frac{\exp\Big\{-\lambda_{\mathcal{M}}\pi r_{\mathfrak{m}}^2[\rho(\mho,\alpha_i) + \frac{\lambda_{\mathcal{S}}}{\lambda_{\mathcal{M}}}\frac{\pi}{2}\sqrt{\frac{P_{\mathcal{S}}G_{\mathcal{S}}}{P_{\mathcal{M}}G_{\mathcal{M}}}\mho} + 1]\Big\} 2\pi\lambda_{\mathcal{M}} r_{\mathfrak{m}}}{1 + \frac{\mho\gamma\epsilon P_{\tilde{a}}G_{\tilde{a}} r_{\mathfrak{m}}^{\alpha_i}}{r_{\tilde{a}\mathfrak{m}}^{\alpha_i} P_{\mathcal{M}}G_{\mathcal{M}}\pi^2\lambda_{\mathcal{M}}^2}} dr_{\mathfrak{m}}, \tag{5.25}$$

Eq. (5.25) does not have a closed-form expression. However, for specific values of α_i, for example $\alpha_i = 4$ [106], a more tractable form can be obtained for numerical evaluation. Considering $\Im = \lambda_{\mathcal{M}}\pi r_{\mathfrak{m}}^2$, then $dr_{\mathfrak{m}} = \frac{1}{2\lambda_{\mathcal{M}}\pi r_{\mathfrak{m}}} d\Im$. Then Eq. (5.25) becomes:

$$p_{BL} = \int_0^{\infty} \frac{\exp\Big\{-\Im[\rho(\mho,4) + \frac{\lambda_{\mathcal{S}}}{\lambda_{\mathcal{M}}}\frac{\pi}{2}\sqrt{\frac{P_{\mathcal{S}}G_{\mathcal{S}}}{P_{\mathcal{M}}G_{\mathcal{M}}}\mho} + 1]\Big\}}{1 + \frac{\mho\gamma\epsilon P_{\tilde{a}}G_{\tilde{a}}\Im^2}{r_{\tilde{a}\mathfrak{m}}^4 P_{\mathcal{M}}G_{\mathcal{M}}\pi^2\lambda_{\mathcal{M}}^2}} d\Im, \tag{5.26}$$

Considering $\varpi = \frac{1}{1+\Im}$, we get $\Im = \frac{1}{\varpi} - 1$, and $d\Im = -\frac{1}{\varpi^2}$ integrable over region from $0 \to 1$. Hence, a simplified form of Eq. (5.26) is represented as Eq. (5.11).

Backhaul Success Probability when $\kappa = 0$

In case no small-cell transmits over the AL's sub-channels, we can write the success probability p_{BL} as:

$$p_{BL} = \int_0^{\infty} \mathcal{L}_{I_{\mathcal{M}}}(\delta)\mathcal{L}_{I_{\tilde{a}}}(\delta) 2\pi\lambda_{\mathcal{M}} r_{\mathfrak{m}} e^{-\pi\lambda_{\mathcal{M}} r_{\mathfrak{m}}^2} dr_{\mathfrak{m}}, \tag{5.27}$$

where δ is defined in Eq. (5.18). Using $\mathcal{L}_{I_{\mathcal{M}}}(\delta)$ and $\mathcal{L}_{I_{\tilde{a}}}(\delta)$, p_{BL} becomes:

$$p_{BL} = \int_0^{\infty} \exp(-\pi r_{\mathfrak{m}}^2 \lambda_{\mathcal{M}} \rho(\mho, \alpha)) \times \frac{2\pi\lambda_{\mathcal{M}} r_{\mathfrak{m}} \exp(-\pi\lambda_{\mathcal{M}} r_{\mathfrak{m}}^2)}{1 + \gamma\epsilon\mho(r_{\mathfrak{m}}/r_{\tilde{a}\mathfrak{m}})^{\alpha_i} P_{\tilde{a}}/Pc} dr_{\mathfrak{m}}, \tag{5.28}$$

$$p_{BL} = 2\pi\lambda_{\mathcal{M}} \int_0^{\infty} \frac{e^{-\pi\lambda_{\mathcal{M}}(1+\rho(\mho,\alpha_i))r_{\mathfrak{m}}^2}}{1 + \gamma\epsilon\mho(r_{\mathfrak{m}}/r_{\tilde{a}\mathfrak{m}})^{\alpha_i} P_{\tilde{a}}/Pc} r_{\mathfrak{m}} dr_{\mathfrak{m}}, \tag{5.29}$$

Again note that Eq. (5.29) is not a closed-form expression. Again, considering $\alpha_i = 4$, a numerically tractable form for this equation can be evaluated by considering $z = \dfrac{1}{1 + r_{\mathfrak{m}}}$ which is represented as Eq. (5.13).

This completes the proof. ■

Corollary 5.1.1: Effect of AL directivity on the BL

At the backhaul, we have considered an isotropic antenna which can receive signals with equal gain from all directions. On the other hand, AL-antenna transmits with gain $G_{\tilde{a}}$ in direction θ. Hence, in order to capture the effect of directivity of AL-antenna on the BL, we average AL-antenna gain over $\frac{\pi}{2} \rightarrow \frac{3\pi}{2}$ (See Fig. 5.2) to get the following:

When $\kappa \neq 0$

$$\mathcal{Y}_1 = \frac{\gamma\epsilon\mho P_{\tilde{a}}}{P_{\mathcal{M}} G_{\mathcal{M}} \pi^3 \lambda_{\mathcal{M}}^2 r_{\tilde{a}\mathfrak{m}}^4}(\pi - 2\wp). \tag{5.30}$$

When $\kappa = 0$

$$\mathcal{Y}_2 = \frac{\gamma\epsilon\mho P_{\tilde{a}}}{P_{\mathcal{M}} G_{\mathcal{M}} \pi r_{\tilde{a}\mathfrak{m}}^4}(\pi - 2\wp). \tag{5.31}$$

We call the variables $\mathcal{Y}_1$ and $\mathcal{Y}_2$ as the BL's success link parameters. The success link parameters represent the BL's success probability in terms of transmit power and AL-antenna gain. Both $\mathcal{Y}_1$ and $\mathcal{Y}_2$ have been expressed in terms of $P_{\tilde{a}}$ (i.e., AL-antenna transmit power), which we will derive in Section 5.3.3. Next, we will present the success probability of AL transmission.

5.3.2 Access Link's Success Probability

Theorem 5.2: Success Probability for Access Link

The success probability of AL is given as:

$$p_{AL} = \sum_{j=0}^{J} \sum_{\bar{j}=0}^{j} \frac{K^j (-\mho)^{j-\bar{j}}}{e^K j!\,(j-\bar{j})!} \sum_{q=0}^{Q} \frac{(-1)^q \Omega_\kappa^q}{q!} . \frac{1}{P_{\tilde{a}}^q} \mho^{\frac{2q}{\alpha_i}-(j-\bar{j})} \Psi_{(2q/\alpha_i, j-\bar{j})}. \tag{5.32}$$

where

$$\Psi_{(2q/\alpha_i, j-\bar{j})} = \frac{\Gamma(2q/\alpha_i + 1)}{\Gamma(2q/\alpha_i - (j-\bar{j}) + 1)} \tag{5.33}$$

and $\Gamma(.)$ is the Gamma function.

The symbols J, Q are the upper limits for index parameters j, q respectively. The numerical values of J, Q are given in Section 5.6, and Ω_κ is given as:

$$\Omega_\kappa = \pi \bigg(\frac{\gamma \epsilon r_{\tilde{a}v}^{\alpha_o}}{G_{\tilde{a}}} \bigg)^{\frac{2}{\alpha_i}} \bigg(\lambda_{\mathcal{M}} (P_{\mathcal{M}} G_{\mathcal{M}})^{\frac{2}{\alpha_i}} + \kappa \lambda_{\mathcal{S}} (P_{\mathcal{S}} G_{\mathcal{S}})^{\frac{2}{\alpha_i}} \bigg) \beta(\alpha_i). \tag{5.34}$$

and $\beta(.)$ is defined in Eq. (5.21).

Proof

The success probability of AL, denoted by p_{AL}, can be mathematically written as:

$$p_{AL} = \mathbb{E}_{I'_{\tilde{a}}} \Big[\mathbb{P}[h_{\tilde{a},v}^{\omega} > \mho \frac{I_C r_{\tilde{a}\mathfrak{m}}^{\alpha_o} \gamma \epsilon}{P_{\tilde{a}} G(\tilde{a}) G(v)}] \Big], \tag{5.35}$$

Let $I'_{\tilde{a}} = \dfrac{I_C r_{\tilde{a}v}^{\alpha_o} \gamma \epsilon}{P_{\tilde{a}} G(\tilde{a}) G(v)}$, then p_{AL} can be found as:

$$p_{AL} = \mathbb{E}_{I'_{\tilde{a}}} [1 - \mathbb{P}[h_{\tilde{a},v}^{\omega} \leq \mho I'_{\tilde{a}}]], \tag{5.36}$$

The link between AL-antenna $\tilde{a}$ and in-vehicle user's receiver v follows Rician fading. Hence, the channel $h_{\tilde{a},v}^{\omega}$ follows non-central Chi-squared (χ^2) distribution.

In this case, the probability density function for $f_{h^{\omega}_{\tilde{a},v}}(h_{\tilde{a}})$ is given as [Ch:3, [150]]:

$$f_{h^{\omega}_{\tilde{a},v}}(h_{\tilde{a}}) = \frac{K+1}{P_{avg}} e^{\frac{-KP_{avg}-(K+1)h_{\tilde{a}}}{P_{avg}}} I_0(2\sqrt{\frac{K(K+1)h_{\tilde{a}}}{P_{avg}}}), \tag{5.37}$$

where $I_0(.)$ is the modified Bessel function of the first kind of Zeroth order [153] and K (ratio of the power of dominant to the multipath component) denotes the K-factor. For example, $K = 0$ refers to the scenario when the signals completely follow multipath fading with no prominent LoS component. On the contrary, $K = \infty$ depicts the scenarios when a direct LoS link exists between the transmitter and the receiver. The average power received after Rician fading is $P_{avg} = \int_0^{\infty} h_{\tilde{a}} f_{h^{\omega}_{\tilde{a},v}}(h_{\tilde{a}}) dh_{\tilde{a}} = 2\sigma^2(K+1)$ [150]. If the multipath component of the access link is modeled as Gaussian random variable with the variance $\sigma^2 = 1/2$, then $P_{avg} = K+1$. Hence Eq. (5.37) becomes:

$$f_{h^{\omega}_{\tilde{a},v}}(h_{\tilde{a}}) = \frac{I_0(2\sqrt{Kh_{\tilde{a}}})}{e^{Kh_{\tilde{a}}}}. \tag{5.38}$$

The CDF of random variable $h^{\omega}_{\tilde{a},v}$ is denoted as $\mathbb{P}\Big[h^{\omega}_{\tilde{a},v} \leq \mho I'_{\tilde{a}}\Big]$ which we write as F^{ω}_{h}. However, due to the presence of Zeroth order Bessel function, we will use expansion series provided in Eq. (8.447.1) in [154] to solve F^{ω}_{h}. This way, we get the PDF of $h^{\omega}_{\tilde{a},v}$ as:

$$f_{h^{\omega}_{\tilde{a},v}}(h_{\tilde{a}}) = \sum_{j=0}^{\infty} \frac{(Kh_{\tilde{a}})^j}{e^{(K+h_{\tilde{a}})}(j!\,)^2} \tag{5.39}$$

The CDF for Eq. (5.39) is given as:

$$F_{h^{\omega}_{\tilde{a},v}}(h_{\tilde{a}}) = \int_0^{x} \sum_{j=0}^{\infty} \frac{(Kh_{\tilde{a}})^j}{e^{(K+h_{\tilde{a}})}(j!\,)^2} dh_{\tilde{a}} \tag{5.40}$$

$$F_{h^{\omega}_{\tilde{a},v}}(h_{\tilde{a}}) = \sum_{j=0}^{\infty} \frac{(K)^j e^{-K}}{(j!\,)^2} \int_0^{x} h_{\tilde{a}}^{j} e^{-h_{\tilde{a}}} dh_{\tilde{a}} \tag{5.41}$$

So p_{AL} will become:

$$p_{AL} = \sum_{j=0}^{\infty} \sum_{\bar{j}=0}^{j} \frac{e^{K}}{K^j j!\,(j-\bar{j})!} (\mho)^n \eth(\mho, n) \tag{5.42}$$

where $\eth(\mho, n) = \int_0^\infty e^{-y} y^n f_{I'_{\tilde{a}}}(y) dy = (-1)^n D^n \mathcal{L}_{I'_{\tilde{a}}}(\mho)$ and $D^n(.)$ is the n_{th} derivative of the function. The combined Laplace transform of $I'_{\tilde{a}}$ can be written as:

$$\mathcal{L}_{I'_{\tilde{a}}} = \exp\Bigg\{ -\pi\Big(\frac{\mho r_{\tilde{a}v}^{\alpha_o}\gamma\epsilon}{G_{\tilde{a}}\bar{G}_v}\Big)^{2/\alpha_i} . \Bigg(\lambda_{\mathcal{M}}\Big(\frac{P_{\mathcal{M}}G_{\mathcal{M}}\bar{G}_v}{P_{\tilde{a}}}\Big)^{2/\alpha_i} + \kappa\lambda_{\mathcal{S}}\Big(\frac{P_{\mathcal{S}}G_{\mathcal{S}}\bar{G}_v}{P_{\tilde{a}}}\Big)^{2/\alpha_i}\Bigg)\beta(\alpha_i)\Bigg\} \tag{5.43}$$

where $\beta(\alpha)$ is defined in Eq. (5.21), and

$$\eth(\mho, n) = (-1)^n \frac{d^n \mathcal{L}_{I'_{\tilde{a}}}(\mho)}{d\mho^n} = (-1)^n \frac{d^n \exp(-\Omega_\kappa \mho^{2/\alpha_i})}{d\mho^n}. \tag{5.44}$$

where Ω_κ is given in Eq. (5.34).

Let $f(\mho) = \exp(-\Omega_\kappa \mho^{2/\alpha_i})$. Using $e^{(.)} = \sum_{q=0}^{\infty} \frac{(.)^q}{q!}$, we can solve (5.44) as:

$$\eth(\mho, n) = (-1)^n \sum_{q=0}^{\infty} \frac{(-1)^q \Omega_\kappa^q}{q!} \mho^{\frac{2q}{\alpha_i} - n} \frac{\Gamma(2q/\alpha_i + 1)}{\Gamma(2q/\alpha_i - n + 1)}. \tag{5.45}$$

So, p_{AL} will become:

$$p_{AL} = \sum_{j=0}^{\infty} \sum_{\bar{j}=0}^{j} \frac{K^j (-\mho)^{j-\bar{j}}}{e^K j!\,(j-\bar{j})!} \sum_{q=1}^{\infty} \frac{(-1)^q \Omega_\kappa^q}{q!} \frac{1}{P_{\tilde{a}}^q} \mho^{\frac{2q}{\alpha_i} - (j-\bar{j})} \frac{\Gamma(\frac{2q}{\alpha_i} + 1)}{\Gamma(\frac{2q}{\alpha_i} - (j-\bar{j}) + 1)}. \tag{5.46}$$

Eq. (5.46) is a closed-form expression. But we can further define upper limits for parameters j and q as J and Q, respectively. This idea comes from the intuition that for very large values of J, Q, $\frac{1}{J!} \to 0$ and $\frac{1}{Q!} \to 0$. Thus, we can rewrite (5.46) as Eq. (5.32).

This completes the proof. ■

Corollary 5.2.1: Effect of Directivity on AL

Since we have considered isotropic antennas for macro-cell and small-cell transmitters, hence we use $G_{\mathcal{M}} = G_{\mathcal{S}} = 1$. We further average the gain of the AL-antenna from $\frac{-\pi}{2} \to \frac{\pi}{2}$ (see Fig. 5.2) as $G_{\tilde{a}} = \frac{1}{\pi}\int_{-\pi/2}^{\pi/2} (1 + \wp\cos(\theta)) d\theta = 1 + \frac{2\wp}{\pi}$.

Considering $\alpha_i = 4$, we re-write Eq. (5.34) in terms of antenna directivity as:

$$\Omega_\kappa = \frac{(\sqrt{\gamma \epsilon r_{\tilde{a}v}^{\alpha_o}})(\lambda_{\mathcal{M}}\sqrt{P_{\mathcal{M}}} + \kappa\lambda_{\mathcal{S}}\sqrt{P_{\mathcal{S}}})\beta(\alpha_i)}{\sqrt{1+\frac{2\wp}{\pi}}}. \tag{5.47}$$

The highly directional AL-antenna focuses the AL transmission towards in-vehicle users. The secondary effect of directional transmission is the reduced interference on the BL-antenna. To further decrease the interference effect of AL transmission, we will next propose transmit power control scheme.

5.3.3 Access Link Transmit Power Control

Mobile-cell's BL experiences high interference from AL in case both share the same sub-channel. Likewise, AL's signal quality is affected by the neighboring MeNBs and SeNBs. However, due to the use of directional AL-antenna, we have reduced the effect of AL interference on the BL. The directional AL-antenna also ensures high link quality for in-vehicle user even with low transmit power. This is made possible due to strong LoS link between AL-antenna and the receiving VUE.

To further reduce the effect of AL transmission on the BL, we propose that mobile-cell dynamically changes AL-antenna's transmit power ($P_{\tilde{a}}$) to enhance the SIR for backhaul transmission. We ensure that the QoS for commuting cellular users is not compromised. The mobile-cell's CCU controls the transmit power for AL-transmission [145].

If we consider $\alpha_i = 4$ and use the property $e^{(.)} = \sum_{q=0}^{\infty} \frac{(.)^q}{q!}$, the AL's success probability in Eq. (5.46) can be written as:

$$p_{AL} = \exp\left(\frac{-\Omega_\kappa\sqrt{\mho}}{P_{\tilde{a}}}\right) \sum_{j=0}^{\infty}\sum_{\bar{j}=0}^{j} \frac{K^j(-\mho)^{j-\bar{j}}}{e^K j!\,(j-\bar{j})!} \sum_{q=0}^{\infty} \mho^{-(j-\bar{j})} \Psi_{(2q/\alpha_i, j-\bar{j})}, \tag{5.48}$$

where $\Psi_{(2q/\alpha_i, j-\bar{j})}$ is given in Eq. (5.33) and Ω_κ is given in Eq. (5.34). Then, AL antenna's transmit power will be:

$$P_{\tilde{a}} = \frac{\Omega_\kappa\sqrt{\mho}}{\log(\Xi) - \log(p_{AL})}. \tag{5.49}$$

where we define Ξ as:

$$\Xi = \sum_{j=0}^{\infty} \sum_{\bar{j}=0}^{j} \frac{K^j (-1)^{j-\bar{j}}}{e^K j!\,(j-\bar{j})!} \sum_{q=0}^{\infty} \Psi_{(2q/\alpha_i, j-\bar{j})}. \tag{5.50}$$

Note that $P_{\tilde{a}}$ in Eq. (5.49) is the function of AL's success probability (p_{AL}). Mobile-cell's CCU controls the p_{AL}. Other parameters like ϵ, γ, and K-factor for Rician channel are assumed to be pre-determined. The parameters $\lambda_{\mathcal{M}}$ and $\lambda_{\mathcal{S}}$ are broadcasted by A-MeNB [22]. The transmission power of the macro-cell layer is assumed to be fixed.

The expressions for BL's success probability are given as Eq. (5.11) and Eq. (5.13) for the cases when $\kappa \neq 1$ and $\kappa = 0$, respectively. Given the power control expression for the AL, success-link parameters ($\mathcal{Y}_1$ and $\mathcal{Y}_2$) for backhaul get modified by inserting $P_{\tilde{a}}$ from Eq. (5.49) as follows:

When $\kappa \neq 0$:

$$\mathcal{Y}_1 = \Big(\frac{\gamma\epsilon\mho(\pi - 2\wp)}{P_{\mathcal{M}}\pi^2\lambda_{\mathcal{M}}^2 r_{\tilde{a}\mathfrak{m}}^4}\Big)\Big(\frac{\Omega_\kappa\sqrt{\mho}}{\log(\Xi) - \log(p_{AL})}\Big). \tag{5.51}$$

When $\kappa = 0$:

$$\mathcal{Y}_2 = \Big(\frac{\gamma\epsilon\mho(\pi - 2\wp)}{P_{\mathcal{M}}\pi r_{\tilde{a}\mathfrak{m}}^4}\Big)\Big(\frac{\Omega_\kappa\sqrt{\mho}}{\log(\Xi) - \log(p_{AL})}\Big). \tag{5.52}$$

Next, we will formulate the effect of resource sharing on the success probability of users of fixed small-cell.

5.3.4 Effect of Resource Sharing on Small-Cell Transmission

Following Eq. (5.10), the success probability for small-cell users can be written as:

$$p_{SC} = \int_0^{R_{\mathcal{S}}} f_{\mathcal{R}}(r_s)\mathbb{P}[\frac{P_{\mathcal{S}} G_{\mathcal{S}} \bar{G}_s r_{\mathcal{S}s}^{-\alpha_i} h_{\mathcal{S},s}^{\omega}}{I_C + I_{\tilde{a}}\epsilon} > \mho] dr_s, \tag{5.53}$$

$$p_{SC} = \int_0^{R_\mathcal{S}} f_\mathcal{R}(r_s)\, \mathbb{P}[h^\omega_{S,s} > \frac{\mho r^{\alpha_i}_{Ss}(I_C + I_{\tilde{a}}\epsilon)}{P_\mathcal{S} G_\mathcal{S} \bar{G}_s}]dr_s, \tag{5.54}$$

Considering $\alpha_i = 4$ and $G_\mathcal{S} = \bar{G}_s = 1$, we get:

$$p_{SC} = \frac{1 - \exp(-\pi\lambda_\mathcal{S} R^2_\mathcal{S}(1 + \varkappa))}{(1 + \varkappa)(1 - \exp(-\pi\lambda_\mathcal{S} R^2_s))}. \tag{5.55}$$

where

$$\varkappa = \sqrt{\mho}\Big[\tan^{-1}\sqrt{\mho} + \sqrt{\frac{P_\mathcal{M}}{P_\mathcal{S}}}\frac{\lambda_\mathcal{M}}{\lambda_\mathcal{S}}\tan^{-1}\sqrt{\frac{\mho P_\mathcal{M}}{P_\mathcal{S}}} + \sqrt{\frac{\epsilon P_{\tilde{a}}}{P_\mathcal{S}}}\frac{\lambda_m}{\lambda_\mathcal{S}}\tan^{-1}\sqrt{\frac{\mho\epsilon P_{\tilde{a}}}{P_\mathcal{S}}}\Big]. \tag{5.56}$$

In case when A-MeNB does not transmit to the mobile-cell on BL, mobile-cell's AL share sub-channel with out-of-vehicle macro-cell user which is presented in the next section.

5.4 Resource Sharing with Macro-Cell users

The mobile-cell's AL will share the sub-channel with the MUE in case there is no backhaul transmission (See Fig. 5.4). We will first derive the expression for the success probability of the macro-cell user in terms of its distances from the mobile-cell and A-MeNB. Based on this expression, we will propose an algorithm for selecting MUE that experiences minimal interference from the mobile-cell's AL. The selected MUE and mobile-cell's AL will share a single sub-channel. Following Eq. (5.7), the success probability for downlink cellular transmission for MUE is given as:

$$p_{MUE} = \mathbb{P}\Big[h^\omega_{\mathcal{M},m} > \frac{\mho r^{\alpha_i}_m}{P_\mathcal{M} G_\mathcal{M} \bar{G}_m}(I_{\mathcal{M}'} + I_{\mathcal{S}'} + I'_{\tilde{a}})\Big], \tag{5.57}$$

Using CCDF of $h^\omega_{\mathcal{M},m}$, we get:

$$p_{MUE} = \mathbb{E}\Big[\exp\Big\{-\frac{\mho r^{\alpha_i}_m}{P_\mathcal{M} G_\mathcal{M} \bar{G}_m}(I_{\mathcal{M}'} + I_{\mathcal{S}'} + I'_{\tilde{a}})\Big\}\Big], \tag{5.58}$$

We use $G_\mathcal{M}, G_\mathcal{S} = 1$, as mentioned earlier in Corollary 5.1.1. The gain of the interfering mobile-cell's AL-antenna is $G_{\tilde{a}'} = \frac{1}{2\pi}\int_0^{2\pi}(1 + \wp\cos(\phi))d\phi = 1$ in the azimuthal plane, where ϕ is the horizontal angle for the antennas. The expectation in Eq. (5.58) is with respect to the i.i.d. random variables $I_{\mathcal{M}'}, I_{\mathcal{S}'}$, and $I'_{\tilde{a}}$. Considering $\alpha_i = 4$ we can solve p_{MUE} by applying the following Laplace transforms on Eq. (5.58),

$$\mathcal{L}_{I'_{\mathcal{M}}}(\mathfrak{s}) = \exp\left\{\frac{-\pi r_m^2 \lambda_{\mathcal{M}}}{2}\sqrt{\frac{P_{\mathcal{M}}\mho}{P_{\mathcal{M}}}}\right\}, \tag{5.59}$$

$$\mathcal{L}_{I'_{\mathcal{S}}}(\mathfrak{s}) = \exp\left\{\frac{-\pi r_m^2 \lambda_{\mathcal{S}}\kappa}{2}\sqrt{\frac{P_{\mathcal{S}}\mho}{P_{\mathcal{M}}}}\right\}, \tag{5.60}$$

$$\mathcal{L}_{I'_{\tilde{a}}}(\mathfrak{s}) = \frac{1}{1+\frac{P_{\tilde{a}}\mho\epsilon}{P_{\mathcal{M}}}(\frac{r_m}{r_{\mathfrak{m}m}})^4}, \tag{5.61}$$

The P_{MUE} now becomes:

$$p_{MUE} = \frac{\exp\{\frac{-\pi r_m^2}{2}\sqrt{\frac{\mho}{P_{\mathcal{M}}}}(\lambda_{\mathcal{M}}\sqrt{P_{\mathcal{M}}}+\kappa\lambda_{\mathcal{S}}\sqrt{P_{\mathcal{S}}})\}}{1+\frac{P_{\tilde{a}}\mho\epsilon}{P_{\mathcal{M}}}(\frac{r_m}{r_{\mathfrak{m}m}})^4}. \tag{5.62}$$

It can be observed for Eq. (5.62) that p_{MUE} depends on the distances r_m and $r_{\mathfrak{m}m}$.We can notice that p_{MUE} is monotonically increasing with respect to $r_{\mathfrak{m}m}$ as $r_{\mathfrak{m}m} > 0$. We can verify this statement by taking first-order partial derivative of Eq. (5.62) with respect to $r_{\mathfrak{m}m}$, which yields the following:

$$\frac{\partial\ p_{MUE}}{\partial r_{\mathfrak{m}m}} = \frac{\exp(\frac{-\pi r_m^2}{2}\sqrt{\frac{\mho}{P_{\mathcal{M}}}}(\lambda_{\mathcal{M}}\sqrt{P_{\mathcal{M}}}+\kappa\lambda_{\mathcal{S}}\sqrt{P_{\mathcal{S}}}))\frac{4P_{\tilde{a}}\mho\epsilon r_m^4}{P_{\mathcal{M}}}r_{\mathfrak{m}m}^3}{(r_{\mathfrak{m}m}^4+\frac{P_{\tilde{a}}\mho\epsilon r_m^4}{P_{\mathcal{M}}})^2}. \tag{5.63}$$

Note that $\frac{\partial\ p_{MUE}}{\partial r_{\mathfrak{m}m}} > 0$. This suffices the condition for an increasing monotonic function [155].

Simultaneously, Eq. (5.62) is a monotonically decreasing function with respect to r_m i.e., as the distance of MUE from A-MeNB increases, its success probability decreases. The first order partial derivative with respect to r_m gives:

$$\frac{\partial\ p_{MUE}}{\partial r_m} = -2r_m e^{-\mathfrak{A}\ r_m^2}\left[\frac{2\mathfrak{A}r_m(1+\mathfrak{B}r_m^4)+4\mathfrak{B}r_m^3}{(1+\mathfrak{B}r_m^4)^2}\right]. \tag{5.64}$$

Algorithm 2 Dynamic User Scheduling Algorithm

A-MeNB, ω : Associated MeNB, sub-channel.
$|\mathfrak{M}|$: Number of MUEs registered with A-MeNB.
r_m : Distance between A-MeNB and MUEs (m).
$r_{\mathfrak{m}m}$: Distance between mobile-cell $\mathfrak{m}$ and MUE (m).
$\bar{t}$: Unit of time.
for all $\bar{t} > 0$ **do**
  A-MeNB knows mobile-cells' location at time $\bar{t}$.
  A-MeNB knows r_m and $r_{\mathfrak{m}m}$.
  if no transmission for backhaul link **then**
    A-MeNB assigns ω to MUE ($\hat{m}$) such that:
    for all $i \leq |\mathfrak{M}|$ **do**
      $\min \text{sort } \dfrac{r_m}{r_{\mathfrak{m}m}} \ \forall\ r_m | r_{\mathfrak{m}m}$
    end for
    mobile-cell AL shares ω with MUE ($\hat{m}$) DL such that:
     i. $\dfrac{r_{\hat{m}}}{r_{\mathfrak{m}\hat{m}}} < 1$
     ii. $\dfrac{r_{\hat{m}}}{r_{\mathfrak{m}\hat{m}}} < \dfrac{r_m}{r_{\mathfrak{m}m}} \ \forall\ \hat{m} \neq m,\ m \in \{1, 2, 3, ...|\mathfrak{M}|\}$.
  end if
end for

where $\mathfrak{A} = \frac{\pi}{2}\sqrt{\frac{\mho}{P_{\mathcal{M}}}}\left(\lambda_{\mathcal{M}}\sqrt{P_{\mathcal{M}}}+\kappa\lambda\sqrt{P_{\mathcal{S}}}\right)$ and $\mathfrak{B} = 1+\frac{P_{\tilde{a}}\mho\epsilon}{P_{\mathcal{M}} r_{\mathfrak{m}m}}$. Since $\frac{\partial\, p_{MUE}}{\partial r_m} < 0$ in Eq. (5.64), the condition that Eq. (5.62) decreases monotonically with respect to r_m is satisfied [155].

To summarize, an MUE will have high success probability if it is located closer to A-MeNB, while at the same time positioned at a farther distance away from the mobile-cell which shares the sub-channel ω. Next, we will present an algorithm to select a MUE that suffices the above mentioned condition.

5.4.1 Dynamic User Scheduling Algorithm

We propose dynamic user scheduling algorithm (DUSA) to select a MUE which is farthest away from the mobile-cell, while at the same time closer to the A-MeNB. Without the loss of generality, we now focus our analysis on those MUEs that are associated only to A-MeNB. The A-MeNB-to-MUE association is based on the distance which means that the macro-cell users within the coverage radius of $R_{\mathcal{M}}$ around A-MeNB are associated with A-MeNB. Mathematically, our goal is to choose an MUE that minimizes $\frac{r_m}{r_{\mathfrak{m}m}}$.

The MUEs associated with A-MeNB are distributed as stationary point process $\Phi_m \sim \mathrm{PPP}(\lambda_m)$. If $\mathfrak{M}$ MUEs are registered with A-MeNB, then average number of MUEs is $|\mathfrak{M}| = \lambda_m |B|$, and $|B| = \pi R_{\mathcal{M}}^2$ is the area-bound around A-MeNB. Conditioned on this area-bound $|B|$, with slight abuse of terminology, we can say that $\hat{\Phi}_{\mathfrak{M}}$ is a binomial point process (BPP) with $|\mathfrak{M}|$ points [Sec. 2.2.2, [128]]. Each MUE is located at a different and unique geographic location around A-MeNB. According to DUSA, for each time unit, the A-MeNB sorts the list of MUEs in the increasing order of the ratio $\frac{r_m}{r_{\mathfrak{m}m}}$. A-MeNB assigns sub-channel ω to AL of mobile-cell $\mathfrak{m}$ and MUE $\hat{m}$ such that $\frac{r_{\hat{m}}}{r_{\mathfrak{m}\hat{m}}} < 1$ and $\frac{r_{\hat{m}}}{r_{\mathfrak{m}\hat{m}}} < \frac{r_m}{r_{\mathfrak{m}m}}\ \forall\ \hat{m} \neq m,\ m \in \{1, 2, 3, ...|\mathfrak{M}|\}$. This arrangement ensures that interference from the mobile-cell's AL to the downlink transmission of MUE remains low.

Another parameter of interest while proposing resource sharing is the ergodic rate per sub-channel at each link. It is essential that each link achieves high ergodic rate, for which, we will provide analysis in the next section.

5.5 Ergodic Rate and Sub-Channel Reuse

The cellular users are more concerned about the data rate that they acheive per link. We have measured the same in terms of ergodic rate in nats/sec/Hz (1 nat $\approx$ 1.443 bits). Later on, the analysis for sub-channel reuse parameter is also presented in this section.

5.5.1 Backhaul Link

The ergodic rate for backhaul link is given as [106]:

$$T_{BL} = \int_0^\infty \mathbb{E}[\ln(1 + \Upsilon_1(\omega, M \to m))] f(r_{\mathfrak{m}}) dr_{\mathfrak{m}}, \tag{5.65}$$

For a positive random variable ζ, $\mathbb{E}[\zeta] = \int\limits_{\tau>0} \mathbb{P}(\zeta > \tau) d\tau$ [106].

$$T_{BL} = \int_0^\infty \int_0^\infty \mathbb{E}[\, \ln(1 + \frac{P_{\mathcal{M}} r_{\mathfrak{m}}^{-\alpha_i} h_{M,\mathfrak{m}}^{\omega}}{I_{\mathcal{M}} + I_{\mathcal{S}} + I_{\tilde{a}} \gamma \epsilon})] d\tau dr_{\mathfrak{m}}, \tag{5.66}$$

For $\alpha_i = 4$, and $\bar{\iota} = \lambda_{\mathcal{M}} \pi r_{\mathfrak{m}}^2$, the rate expression can be written as:

$$T_{BL} = \int_{\bar{\iota}=0}^{\infty}\int_{\tau=0}^{\infty} \exp\Big\{\bar{\iota}\Big[1+\sqrt{e^{\tau}-1}\Big(\frac{\pi}{2}-\tan^{-1}\frac{1}{\sqrt{e^{\tau}-1}}+ \frac{\kappa}{2}\frac{\lambda_{\mathcal{S}}}{\lambda_{\mathcal{M}}}\sqrt{\frac{P_{\mathcal{S}}}{P_{\mathcal{M}}}}\Big)\Big]\Big\} \times \frac{1}{1+\frac{(e^{\tau}-1)\mathcal{F}\bar{\iota}^2}{\pi^2\lambda_{\mathcal{M}}^2}}\, d\tau\, d\bar{\iota}, \quad (5.67)$$

where $\mathcal{F} = \dfrac{P_{\tilde{a}}\gamma\epsilon}{P_{\mathcal{M}} r_{\tilde{a}\mathfrak{m}}^4}$. Note that Eq. (5.67) is the combination of two improper integrals and remains intractable in this current form. Considering $g = \dfrac{1}{1+\tau}$ and $\sigma = \dfrac{1}{1+\bar{\iota}}$, we get the definite integral form for Eq. 5.67 which can be solved using numerical integration method [106].

$$T_{BL} = \int_0^1\int_0^1 \exp\Big\{-\Big[1+\sqrt{e^{\frac{1}{g}-1}-1}\Big(\frac{\pi}{2}-\tan^{-1}\frac{1}{\sqrt{\exp(1/g-1)-1}}+\frac{\kappa\lambda_{\mathcal{S}}}{2\lambda_{\mathcal{M}}}\sqrt{\frac{P_{\mathcal{S}}}{P_{\mathcal{M}}}}\Big)\Big] \Big(\frac{1}{\sigma}-1\Big)\Big\} \times \frac{1}{g^2\sigma^2\Big[1+(\frac{1}{\sigma}-1)^2\Big(\frac{\mathcal{F}\exp(1/g-1)-1}{\lambda_{\mathcal{M}}^2\pi^2}\Big)\Big]}\, d\sigma\, dg. \quad (5.68)$$

5.5.2 Access Link

The ergodic rate for access link can be found as:

$$T_{AL} = \mathbb{E}[\ln(1+\Upsilon_3) > \psi], \quad (5.69)$$

$$T_{AL} = \int_{\psi>0} \mathbb{E}_{I_{\mathcal{M}}}[P[h_{\tilde{a}} > (e^{\psi}-1)\frac{\epsilon I_{\mathcal{M}} r_{\tilde{a}v}^{\alpha_o}}{P_{\tilde{a}}}]]d\psi, \quad (5.70)$$

$$T_{AL} = \int_{\psi>0} \mathbb{E}[1-F_{h_{\tilde{a}}}(X)]d\psi, \quad (5.71)$$

$$T_{AL} = \int_{\psi>0}\sum_{j=0}^{\infty}\sum_{\bar{j}=0}^{j}\frac{K^j(1-e^{\psi})^{j-\bar{j}}}{e^K.j!\,(j-\bar{j})!} \sum_{q=0}^{\infty}\frac{(-1)^q\Omega^q}{q!}(e^{\psi}-1)^{2q/\alpha_i-(j-\bar{j})}\Psi_{(2q/\alpha_i,j-\bar{j})}d\psi, \quad (5.72)$$

where $\Psi_{(2q/\alpha_i, j-\bar{j})}$ is given in Eq. (5.33).

$$T_{AL} = \int\limits_{\psi>0} \sum_{j=0}^{\infty} \sum_{\bar{j}=0}^{j} \sum_{q=1}^{\infty} \frac{K^j (-1)^{j-\bar{j}+q} (e^{\psi} - 1)^{2q/\alpha_i}}{e^K . j! \, (j-\bar{j})!} \frac{\Omega^q}{q!} \Psi_{(2q/\alpha_i, j-\bar{j})} \, d\psi, \tag{5.73}$$

Considering $g = \dfrac{1}{1+\psi}$, Eq. (5.73) can be further simplified as:

$$T_{AL} = \int\limits_0^1 \frac{1}{g^2} \sum_{j=0}^{\infty} \sum_{\bar{j}=0}^{j} \sum_{q=1}^{\infty} \frac{K^j (-1)^{j-\bar{j}+q} (e^{\frac{1}{g}-1} - 1)^{2q/\alpha}}{e^K j! \, (j-\bar{j})!} \frac{\Omega_k^q}{q!} \Psi_{(2q/\alpha_i, j-\bar{j})} \, dg. \tag{5.74}$$

5.5.3 Out-of-vehicle Cellular-link

Finally, the ergodic rate of MUE m is given as:

$$T_{MUE} = \int_0^1 \frac{\exp\big(- \tilde{A} \sqrt{e^{\frac{1}{\tilde{g}}-1} - 1} \big)}{\tilde{g}^2 (1 + \tilde{B}(e^{\frac{1}{\tilde{g}}-1} - 1))} d\tilde{g}. \tag{5.75}$$

where $\tilde{A} = \dfrac{\pi r_m^2 (\lambda_{\mathcal{M}} + \lambda_{\mathcal{S}} \kappa \sqrt{\frac{P_{\mathcal{S}}}{P_{\mathcal{M}}}})}{2}$ and $\tilde{B} = \dfrac{1}{P_{\mathcal{M}}} \Big(\dfrac{r_m}{r_{\mathfrak{m}m}} \Big)^2$.

The proof for T_{MUE} is trivial and follows the steps used to derive Eq. (5.68). Note that we have used numerical integration to solve Eq. (5.68), Eq. (5.74) and Eq. (5.75). The results are reported in Section 5.6. Next, we will present the sub-channel reuse parameter to demonstrate the spectral efficiency of proposed resource sharing scheme.

5.5.4 Sub-channel Reuse Parameter

The sub-channel reuse parameter ($\mathcal{Q}_\omega$) specifies the number of links that share a sub-channel under A-MeNB's coverage. Mathematically, we can write this parameter as:

$$\mathcal{Q}_\omega = 2 + \sum_{\eta=1}^{\lambda_{\mathcal{S}}|B|} \kappa_\eta. \tag{5.76}$$

Table 5.2: Parameters for Monte-Carlo simulations.

Parameter	Values
Total simulation runs	10,000
Simulation area	40×40 Km^2
α_i, α_o	4, 3.5
$\lambda_{\mathcal{M}}$	2×10^{-6}
$\lambda_{\mathcal{S}}$	$10\lambda_{\mathcal{M}}$
$r_{\tilde{a}v}, r_{\tilde{a}\mathfrak{m}}$	8 meters, 5 meters
κ	0, 1
$P_{\mathcal{S}}$	3, 23 dBm

where κ_η is an indicator function such that $\kappa_\eta \in 0, 1$. When small-cell η transmits on the sub-channel ω then $\kappa_\eta = 1$, and $\kappa_\eta = 0$ when small-cell is silent. It can be observed from Eq. (5.76) that $\mathcal{Q}_\omega$ has a linear relationship with the small-cells' density ($\lambda_{\mathcal{S}}$) along with the indicator function κ_η. Intuitively, when no small-cell shares ω with mobile-cell, then $\mathcal{Q}_\omega = 2$.

In the next section, we will provide the results of our analysis and Monte-Carlo simulation for the proposed resource sharing scheme.

5.6 Results and Discussion

To demonstrate the validity of our analysis of the proposed schemes, we have performed Monte-Carlo simulations. In Table 5.2, we have presented the most important parameters used in our simulations.

Backhaul link's Performance

The success probability of backhaul link over a given SIR range is shown in Figure 5.5. We have considered following cases: (i) $\kappa = 0$, (ii) $\kappa = 1$ with $P_{\mathcal{S}} = 3$ dBm, and (iii) $\kappa = 1$ with $P_{\mathcal{S}} = 23$ dBm. It can be seen that the success probability remains almost the same for the two cases (i) when $\kappa = 0$, and (ii) when small-cells' transmit power is low ($P_{\mathcal{S}} = 3$ dBm). On the contrary, when the small-cells transmit with high power, success probability is lower than the other two cases. It can be deduced from Figure 5.5 that the main contributor to interference on BL is the spatially closer AL-antenna. On the other hand, the low-powered small-cell transmission only marginally affects the success probability of BL.

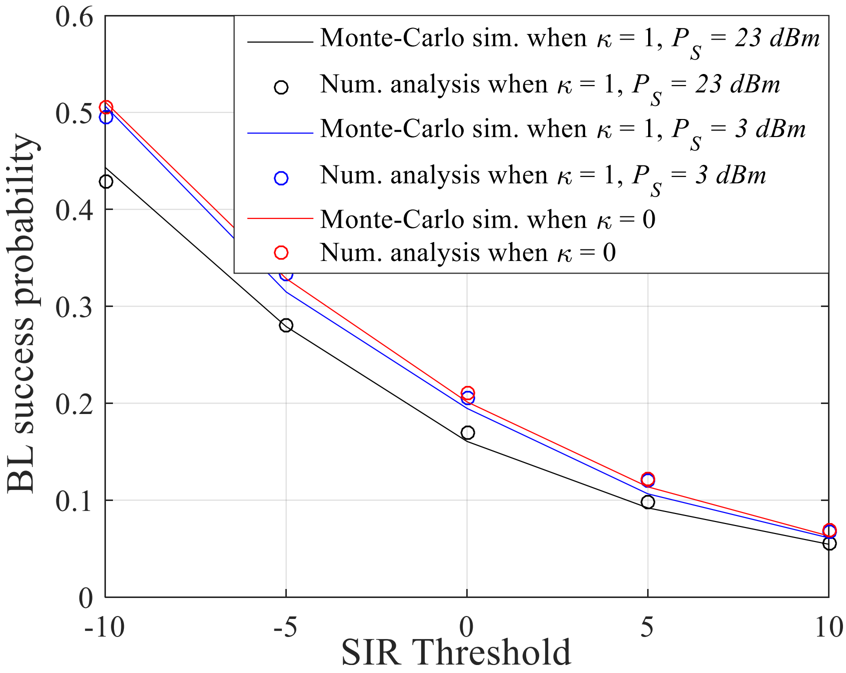

Figure 5.5: Success probability of backhaul link with $\lambda_{\mathcal{M}} = 2 \times 10^{-6}, \lambda_{\mathcal{S}} = 10\lambda_{\mathcal{M}}$, $\epsilon = 0.1$, $\gamma = 1$ (i.e., No SIC), and $\wp = 0.1$. © 2019 IET [39].

A combined effect of $\mho, \epsilon$ on backhaul is shown in Figure 5.6. It can be observed that BL's quality gets higher as ϵ gets lower, especially for lower SIR-thresholds regions. Figure 5.7 shows the impact of successive SIC on the BL. Intuitively, for ideal SIC-enabled reception, higher success probability for the link is achieved. In the absence of SIC, link quality degrades drastically, particularly in regions with high SIR-threshold values. The slight differences between the analytical and simulation results (see Fig. 5.7 and Fig. 5.8) are because of the use of numerical approximations in Eq. 5.11 and Eq. 5.13 in Section 5.3, and Eq. 5.67 in Section 5.5.

The ergodic capacity for the BLs are shown in Figure 5.8. It can be observed that the capacity per sec/Hz increases if SIC is enabled at the backhaul. Note that even if the macro-cell deployment is sparse (e.g., when $\lambda_{\mathcal{M}} = 2 \times 10^{-6}$), backhaul's ergodic rate with 90% SIC is much higher as compared to the case when macro-cells are densely deployed (e.g., $\lambda_{\mathcal{M}} = 4 \times 10^{-6}$), but with no SIC. Next, we will present the performance of the access link of mobile-cell.

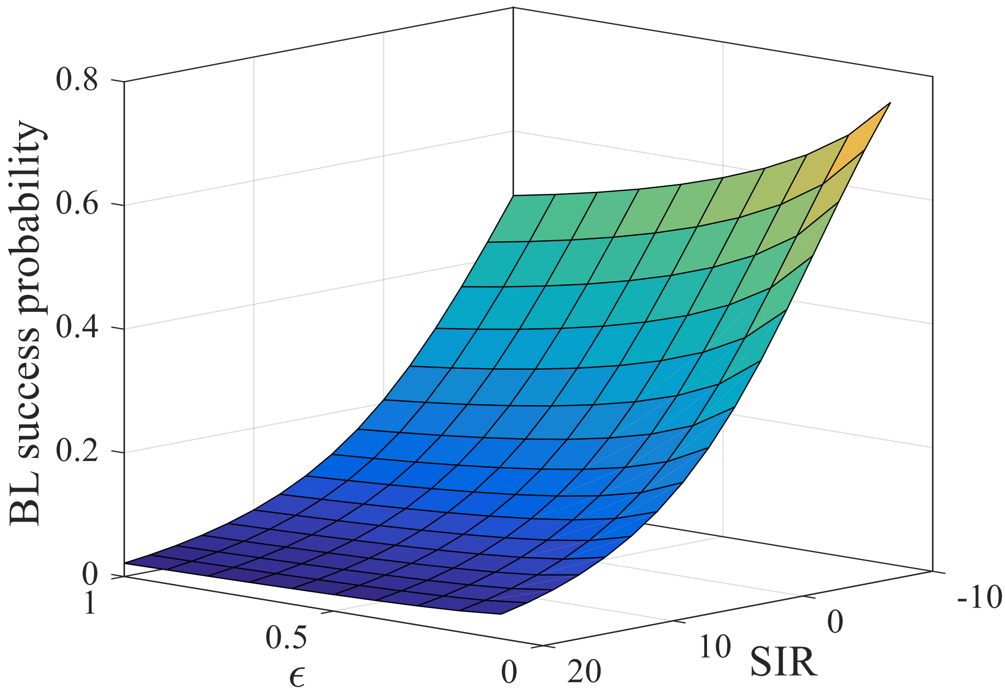

Figure 5.6: Dependence of backhaul link's success probability on SIR and ϵ ($\lambda_{\mathcal{M}} = 2 \times 10^{-6}, \kappa = 1, P_{\mathcal{S}} = 3dB, \wp = 0.1$). © 2019 IET [39].

Access Link's Performance

The AL experiences strong LoS component of the transmission from AL-antenna. For this reason, very high success probability is achievable, even at higher values of $\mho$ and ϵ. This is evident from the results presented in Figure 5.9. Note that the success probability reaches 1 when high vehicular penetration loss prevents out-of-vehicle interference ($\epsilon = 0.1$). Furthermore, the success probability for AL deteriorates significantly at high SIR regions, for poorly isolated mobile-cell's structure ($\epsilon = 0.8$). We have assumed Rician K-factor as 2 dB, which means that there exists a nominally dominant LoS component as compared to the multipath components. If we assume a very strong LoS, then the quality of AL will be very high in all cases. However, in practice, K does not attain such high values.

Figure 5.10 shows the relationship between success probabilities of access and backhaul links. The AL's success probability increases with an increase in AL-antenna's transmit power. The subsequent effect of AL's success probability on the BL can be observed on the y-axis of Figure 5.10. It can be observed that

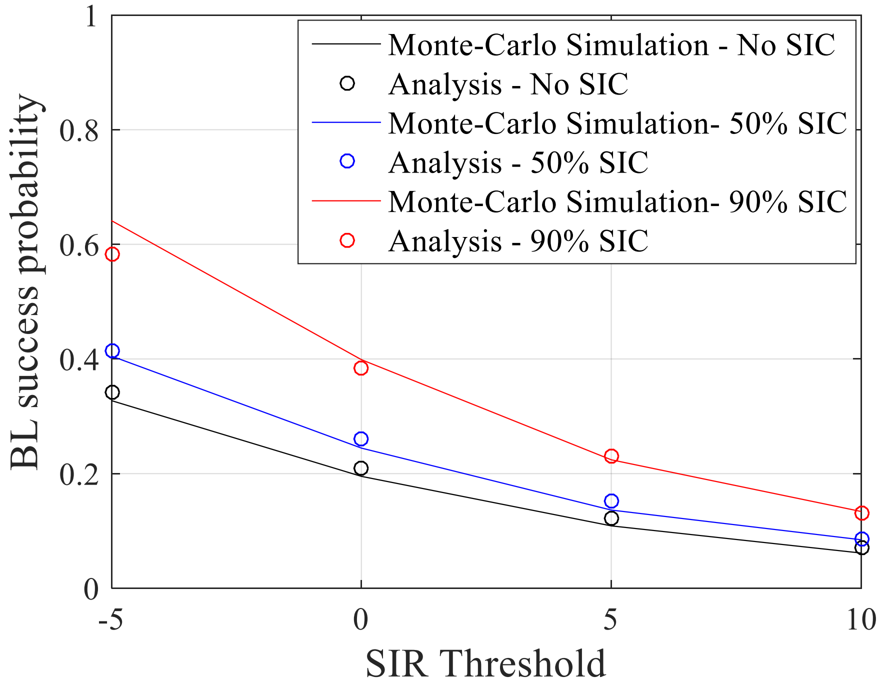

Figure 5.7: SIC effect on backhaul link ($\epsilon = 0.1$, $\lambda_{\mathcal{M}} = 2 \times 10^{-6}, \kappa = 0, \wp = 0.1$). © 2019 IET [39].

with high vehicular penetration loss along with using accurate SIC suppression both links acheive high success probabilities. For example, when $\epsilon = \gamma = 0.1$, $\kappa = 1$ and AL's success probability is greater than or equal to 70%, backhaul coverage does not get lower than 65%. The QoS of both links depends, among other factors, on the transmission power of AL-antenna (see Eq. (5.49)). It follows that by adjusting AL-antenna's transmit power ($P_{\tilde{a}}$), we can enhance the link quality at the backhaul.

Performance of MUE's Downlink

We have proposed that resource sharing between access link and out-of-vehicle macro-cell user is enabled using DUSA algorithms. We have compared DUSA with the random-selection (RS) scheme in Figure 5.11. In a RS scheme, a randomly selected MUE shares sub-channel ω with mobile-cell's AL. During each iteration, we randomly deployed a single mobile-cell and $|\mathfrak{M}| = \lambda_m \pi R_{\mathcal{M}}^2$ MUEs under the coverage radius of 1 Km around A-MeNB. The results in Figure 5.11 show that DUSA significantly improves the quality of downlink success probability for MUEs by selecting each device that is closest to A-MeNB and farther away

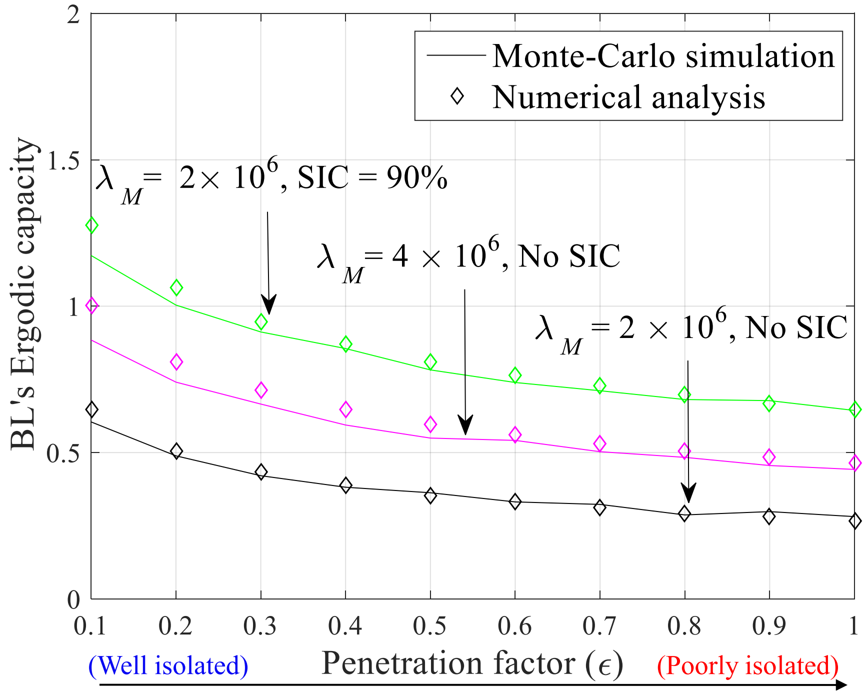

Figure 5.8: Ergodic rate for backhaul link in nats/sec/Hz. © 2019 IET [39].

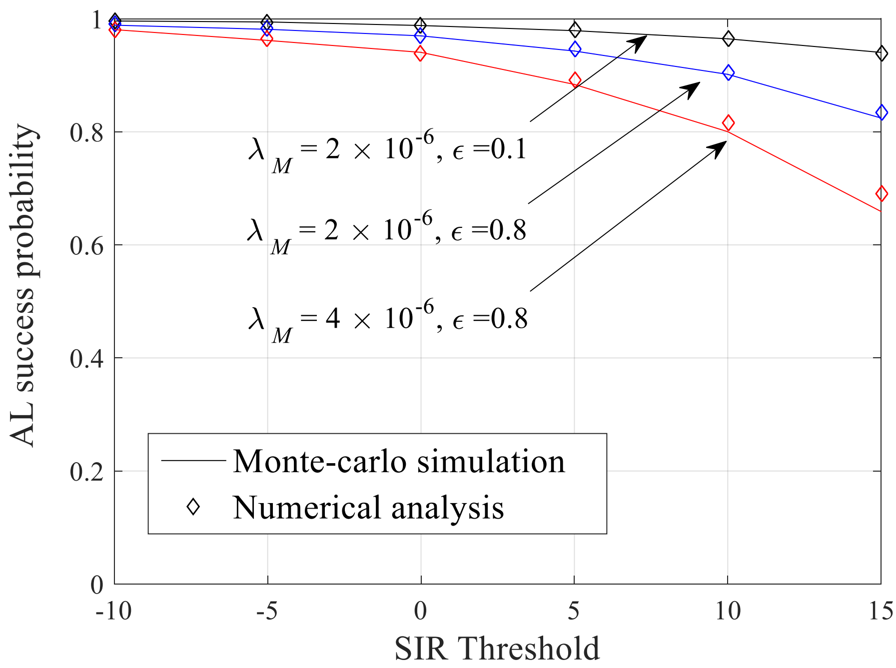

Figure 5.9: Success probability for access link ($\kappa = 0$, $\gamma = 1$(i.e., No SIC), $\wp = 0.1$, $J, Q = 70$.) © 2019 IET [39].

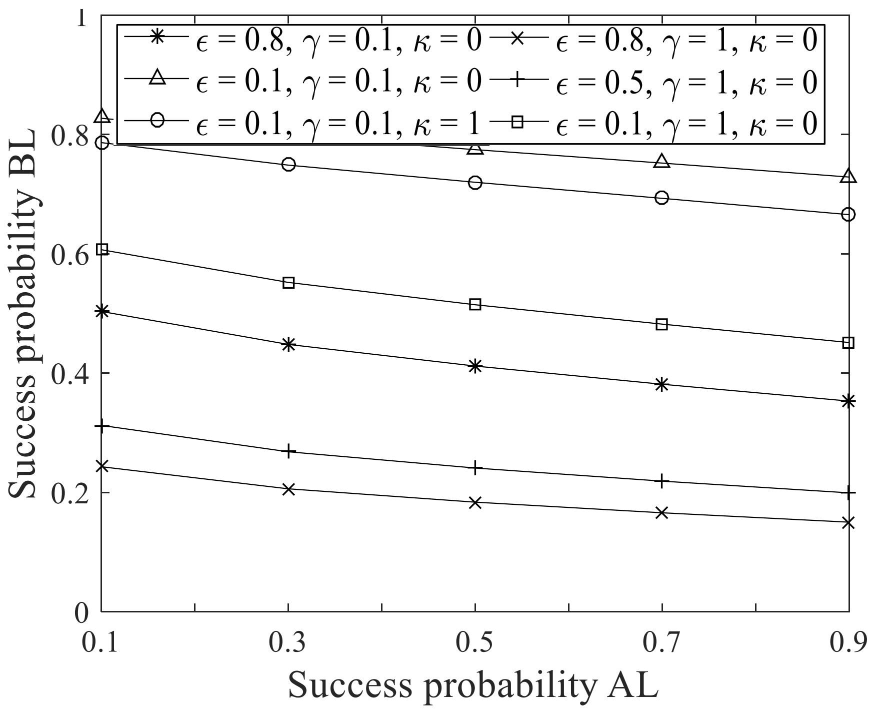

Figure 5.10: Success probability: Backhaul vs Access links $(\lambda_{\mathcal{M}}, \kappa, \mho, \wp = \{2 \times 10^{-6}, 0, -10, 0.1)\}$. © 2019 IET [39].

from the mobile-cell. The success probability for DUSA degrades when there is sparse population of MUE (e.g., $\lambda_m = 3.18 \times 10^{-5}$), particularly at high SIR thresholds. However, this reduced success probability is still distinctively greater than the performance achieved by RS algorithm. We can observe that λ_m has little effect on the performance of RS algorithm and very low success probability for MUEs is achieved in all cases. We will show the impact of mobile-cell's mobility on the success probability of MUE in the next sub-section.

Effect of Mobility on MUE

Figure 5.12 shows the impact of mobile-cell's mobility on the success probability of macro-cell user. We have selected three "mobile-cell and MUE" pairs using DUSA. We considered the worst case scenario when a mobile-cell moves with a high speed (150 Km/hr $\approx$ 42 m/s) towards the MUE. We have observed the sub-channel sharing for a 1-second interval. The distances are normalized such that the maximum distance between mobile-cell and MUE is $r_{\mathfrak{m}m} \approx 42$ m. The mobile-cell moves in a straight line towards MUE [43, 60].

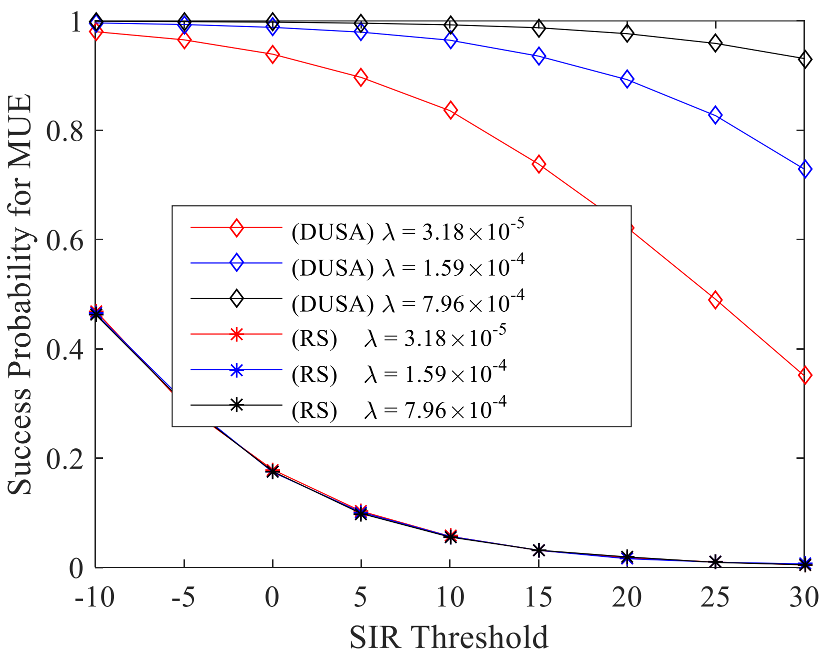

Figure 5.11: DUSA versus RS ($R_{\mathcal{M}} = 1$ Km, $\lambda_{\mathcal{M}} = 2 \times 10^{-6}, \lambda_{\mathcal{S}} = 10\lambda_{\mathcal{M}}, \epsilon = 0.1, \kappa = 1, P_{\mathcal{M}}, P_{\mathcal{S}}, P_{\tilde{a}} = 45, 23, 3$ dBm). © 2019 IET [39].

Interestingly, the performance of MUE that is closer to A-MeNB does not deteriorate due to mobile-cell's mobility because $P_{\mathcal{M}} >> P_{\tilde{a}}$, and the effect of mobile-cell's AL-interference is very low.

5.7 Conclusion

In this chapter, we have proposed a resource sharing scheme for mobile-cell's AL with out-of-vehicle links, including BL and macro-cell users. According to our scheme, the downlink AL will share the sub-channel with the BL when A-MeNB transmits to the mobile-cell. In case there is no transmission from A-MeNB to the mobile-cell, AL will share the sub-channel with the downlink transmission of out-of-vehicle macro-cell user. We have proposed an algorithm to select the MUE such that it receives minimum interference from AL transmission. We have used directional antenna for AL and exploited successive interference cancellation at the backhaul to ensure that such aggressive resource sharing does not deteriorate performance of any of the links. The directional AL-antenna ensures high QoS for in-vehicle users even at low transmit power, while at the same time minimizes the

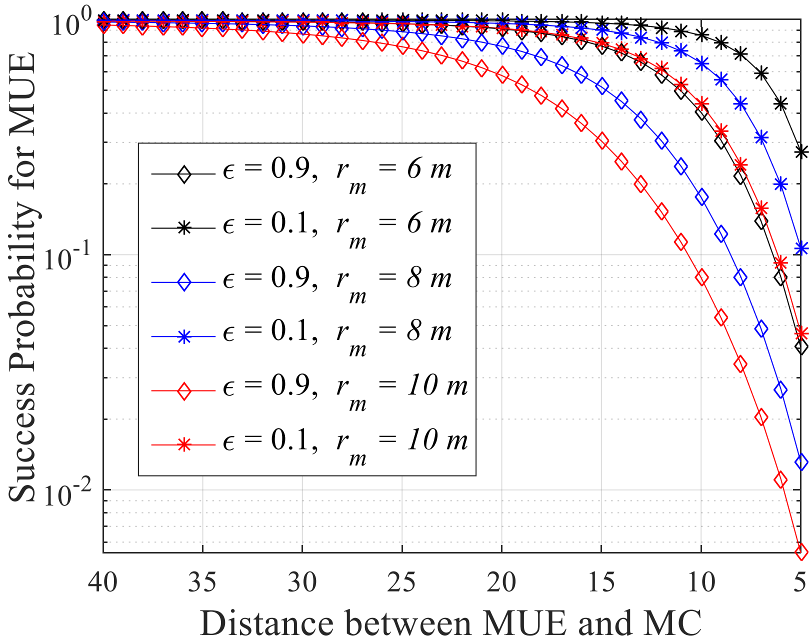

Figure 5.12: Mobile-cells mobility towards m ($\lambda_{\mathcal{M}} = 2 \times 10^{-6}, \lambda_{\mathcal{S}} = 10\lambda_{\mathcal{M}}, \mho = 20$ dB, $\kappa = 1, P_{\mathcal{M}}, P_{\mathcal{S}}, P_{\tilde{a}} = 45, 23, 3$ dBm). © 2019 IET [39].

interference to spatially closer BL-antenna. On the other hand, vehicular penetration loss is exploited to further reduce the interference between in-vehicle and out-of-vehicle resource sharing links. We have demonstrated, through analysis and simulation, that high success probabilities and ergodic rates are achievable for all resource sharing links when VPL is high and SIC is highly efficient. We have also proposed transmit power control for AL transmission to further enhance SIR at the BL without compromising on the in-vehicle link quality. We have also demonstrated the effect of mobile-cell's mobility on the proposed resource sharing scheme. The results have shown that the resource sharing achieves high success probability for out-of-vehicle cellular user even when mobile-cell is traveling at high speed towards the user.

In the next chapter, we will present resource sharing for uplink access link with sidehaul link between mobile-cells and out-of-vehicle cellular user.

5.8 Related Publications

- **Shan Jaffry**, Syed Faraz Hasan, Xiang Gui, "Shared Spectrum for Mobile-Cell's Backhaul and Access Link", IEEE Global Communications Conference (IEEE Globecom), December 2018, Abu-Dhabi, UAE.
- **Shan Jaffry**, Syed Faraz Hasan, Xiang Gui, "Interference Management and Resource Sharing in Moving Networks", IET Communications, (*under review*).

Chapter 6

Sidehaul and Uplink Access Link Resource Sharing

6.1 Introduction

We have proposed resource sharing for mobile-cell's downlink access link (AL) with backhaul transmission or out-of-vehicle macro-cell user in the previous chapter. In this chapter, we now focus on resource sharing between mobile-cell's uplink AL and sidehaul link (SL), along with uplink communication for the macro-cell cellular user (CU). Like before, we will derive expressions for success probability and ergodic rates of all the resource sharing links.

A mobile-cell's in-vehicle antenna provides cellular services to commuters over the AL and communicates with the core network over backhaul link (BL). The communication between neighboring mobile-cells, or between mobile-cell and out-of-vehicle cellular user is established over the SLs (see Fig. 6.1). An out-of-vehicle antenna is installed on the roof of the vehicle for backhaul and sidehaul communication. Mobile-cell's SL is essential to exchange data, such as cached content, with its neighbors [26]. In [23, 30], the authors have shown that the SL may provide connectivity in regions with low or no cellular coverage. In [31], the authors have demonstrated that mobile-cells can provide services to the cell-edge users using SLs to enhance coverage of cellular network.

Resource allocation problems for mobile-cells' links are uniquely challenging. On the one hand resources assigned to mobile-cells' multiple wireless links should not deteriorate the spectral efficiency of the network. On the other hand, these links should minimally interfere with the out-of-vehicle cellular users. In

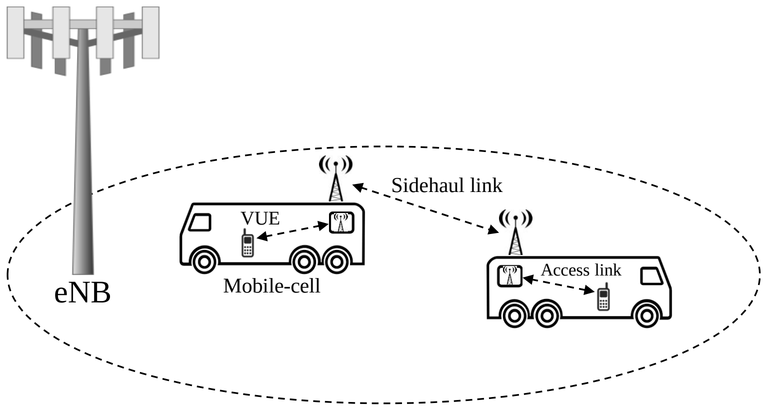

Figure 6.1: Mobile-cells communicating over ALs and SL.

Chapter 2, we have already discussed that most of the related works assigned dedicated frequency resources to the individual mobile-cells' links [26, 123, 144]. However, the solutions that assign dedicated resources to individual links are spectrally inefficient and require additional sub-channels. Given the limited availability of spectral resources, such schemes may not be very practical. Hence, in this Chapter, our focus is to provide spectrally efficient scheme so that mobile-cell does not require additional resources from the cellular spectrum.

6.1.1 Research Contribution

Our contribution in this chapter is to enable the resource sharing among the following three links: (i) CUs transmitting to eNB, (ii) mobile-cell's uplink AL and (iii) SL between neighboring mobile-cells. For successful resource sharing, we will exploit VPL and successive interference cancellation (SIC) technique. Note that due to VPL, the strength of wireless signal may drastically reduce as it travels through metallic body of the vehicle. Exploiting this fact, we can utilize the same sub-channel for in-vehicle and out-of-vehicle transmissions. On the other hand, we will employ SIC to enhance the signal-to-interference ratio (SIR) for the sidehaul signals [156]. We have mathematically formulated the success probabilities and ergodic rates for all the resource sharing links. Our scheme will ensure that the access and sidehaul links of a mobile-cell do not require additional spectral resources.

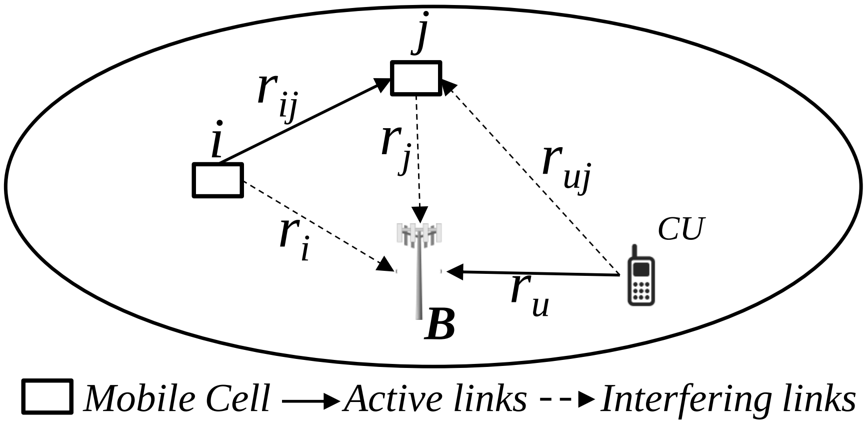

Figure 6.2: A mobile-cell communication scenario with active and interfering links. The uplink AL for MC j is not presented. © 2019 IEEE [40].

6.1.2 Chapter Organization

The rest of this chapter contains the following: The system model is presented in Section 6.2. In Section 6.3 we will derive the expressions for success probabilities and ergodic rates for all the resource sharing links which will act as the basis for the algorithms that we will propose in Section 6.4. We will discuss results in Section 6.5 and conclude this chapter in Section 6.6. The publication related to this chapter is presented in Section 6.7

6.2 System Model

We have considered a single-cell environment in which eNB B is at the origin as shown in Figure 6.2. The out-of-vehicle CUs form a set $\mathcal{U}$ and mobile-cells form a set $\mathcal{M}$. All CUs and mobile-cells are distributed uniformly and randomly with density λ_u and λ_m (per m^2), respectively. All CUs are considered static at all times and are denoted as $u \in \{1, 2, 3, ...|\mathcal{U}|\}$, where $|.|$ shows the cardinality of the set. Without the loss of generality, we consider $i, j \in \mathcal{M}$ as two neighboring mobile-cells where i is the transmitter and j is the receiver in a sidehaul communication. We employ SIC at the sidehaul receiver. A common communication control unit (CCU) manages the communication process within mobile-cells [145]. The CCU performs the decoding and cancellation of the stronger AL interfering signal at the out-of-vehicle antenna to increase the quality of SL [156]. We assume that the mobile-cells are not aware of the SIC capabilities of the respective neighbors. Each device (i.e., mobile-cell and cellular users) is equipped with a localization system, for example as discussed in [147], which can determine device's location. The devices may transmit their positioning information to eNB on periodic basis over the control channels. Hence, the eNB knows the devices' locations for any given time-slot T. Note that T is a very short time period, typically in the scales of milli-seconds. The mobile-cells remain static only during T [124, 126].

The number of commuting users inside a vehicle may vary. However, for the sake of mathematical tractability and without the loss of generality, we consider a single in-vehicle user equipment (VUE) v_m having active uplink access link communication inside mobile-cell $m \in \mathcal{M}$, and $\tilde{a}_m$ represents the AL-antenna of m. The sub-channel $\omega \in \mathcal{W}$ is shared across three links: $u \to B$, $i \to j$, and $v_j \to \tilde{a}_j$. We collectively call these resource sharing links as a 'trio'. The total number of sub-channels are $|\mathcal{W}|$ where $\mathcal{W}$ is the set denoting individual sub-channel ω, such that $\omega = \{1, 2, 3, ...|\mathcal{W}|\}$.

All links follow standard pathloss model $r^{-\alpha}$ as slow fading, where r is the transmitter-to-receiver distance and α is the general pathloss exponent. In particular, we have considered α_o as out-of-vehicle pathloss exponent and α_{in} as in-vehicle pathloss exponent. The quasi-static Rayleigh channel represents fast fading [126]. We have further considered the additive white Gaussian noise with constant average power η^2.

The signal-to-interference-plus-noise ratio (SINR) of CU u's uplink transmission at eNB B at a given time-slot T over ω is:

$$\Upsilon_{UL}^{T} = \frac{P_u r_u^{-\alpha_o} h_{uB}^{\omega}}{I_i + I_{v_j}\varepsilon + \eta^2}. \tag{6.1}$$

where P_{t_x} is the transmit power from transmitter t_x and $h_{t_x t_r}^{\omega}$ denotes exponentially distributed fading power of ω between transmitter-receiver pair $t_x - t_r$. $I_i = P_i r_i^{-\alpha_o} h_{iB}^{\omega}$, $I_{v_j} = P_{v_j} r_j^{-\alpha_o} h_{jB}^{\omega}\varepsilon$ are the interferences from the SL transmission of mobile-cell i and from VUE v_j's AL, respectively. The distances from $u, i, j \to B$ are given as r_u, r_i, r_j, respectively. The VPL factor is denoted by ε such that $0 < \varepsilon \leq 1$. As before, the VPL factor represents the quality of isolation between in-vehicle and out-of-vehicle links. The higher values of ε represent lower isolation.

Table 6.1: System model parameters

Symbol	Definition
B	Macro-cell eNB.
$\mathcal{M}$,$\mathcal{U}$	Set of mobile-cells and out-of-vehicle cellular users.
$\lambda_{\mathcal{M}}, \lambda_{\mathcal{U}}$	Density of mobile-cells, and CUs.
m, u, v_m	Single mobile-cell, cellular user, in-vehicle user inside m.
i, j	Transmitter for sidehaul link, receiver for sidehaul link.
$\tilde{a}_j$	In-vehicle access link antenna.
r_u, r_i, r_j	Distance $u \to B,\ i \to B,\ j \to B$.
$P_u,\ P_i,\ P_{v_j}$	Uplink transmit power for u, MC i, and in-vehicle user.
α_{in}, α_o	In-vehicle and out-of-vehicle pathloss exponents.
$h^{\omega}_{t_x,t_r}$	Exponentially distributed fading power of channel between $t_x - t_r$ pair for sub-channel ω.
ε, γ	VPL factor, SIC factor $(0 < \epsilon \leq 1)$ $(0 \leq \gamma \leq 1)$.

SINR for uplink AL from VUE v_j to AL-antenna $\tilde{a}_j$ is:

$$\Upsilon^{T}_{_{AL}} = \frac{P_{v_j} l_{v_j}^{-\alpha_{in}} h^{\omega}_{v_j \tilde{a}_j}}{I_u \varepsilon + I_{ij}\varepsilon + \eta^2}. \tag{6.2}$$

where l_{v_j} is the distance between $v_j \to \tilde{a}_j$. $I_u = P_u r_{uj}^{-\alpha} h^{\omega}_{uj}$ and $I_{ij} = P_i r_{ij}^{-\alpha} h^{\omega}_{ij}$ are the interferences from the cellular link and i's sidehaul transmission, respectively. r_{uj} and r_{ij} are the distances between $j \to u$, and $i \to j$, respectively.

As for SL from mobile-cell i to j, if γ is the SIC parameter such that $\gamma \in [0, 1]$, then SINR is:

$$\Upsilon^{T}_{_{SL}} = \frac{P_i r_{ij}^{-\alpha_o} h^{\omega}_{ij}}{I_u + I_{v_j}\varepsilon\gamma + \eta^2}. \tag{6.3}$$

Note that in Eq. (6.3), $\gamma = 0.1$ represents 90% successful SIC. Likewise, $\gamma = 0.9$ indicates that there is only 10% success in SIC. The performance of SIC depends on the effectiveness of mobile-cell's CCU that manages communication for mobile-cell's links [145]. A list of all variables and their associations are presented in Table 6.1 for the readers' convenience. In the next section, we will mathematically formulate the parameters of success probabilities and ergodic rates for the resource sharing links.

6.3 Link Analysis

6.3.1 Success Probability

Ideally, in a wireless system, a unique sub-channel should be assigned to all individual users. However, when more than one user share a sub-channel then the signal from the intended transmitter is successfully decoded by the receiver if the received signal strength, measured in terms of SINR (Υ), is above a certain threshold level. Mathematically, this so-called success probability is defined as $\mathbb{P}\Big[\Upsilon > \theta\Big]$, where $\mathbb{P}$ denotes the probability of an event and θ is the SINR threshold.

For cellular users transmitting over sub-channel ω, the success probability can be written as:

$$p^{\omega}_{_{UL}} = \mathbb{P}[\Upsilon_{_{UL}} > \theta]. \tag{6.4}$$

$$p^{\omega}_{_{UL}} = \mathbb{E}\Bigg[\exp\Bigg(-\theta\frac{r_u^{\alpha_o}}{P_u}(I_i + I_{v_j}\varepsilon + \eta^2)\Bigg)\Bigg]. \tag{6.5}$$

$$p^{\omega}_{_{UL}} = \mathbb{E}\Bigg[\exp\Bigg(-\Big(\frac{r_u}{r_i}\Big)^{\alpha_o}\frac{\theta P_i h^{\omega}_{ui}}{P_u}\Bigg)\Bigg]\mathbb{E}\Bigg[\exp\Bigg(-\Big(\frac{r_u}{r_j}\Big)^{\alpha_o}\frac{\theta P_{v_j}\varepsilon h^{\omega}_{uj}}{P_u}\Bigg)\Bigg]e^{-\frac{\theta r_u^{\alpha_o}\eta^2}{P_u}}. \tag{6.6}$$

$$p^{\omega}_{_{UL}} = \frac{e^{-\theta r_u^{\alpha_o}\eta^2/P_u}}{[1+\theta\frac{P_i}{P_u}(\frac{r_u}{r_i})^{\alpha_o}][1+\theta\varepsilon\frac{P_{v_j}}{P_u}(\frac{r_u}{r_j})^{\alpha_o}]}. \tag{6.7}$$

where Eq. (6.5) follows the complimentary cumulative density function (CCDF) of exponentially distributed random variable $h^{\omega}_{uB} \sim \exp(1)$. The expectation $\mathbb{E}[.]$ is with respect to the random interference. Eq. (6.6) follows the independence of random variables h^{ω}_{iB} and h^{ω}_{jB}, and Eq. (6.7) follows the property of Laplace Transform for random variables, i.e., $\mathcal{L}_X(s) = \mathbb{E}[e^{-sX}]$. For $h^{\omega}_{t_x t_r} \sim \exp(1)$, $\mathcal{L}_{h^{\omega}_{t_x t_r}}(s) = \dfrac{1}{1+s}$.

Similarly, the success probabilities for AL is:

$$p^{\omega}_{_{AL}} = \frac{e^{-\theta l_{v_j}^{\alpha_{in}}\eta^2/P_{v_j}}}{[1+\theta\varepsilon\frac{P_u}{P_{v_j}}(\frac{l_{v_j}}{r_{uj}})^{\alpha_o}][1+\theta\varepsilon\frac{P_i}{P_{v_j}}(\frac{l_{v_j}}{r_{ij}})^{\alpha_o}]}. \tag{6.8}$$

For SL, success probability is calculated as:

$$p^{\omega}_{SL} = \frac{e^{-\theta r_{ij}^{\alpha_o}\eta^2/P_i}}{[1+\theta\frac{P_u}{P_i}(\frac{r_{ij}}{r_{uj}})^{\alpha_o}][1+\theta\varepsilon\gamma\frac{P_{v_j}}{P_i}(\frac{r_{ij}}{l_{v_j}})^{\alpha_o}]}. \tag{6.9}$$

Note that in Eq. (6.9) only α_o is considered because the AL signal will only act as the interference for all out-of-vehicle receivers.

6.3.2 Ergodic Rate

An important parameter when considering resource sharing by multiple links is the ergodic rate per link. Even if the signal is decoded successfully, it is of utmost importance that each link achieves high rates. We calculate the ergodic rate per sub-channel in nats/sec/hz (1 nat ≈ 1.443 bits). For a cellular user's uplink, the rate is given as:

$$T^{\omega}_{UL} = \mathbb{E}[\ln(1+\Upsilon_{UL})] \tag{6.10}$$

For a random variable $\zeta > 0$, $\mathbb{E}[\zeta] = \int\limits_{\sigma>0} \mathbb{P}[\zeta > \sigma] d\sigma$ [106]. Hence:

$$T^{\omega}_{UL} = \int\limits_{\sigma>0} \mathbb{P}\Big[h^{\omega}_{uB} > (e^{\sigma}-1)\Big[\frac{(I_i + I_{v_j}\varepsilon + \eta^2) r_u^{\alpha_o}}{P_u}\Big]\Big] d\sigma \tag{6.11}$$

$$T^{\omega}_{UL} = \int\limits_{\sigma>0} \mathbb{E}[\exp\big(-(e^{\sigma}-1)\frac{r_u^{\alpha_o}}{P_u} I_i - (e^{\sigma}-1)\frac{r_u^{\alpha_o}}{P_u} I_{v_j}\varepsilon)] e^{\frac{-(e^{\sigma}-1) r_u^{\alpha_o}\eta^2}{Pu}} d\sigma \tag{6.12}$$

Using $I_i = P_i r_i^{-\alpha_o} h^{\omega}_{iB}$, $I_{v_j} = P_{v_j} r_j^{-\alpha_o} h^{\omega}_{jB}\varepsilon$, we consider $s_1 = (e^{\sigma}-1)\Big(\frac{r_u}{r_i}\Big)^{\alpha_o}\Big(\frac{P_i}{P_u}\Big)$ and $s_2 = (e^{\sigma}-1)\Big(\frac{r_u}{r_j}\Big)^{\alpha_o}\Big(\frac{P_{v_j}}{P_u}\Big)\varepsilon$. Using Laplace Transform for random variable $\tilde{h} \sim \exp(1)$, we get:

$$T^{\omega}_{UL} = \int\limits_{0}^{\infty} \frac{e^{\frac{-(e^{\sigma}-1) r_u^{\alpha_o}\eta^2}{Pu}}}{(1+s_1)(1+s_2)} d\sigma \tag{6.13}$$

$$T^{\omega}_{UL} = \int_{0}^{\infty} \Bigg(\frac{e^{\frac{-(e^{\sigma}-1)r_u^{\alpha_o}\eta^2}{Pu}}}{[1+(e^{\sigma}-1)\mathcal{X}][1+(e^{\sigma}-1)\mathcal{Y}]}\Bigg) d\sigma \tag{6.14}$$

where $\mathcal{X} = \left(\frac{r_u}{r_i}\right)^{\alpha_o}\left(\frac{P_i}{P_u}\right)$ and $\mathcal{Y} = \left(\frac{r_u}{r_j}\right)^{\alpha_o}\left(\frac{P_{v_j}}{P_u}\right)\varepsilon$.

Since $\eta^2 << 1$, we use the fact that $\lim_{n\to 0} e^n \approx 1$ for smaller values of n [157],

$$T^{\omega}_{UL} \approxeq \int_{0}^{\infty} \Bigg(\frac{1}{[1+(e^{\sigma}-1)\mathcal{X}][1+(e^{\sigma}-1)\mathcal{Y}]}\Bigg) d\sigma \tag{6.15}$$

Now letting $\breve{a} = e^{\sigma} - 1$, we get:

$$T^{\omega}_{UL} = \int_{0}^{\infty} \Bigg(\frac{1}{[1+\breve{a}\mathcal{X}][1+\breve{a}\mathcal{Y}]}\Bigg) d\sigma \tag{6.16}$$

For $\breve{a} = e^{\sigma} - 1$, taking derivative on both sides with respect to σ, we get $d\sigma = \frac{1}{e^{\sigma}} d\breve{a} \Rightarrow \frac{1}{\breve{a}+1} d\breve{a}$. Hence, we can now write Eq. (6.16)as:

$$T^{\omega}_{UL} = \int_{0}^{\infty} \left(\frac{1}{1+\breve{a}}\right)\left(\frac{1}{1+\breve{a}\mathcal{X}}\right)\left(\frac{1}{1+\breve{a}\mathcal{Y}}\right) d\breve{a}, \tag{6.17}$$

Using the technique of Feynman Parametrization [158], Eq. (6.17) can be solved as:

$$T^{\omega}_{UL} = \frac{(\mathcal{X}-1)\mathcal{Y}\ln(\mathcal{Y}) - \mathcal{X}\ln(\mathcal{X})\mathcal{Y} + \mathcal{X}\ln(\mathcal{X})}{(\mathcal{X}-1)(\mathcal{Y}-1)(\mathcal{Y}-\mathcal{X})}. \tag{6.18}$$

Similarly, the ergodic rates for AL is computed as:

$$T^{\omega}_{AL} = \frac{(\mathcal{P}-1)\mathcal{Q}\ln(\mathcal{Q}) - \mathcal{P}\ln(\mathcal{P})\mathcal{Q} + \mathcal{P}\ln(\mathcal{P})}{(\mathcal{P}-1)(\mathcal{Q}^2 - (\mathcal{P}+1)\mathcal{Q} + \mathcal{P})}. \tag{6.19}$$

where $\mathcal{P} = \left(\frac{l_{v_j}^{\alpha_{in}}}{r_{uj}^{\alpha_o}}\right)\left(\frac{P_u}{P_{v_j}}\right)\varepsilon$ and $\mathcal{Q} = \left(\frac{l_{v_j}^{\alpha_{in}}}{r_{ij}^{\alpha_o}}\right)\left(\frac{P_i}{P_{v_j}}\right)\varepsilon$.

Finally, the ergodic rate for SL is:

$$T^{\omega}_{SL} = \frac{(\mathcal{K}-1)\mathcal{J}\ln(\mathcal{J}) - \mathcal{K}\ln(\mathcal{K})\mathcal{J} + \mathcal{K}\ln(\mathcal{K})}{(\mathcal{K}-1)(\mathcal{J}^2 - (\mathcal{K}+1)\mathcal{J} + \mathcal{K})}. \tag{6.20}$$

where $\mathcal{K} = \left(\frac{r_{ij}}{r_{uj}}\right)^{\alpha_o}\left(\frac{P_u}{P_i}\right)$ and $\mathcal{J} = \left(\frac{r_{ij}}{l_{v_j}}\right)^{\alpha_o}\left(\frac{P_{v_j}}{P_i}\right)\varepsilon\gamma$.

With the mathematical expression of success probability and ergodic rates derived in this section, the next section presents the resource sharing algorithm.

6.4 Resource Sharing Algorithm

Our main goal is to maximize the ergodic rate while enabling resource sharing for the trio. The total ergodic rate (R) for N trios is:

$$R = \sum_{\omega=1}^{N} R_{\omega}. \tag{6.21}$$

where $R_\omega = T_{UL}^{\omega} + T_{AL}^{\omega} + T_{SL}^{\omega}\ \forall\ \omega$.

Our main objective is:

$$\max \sum_{\omega=1}^{N} R_{\omega}. \tag{6.22}$$

$$\text{subject to (i)} \ \sum_{L} \beta_L^{\omega} \leq 3,$$

$$\text{(ii)} \ \ \beta_{v_i\tilde{a}_i}^{\omega}\beta_{ij}^{\omega} = 0,\ \ \beta_{v_j\tilde{a}_j}^{\omega}\beta_{ij}^{\omega} = 1$$

where β_L^{ω} is the binary indicator such that $\beta_L^{\omega} = 1$ if ω is assigned to link L and $\beta_L^{\omega} = 0$ otherwise. Constraint (i) ensures that a maximum of 3 links can be shared over ω, and constraint (ii) guarantees that ω is not assigned to VUE in i and is only assigned to VUE in j. This constraint guarantees minimal interference for the low-powered ALs.

While the brute-force (BF) search can provide optimal solution to the problem presented in Eq. (6.22), the associated computational costs will be high, especially for large number of mobile-cells and CUs. BF search calculates maximum R_ω by comparing all possible “CU to mobile-cell” combinations before forming a trio. This takes considerable time to converge, in particular when the number of CUs around eNB is very large. Random selection (RS) scheme may provide a quick solution by randomly selecting the nodes to form a trio, but cannot guarantee optimal rates. Hence, we propose two sub-optimal, yet less time consuming,

Algorithm 3 Dynamic Resource Sharing for mobile-cell

$\mathcal{U}, \mathcal{M}, \mathcal{W}$: Cellular users, Mobile-Cells, Sub-channels.
for time slot T **do**
  for all mobile-cell $i = 1 : \mathcal{M}$ **do**
    1. Select mobile-cell j as neighboring mobile-cell to establish SL
    2. Assign resource ω for
      (i) SL link between mobile-cell i and j
      (ii) AL for mobile-cell j
      (iii) Select $x, y, z \in \mathcal{U}$, such that
        $\forall \frac{r_u}{r_i} < 1$, $\frac{r_x}{r_i} = \min(\frac{r_u}{r_i})$
        $\forall \frac{r_u}{r_j} < 1$, $\frac{r_y}{r_j} = \min(\frac{r_u}{r_j})$
        $\forall \frac{r_{ij}}{r_{uj}} < 1$, $\frac{r_z}{r_j} = \min(\frac{r_{ij}}{r_{uj}})$
    3. Assign resource ω to CU u such that
        $u \in \{x, y, z\}$ and $r_u = \min(r_x, r_y, r_z)$
  end for
end for

algorithms to solve resource sharing problem. The basis for these algorithms originates from the analysis presented in Section 6.3. It is evident from Eqs. (6.7)-(6.9) and Eqs. (6.18)-(6.20) that the success probabilities and the ergodic rates are inversely related to the distance ratios $\frac{r_u}{r_i}$, $\frac{r_u}{r_j}$, and $\frac{r_{ij}}{r_{uj}}$. Therefore, in order to achieve high success probabilities, according to Eqs. (6.7)-(6.9), the ratios $\frac{r_u}{r_i}, \frac{r_u}{r_j}, \frac{r_{ij}}{r_{uj}}$, which depend on the selection of devices in euclidean plane, should be less than 1. The same condition applies for ergodic rates in Eqs. (6.18)-(6.20). We therefore have an additional constraint to ensure the distance limitation for all devices in a trio. Mathematically, we can write this constraint as:

$$\text{(iii)} \quad \frac{r_u}{r_i}, \frac{r_u}{r_j}, \frac{r_{ij}}{r_{uj}} < 1$$

It is important to note that $\frac{l_{v_j}^{\alpha_{in}}}{r_{uj}^{\alpha_o}}, \frac{l_{v_j}^{\alpha_{in}}}{r_{ij}^{\alpha_o}} < 1$ because generally $l_{v_j} < \{r_{uj}, r_{ij}\}$, but more importantly because $\alpha_{in} < \alpha_o$. The condition that $\alpha_{in} < \alpha_o$ is true because the in-vehicle AL often experiences good channel conditions between the transmitting VUE and the receiving AL-antenna ($\tilde{a}_j$) as compared to out-of-vehicle communication. On the other hand, note that in Eq. (6.9), $\frac{r_{ij}}{l_{v_j}} > 1$. This

Algorithm 4 Quadrant-based Resource Sharing for mobile-cell

$\mathcal{U}, \mathcal{M}, \mathcal{W}$: Cellular users, Mobile-Cells, Sub-channels.
Q^n_{no} : Quadrant no around eNB for device n
eNB split the coverage area into 4 quadrants, i.e., $no = 4$.
for time slot T **do**
  for all Mobile-cell $i = 1 : \mathcal{M}$ **do**
    1. Select mobile-cell j as neighboring mobile-cell to establish SL
    2. Assign resource ω for
      (i) SL link between mobile-cell i and j
      (ii) AL for mobile-cell j
    3. Shortlist all CUs in quadrant $Q_{no} = Q^j_{no} + 2$
      Select $x, y, z \in \mathcal{U}$ in Q_{no}, such that
        $\forall \frac{r_u}{r_i} < 1$, $\frac{r_x}{r_i} = \min(\frac{r_u}{r_i})$
        $\forall \frac{r_u}{r_j} < 1$, $\frac{r_y}{r_j} = \min(\frac{r_u}{r_j})$
        $\forall \frac{r_{ij}}{r_{uj}} < 1$, $\frac{r_z}{r_j} = \min(\frac{r_{ij}}{r_{uj}})$
    4. Assign resource ω to CU u such that
        $u \in \{x, y, z\}$ and $r_u = \min(r_x, r_y, r_z)$
  end for
end for

means that the success probability and ergodic rates for SLs may remain low. This effect is subsided by employing SIC at the SL. SIC will enhance the SIR for the sidehaul signals by canceling out the interfering AL transmission.

Our proposed algorithms given as, Algorithm 3 (Al-3) and Algorithm 4 (Al-4), aim to solve the problem presented in Eq. (6.22) while strictly following constraints (i)-(iii). Both Al-3 and Al-4 only consider those out-of-vehicle cellular users that satisfy constraint (iii), while also abiding by the constraints (i) and (ii). Unlike BF method, the proposed algorithms reduce the number of computations required to select the best possible cellular user to form a trio. In both algorithms (i.e., Al-3 and Al-4), the mobile-cells i and j will share sub-channel ω for sidehaul and access links, respectively. The out-of-vehicle user is then selected by eNB such that the selected CU satisfies the constraint (iii) of the problem specified in Eq. (6.22). Unlike Al-3, Al-4 divides the region around eNB in four quadrants (Q_{no}), where Q^j_{no} denotes resident-quadrant for mobile-cell j. The intuition behind Al-4 is that the cellular user in the resource sharing trio is selected from the quadrant opposite to j (i.e., recipient of the sidehaul

Table 6.2: Parameters for Monte-Carlo simulations.

Parameter	Values
Cell radius	500 meters
λ_u	7.64×10^{-4}
λ_m	1.9×10^{-5}
α_o, α_{in}	3, 2.5
l_{v_j}	5 meters
η^2	-130 dBm/Hz
Baseline algorithms	Random Select (RS), Brute Force (BF)

transmission). Thus, Al-4 further reduces computations compared to Al-3 as this algorithm will consider lesser number of CUs as compared to Al-3. A detailed performance analysis for these algorithms, with comparison to brute-force and random-select (RS) methods will be presented in Section 6.5.

Finally, in order to further evaluate the performance of the proposed algorithms, we have calculated the CCDF of ergodic-rate (δ) for all resource sharing links in a trio. The derivation for CCDF follows the approach adopted in Section 6.3.1. The CCDF for uplink ($\mathcal{C}^{\omega}_{T_{UL}}$), AL ($\mathcal{C}^{\omega}_{T_{AL}}$) and SL ($\mathcal{C}^{\omega}_{T_{SL}}$) are given as:

$$\mathcal{C}^{\omega}_{T_{UL}} = \frac{e^{-(e^{\delta}-1)r_u^{\alpha_o}\eta^2/P_u}}{\left[1+(e^{\delta}-1)\frac{P_i}{P_u}\left(\frac{r_u}{r_i}\right)^{\alpha_o}\right]\left[1+(e^{\delta}-1)\left(\frac{r_u}{r_j}\right)^{\alpha_o}\frac{P_{v_j}}{P_u}\varepsilon\right]}. \tag{6.23}$$

$$\mathcal{C}^{\omega}_{T_{AL}} = \frac{e^{-(e^{\delta}-1)l_{v_j}^{\alpha_{in}}\eta^2/P_{v_j}}}{\left[1+(e^{\delta}-1)\varepsilon\frac{P_u}{P_{v_j}}\left(\frac{l_{v_j}^{\alpha_{in}}}{r_{uj}^{\alpha_o}}\right)\right]\left[1+(e^{\delta}-1)\varepsilon\frac{P_i}{P_{v_j}}\left(\frac{l_{v_j}^{\alpha_{in}}}{r_{ij}^{\alpha_o}}\right)\right]}. \tag{6.24}$$

$$\mathcal{C}^{\omega}_{T_{SL}} = \frac{e^{-(e^{\delta}-1)r_{ij}^{\alpha_o}\eta^2/P_i}}{\left[1+(e^{\delta}-1)\frac{P_u}{P_i}\left(\frac{r_{ij}}{r_{uj}}\right)^{\alpha_o}\right]\left[1+(e^{\delta}-1)\varepsilon\gamma\frac{P_{v_j}}{P_i}\left(\frac{r_{ij}}{l_{v_j}}\right)^{\alpha_o}\right]}. \tag{6.25}$$

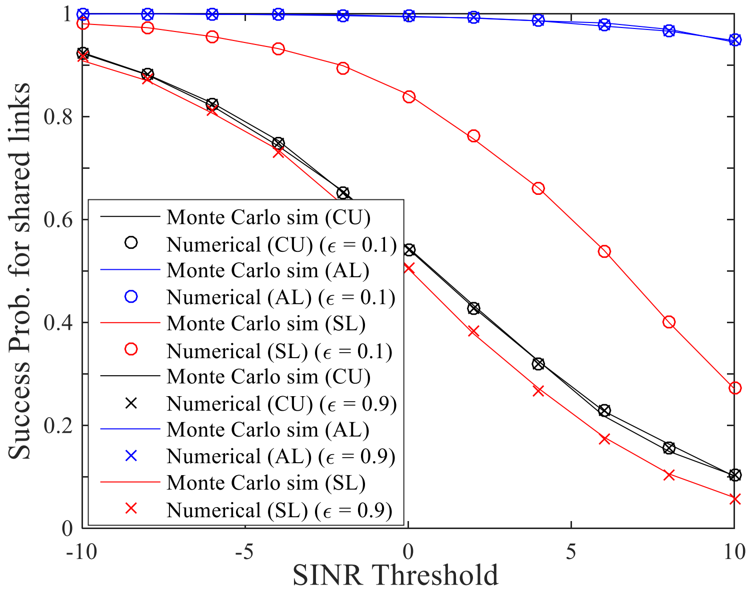

Figure 6.3: Link success probabilities ($P_u, P_{v_j}, P_i = 18, 3, 18$ dBm, $\gamma = 0.1$). © 2019 IEEE [40].

6.5 Results and Discussion

In this section, we present the performance evaluation for the analysis of the proposed algorithms. We have performed Monte-Carlo simulation in which mobile-cells and cellular users are distributed on the euclidean plane independently and randomly. We call this device distribution on 2D plane as a 'topology'. The device distribution densities for cellular users and mobile-cells and rest of the other parameters are mentioned in Table 6.2, unless otherwise stated.

It is obvious from Figure 6.3 and Figure 6.4 that the outcomes from the analysis accurately match the simulation results. Note that the results in Figure 6.3 and 6.4 show the effect of SIC and VPL on success probability and ergodic rates, respectively. A single trio was selected whose devices' follow the distance ratios: $\left(\frac{r_u}{r_i}, \frac{r_u}{r_j}, \frac{r_{ij}}{r_{uj}}, \frac{l_{v_j}}{r_{ij}}, \frac{l_{v_j}}{r_{uj}} = 0.75, 0.66, 0.57, 0.15, .09\right)$. We call this particular orientation as Topology-A. It is clear from Figure 6.3 that high success probability is achieved for SL when VPL is high (i.e., lower value of ε). Recall that the lower values of ε represents high isolation between in-vehicle and out-of-vehicle links. On the other hand, Figure 6.4 shows the effect of vehicular penetration loss (ε) on the ergodic rates of each link. It can be seen that for higher value of ε, the rates for ALs and SLs reduce. These results explain that if VPL is low, the

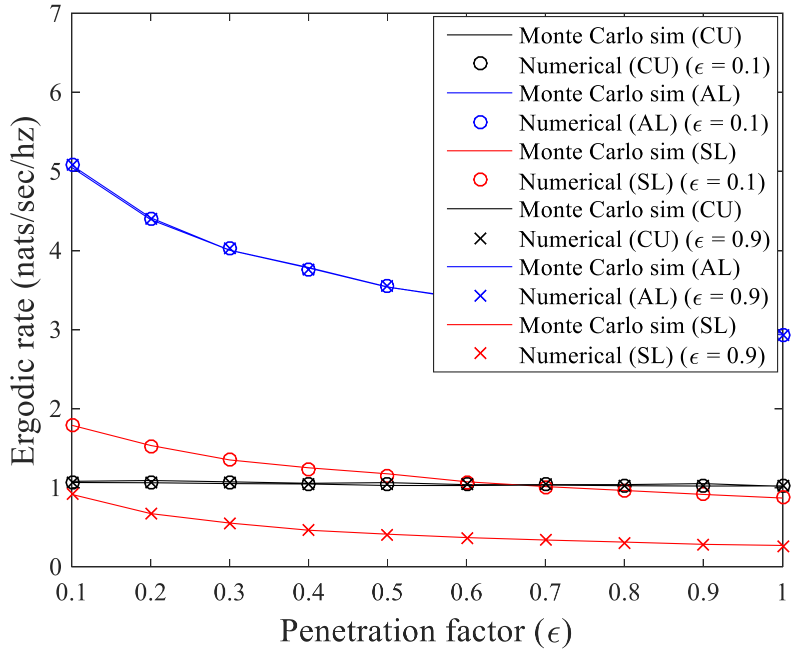

Figure 6.4: Ergodic rate vs VPL ($P_u, P_{v_j}, P_i = 18, 3, 18$ dBm). © 2019 IEEE [40].

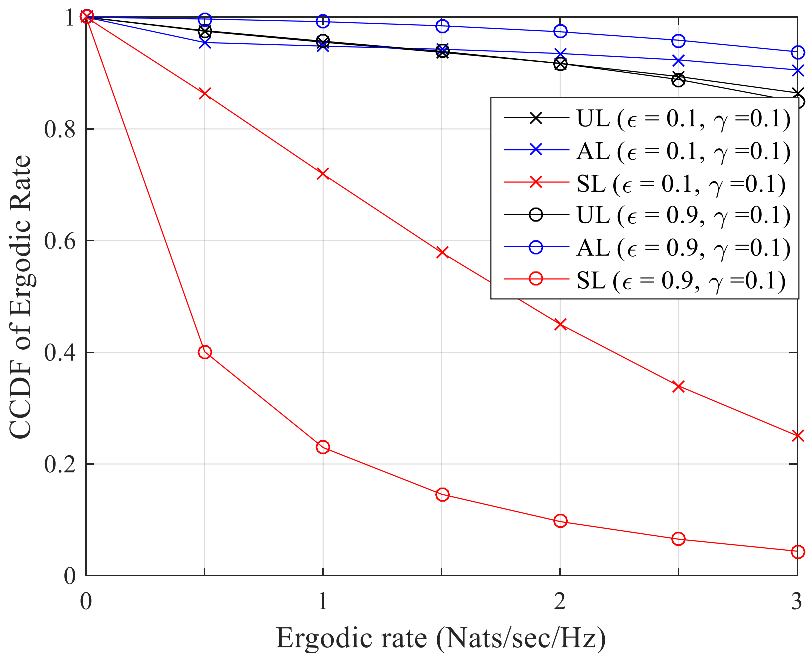

Figure 6.5: Aggregate CCDF of ER for a single topology ($P_u, P_{v_j}, P_i = 15, 6, 18$ dBm).

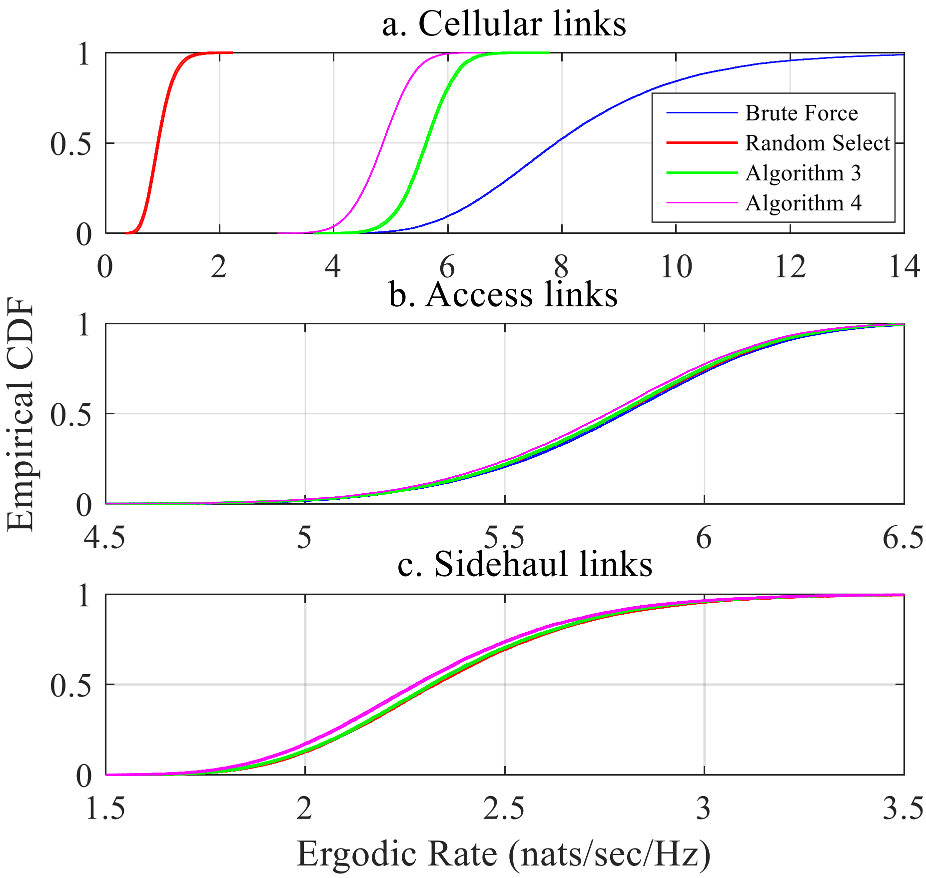

Figure 6.6: Empirical CDF of ER (P_u, P_{v_j}, P_i=15, 6, 18 dBm, SL communication range = 50 m, $\epsilon, \gamma = 0.1$.) © 2019 IEEE [40].

interference from the resource sharing links is high. Interestingly, the rates for the CUs remain unaffected. This is due to the fact that cellular users' transmissions are not affected by the low-powered in-vehicle communication. Furthermore, the reason that ALs are also not affected by the change in VPL is that the distance between in-vehicle antenna and receiver is very small. Therefore, the AL's signal strength at the AL-antenna is higher than the interference from CU and sidehaul transmission.

Figure 6.5 shows the VPL's effect on the aggregate CCDF of the ergodic rates for all links. It is obvious from the figure that as penetration factor increases, the total CCDF of ergodic rate for SL deteriorates. This deterioration is due to the fact that the dominant AL interference reduces the SIR for SL. In contrast, the cellular link remains almost unaffected by the change in the VPL. The variation in the ergodic rate of AL is negligible. This is due to the fact that the small

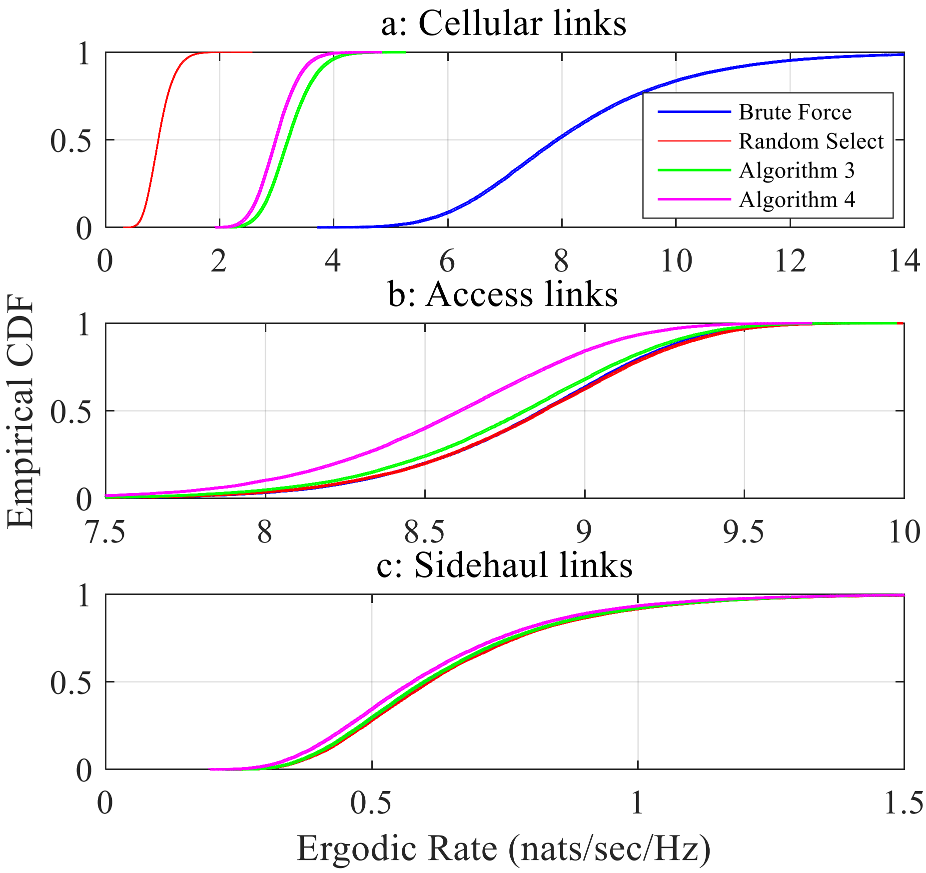

Figure 6.7: Empirical CDF of ER (P_u, P_{v_j}, P_i=15, 6, 18 dBm, SL communication range = 150 m, ϵ, γ = 0.1.) © 2019 IEEE [40].

Table 6.3: Mean/Standard Deviation for CU ergodic rates for simulation results in Figure 6.6 and Fig. 6.7. © 2019 IEEE [40].

SL comm. range	Parameter	BF	RS	Al-3	Al-4
50 meters	Mean	8.20	0.94	5.61	4.85
	Std. deviation	1.94	0.23	0.45	0.47
150 meters	Mean	8.24	0.95	3.23	3.00
	Std. deviation	1.96	0.22	0.40	0.36

transmitter-receiver distance for AL communication ensures high received signal strength at the AL-antenna. Consequently, the interfering links do not have adverse effects.

Next, we present the simulation results by averaging the ergodic rates from 1 million topologies. We randomly picked 20 SLs from $i \rightarrow j \ \forall i, j \in \mathcal{M}$ for all simulations (which correspond to 20 trios). We have compared the proposed algorithms (Al-3 and Al-4) with the random-select and the brute-force method. In RS, the eNB randomly selects CUs to form the trios with the mobile-cells. On the other hand, in BF a comprehensive search is performed to select the best possible CU which can maximize the ergodic rate.

Figure 6.6 and Figure 6.7 show the empirical CDF of the ergodic rates for all links when sidehaul communication ranges are 50 and 150 meters, respectively. It is obvious from both figures that the proposed algorithms ensure better rates for uplink cellular transmissions when compared to the random-select algorithm's results. As expected, the performance of Al-3 and Al-4 is sub-optimal when compared to BF algorithm. Recall, however, that BF requires much larger time to form trios. It is also interesting to note that there is little difference between the ergodic rates of either access or SLs. However, keeping all other factors constant, the ergodic rate of AL increases considerably in Figure 6.7 as compared to the same in Figure 6.6. This is due to the fact that interference from SLs reduces as mobile-cells are placed at larger distances from each other. On the other hand, rates of the SL shown in Figure 6.7 are much lower when compared to those in Figure 6.6.

We can deduce another interesting and important observation from Figure 6.6 and Figure 6.7. It can be seen that the ergodic rates obtained using BF scheme are higher when compared to the proposed algorithms. However, the variation around the mean for Al-3 and Al-4 is very small in comparison to the results obtained through BF. This observation suggests that Al-3 and Al-4 provide more certainty for the ergodic rate of cellular-links compared to BF. Numerically, this observation is summarized for further clarity in Table 6.3. It can be seen that the standard deviation of rates obtained through BF reaches almost 2.0 nats/sec/Hz for SL communication ranges of 50 and 150 meters. On the other hand, the standard deviations for the proposed algorithms remain well below 0.5 nats/sec/Hz in each case.

Table 6.4 presents the relationship between SL's communication range and the mean of the total ergodic rate per sub-channel. For higher ranges, the mean rate per sub-channel decreases for Al-3 and Al-4. However, the rates still remain higher than the ergodic rates achieved using RS scheme. Table 6.5 shows the mean ergodic rates for different transmit powers (P_{t_x}). There is a trade-off in increasing P_{t_x} of a particular link. For example, the ergodic rate for in-vehicle

Table 6.4: SL communication vs ergodic-rate per shared sub-channel ($P_u, P_{v_j}, P_i = 15, 6, 18$ (dBm), $\epsilon, \gamma = 0.1$).

SL comm. range (m)	Algo.	200	150	100	50
Avg. erg. rate/sub-ch.	BF	18.18	17.72	17.07	16.33
	RS	10.97	10.43	9.78	9.06
	Al-3	12.55	12.64	12.91	13.72
	Al-4	12.03	12.19	12.42	12.89

Table 6.5: $P_{t_x}(dBm)$ vs mean rates (SL comm. range = $150m$)

P_u, P_{v_j}, P_i	Algo.	Rate CU	Rate AL	Rate SL	Rate Total
15, 0, 18	Al-3	3.26	7.40	1.16	11.81
	Al-4	3.02	7.20	1.09	11.32
15, 3, 18	Al-3	3.24	8.09	0.87	12.20
	Al-4	3.02	7.88	0.84	11.74
15, 6, 18	Al-3	3.22	8.77	0.65	12.64
	Al-4	3.00	8.57	0.62	12.19
18, 6, 18	Al-3	3.82	8.69	0.64	13.15
	Al-4	3.58	8.44	0.61	12.62
18, 6, 15	Al-3	4.41	9.27	0.45	14.13
	Al-4	4.17	8.96	0.43	13.56

user increases with an increase in P_{v_j} at the expense of lower rates for SLs.

Finally, we study the effect of mobile-cell's mobility on the ergodic rates of the resource sharing links. To this end, we focus only on scenarios when a mobile-cell travels with high speed in the direction of resource sharing receiver. These scenarios are: (i) mobile-cell i moves towards the eNB, and mobile-cell j is static, (ii) mobile-cell i moves towards a static j, (iii) j moves towards resource sharing CU, and i is static. At time $t = 0$ and following Topology-A, the resources are assigned to each device for 1-sec and mobile-cells move at a speed of 22.2 m/s (80 Km/hr) in all cases. Referring to Figure 6.8, high ergodic rates can be observed at each resource sharing link even at the end of 1-sec period. Under normal circumstances, it is expected that as the device moves towards a resource sharing device, the ergodic rates for both devices should decrease drastically because of increased interference. However, it can be deduced from Figure 6.8 that the proposed scheme can withstand the effects of mobile-cell's mobility towards the

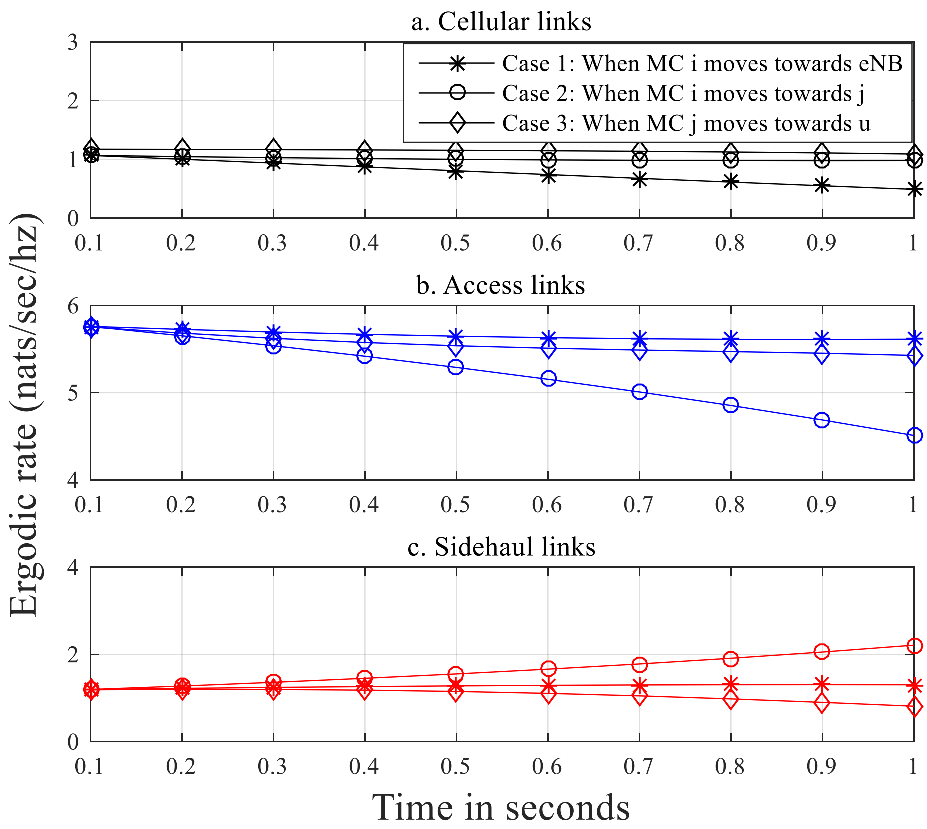

Figure 6.8: Ergodic rates for the mobility scenario following Topology-A at time $t = 0$ (P_u, P_{v_j}, P_i=18, 3, 18 dBm, $\gamma, \epsilon = 0.1$) © 2019 IEEE [40].

resource sharing links.

6.6 Conclusion

Mobile-cells will be an integral part of future heterogeneous networks which will serve cellular users commuting inside public transport vehicles. However, mobile-cells will also introduce multiple wireless links, including sidehaul and access links. Assigning individual spectral resources to each link will be an spectrally inefficient method. Hence, in this chapter, we have proposed two algorithms to ensure that a single resource could be shared by three links: mobile-cell's uplink access link, sidehaul link, and cellular uplink. The algorithms that we have proposed in this chapter provide sub-optimal, yet less time consuming, solutions to the problem of trio formation. Note that the brute-force method is a very reliable way for calculating optimal rates, but at the cost of large processing time. The brute-force search checks every single cellular user in order to attain highest total rate for the trio. On the other hand, the random-selection of devices for the formation of trio may be quicker, but does not ensure high data rate. We have shown that our proposed algorithms also provide results with more certainty as compared to the brute-force search method.

6.7 Related Publications

- **Shan Jaffry**, Syed Faraz Hasan, Xiang Gui, "Efficient resource sharing Algorithms for Mobile-Cell's Sidehaul and Access Links", IEEE Networking Letters, February 2019.

Chapter 7

Final Discussion

7.1 Thesis Conclusion

Mobile-cells will provide in-vehicle cellular connectivity to commuters inside public transport in future heterogeneous networks. Mobile-cells will be installed with an access link antenna to serve on-board users, while the out-of-vehicle antennae will connect mobile-cells to the core network over the backhaul links [38]. The mobile-cells in each others' vicinity will communicate over the sidehaul links [34]. The sidehaul links can only be established after the mobile-cells have knowledge of their neighbors. The neighborhood awareness is achieved during the discovery phase. In a network-centric scheme, a base station may oversee the discovery process. But in the environments where network is not available, neighborhood discovery is a challenging task. Therefore, as its first contribution, this thesis, has proposed an autonomous neighborhood discovery scheme.

The main challenge concerning autonomous discovery is to avoid failures caused due to collision and half-duplexing when devices broadcast beacon messages. In Chapter 3, we have proposed a modified time-frequency frame structure that allows multiple beacon transmission per PSDCH-period. The analytical and simulation results have demonstrated a significant increase in successful discovery probability when the proposed frame structure is used, as compared to the conventional method. However, the proposed solution tends to underperform as the neighborhood density increases. In Chapter 4, we proposed a more comprehensive approach which relies on the neighborhood information to increase discovery probability and to reduce time-to-discovery. In the first instance, we derived an expression for optimal beacon transmission probability. We later introduced a new Information-period which occurs just before PSDCH-period. The devices acquire information about their neighborhood density during the Information-period. The devices then adapt their transmission rates based on the estimated density of neighbors. In case the density of neighbors is very high, each device will lower its beacon transmission rate to avoid collisions and get more opportunities for successful transmission. On the contrary, when neighborhood density is very low, each device will broadcast beacons with high transmission rates to achieve successful discovery in a shorter amount of time. We demonstrated the suitability of the proposed scheme if the discovering device, i.e. mobile-cell, is moving. In order to do so, we developed an analytical model for discovery by a mobile-cell which, to the best of our knowledge, has never been done before.

In Chapter 5 and Chapter 6, we focused on interference management and spectrally efficient resource allocation for mobile-cells which is the second research problem addressed in this thesis. The mobile-cells have multiple wireless links (e.g., AL, BL, and SL) which may interfere with out-of-vehicle cellular users. A naïve way to eliminate interference is to assign separate resources to each individual link. However, given the scarcity of the spectral resources, such a solution is impractical. Instead of assigning individual resources to each wireless link, we focused on resource sharing between mobile-cells' links and out-of-vehicle cellular users. We exploited vehicular penetration loss and utilized successive interference cancellation technique to ensure that the resource sharing links acheive high success probabilities. In Chapter 5, we focused on resource sharing between downlink AL and either BL or out-of-vehicle macrocell user. We proposed two algorithms that work jointly to ensure that additional resources are not required for AL's downlink transmission. Highly directional AL-antenna was used to keep a LoS link between the antenna and the in-vehicle user. The AL power control scheme was proposed to reduce the interference to the BL while maintaining high QoS for in-vehicle users. We also derived expressions for success probabilities and ergodic rates for all resource sharing links. In Chapter 6, we focused on resource sharing between uplink AL with mobile-cell's SL and out-of-vehicle cellular user. Two algorithms have been proposed which ensure that resource sharing, even in dense environments, can maintain high ergodic rate for all three links. The schemes proposed in Chapter 5 and Chapter 6 allow mobile-cells' integration into future cellular networks without requiring additional sub-channels.

This research has identified a number of other interesting directions which, we believe, may find adequate traction within research community. We briefly highlight these directions in the next section.

7.2 Future Directions

Some open questions related to the mobile-cells still exist that need careful investigation and may open exciting new research directions. For example, researchers have explored the idea of providing services to out-of-coverage regions using mobile-cells over SLs [23,32]. The simulations performed in [23,32] assumed ideal connectivity between mobile-cells and the out-of-vehicle users. In practice, the devices must first achieve timing and frequency synchronization before proceeding to neighborhood discovery. Synchronization in a mobile environment is still an unresolved and challenging issue, especially in network-independent and autonomous environments. Third generation partnership project has provided guidelines for device synchronization in out-of-coverage scenarios [159]. However, a detailed analysis for mobile environment still needs serious investigation.

Another dimension for future research into mobile-cells can be the development of effective mobile-caching mechanisms. The distribution of popular contents from the core network to the transport vehicle is a well investigated topic [160–162]. However, content sharing between moving mobile-cells (over SLs) still needs more research. Researchers in [23, 30] have demonstrated that if mobile-cells share contents over SLs, substantial reduction in the consumption of backhaul bandwidth can be achieved. Furthermore, vehicles (or group of vehicles) may travel beyond network coverage in which case, effective caching can ensure the provision of continuous availability of web services to the commuting users. The biggest challenge for mobile environments is the intermittent connectivity between the nodes [162]. Sharing of data, such as multimedia content, requires stable connectivity for sufficient amount of time so as to transfer files of large data sizes. The intermittent connectivity disrupts the effective content sharing. One solution to this problem may be multi-hop data exchange between the mobile-cells. However, as the number of hops between the end-nodes increases, the latency and bandwidth consumption increases. Due to the nature of such complex challenges associated with the content distribution among mobile-cells, more investigation is needed into this open research problem.

In addition to the research challenges, a few practical concerns also warrant considerations. For example, commuters inside buses or trains may use services of different cellular operators. The installation of separate in-vehicle equipment (e.g., antennae or cache components etc.) by each operator will require significant deployment and maintenance cost by all the stakeholders (i.e., mobile operators, and transport service providers, etc.). Therefore, effective mechanisms for sharing physical resources (such as, spectrum, antennae, and caching system) are required to benefit all the stakeholders. This will inevitably encourage considerations of Infrastructure as a Service (IaaS) paradigm.

Recently, the apprehensions that massive amount of 5G base stations will surround our environment have stirred debates related to constant electromagnetic exposures and its impact on human well-being [163]. The idea that AL-antennae within mobile-cells will continuously transmit radio signals to spatially closer in-vehicle users may raise more concerns. Therefore, the domain experts should conduct a comprehensive study to regularize the acceptable transmit power-levels which are not only safe for human well-being but also provide high QoS to users.

This page is intentionally left blank.

References

[1] "Future Works: 5G Use Cases and Requirements," Whitepaper. [Online]. Available: www.networks.nokia.com

[2] P. Cerwall, A. Lundvall, P. Jonsson, R. Möller, S. Bävertoft, S. Carson, and I. Godor, "Ericsson Mobility Report 2018," 2018.

[3] J. Thompson, J. Sun, R. Möller, M. Sintorn, and G. Huston, "Akamai State of Internet Report, Q1 2017," vol. Vol-1, 2017.

[4] Y. Inoue, S. Yoshioka, Y. Kishiyama, J. Kepler, M. Cudak, S. Suyama, and Y. Okumura, "Field experimental trials for 5g mobile communication system using 70 ghz-band," in *2017 IEEE Wireless Communications and Networking Conference Workshops (WCNCW)*. IEEE, 2017, pp. 1–6.

[5] N. Banović-Ćurguz, D. Ilišević, and D. Budimir, "Towards Digital Transformation with 5G Technology," *International Journal of Electrical Engineering and Computing*, vol. 2, no. 2, pp. 101–110, 2018.

[6] J. G. Andrews, S. Buzzi, W. Choi, S. V. Hanly, A. Lozano, A. C. Soong, and J. C. Zhang, "What will 5G be?" *IEEE Journal on selected areas in communications*, vol. 32, no. 6, pp. 1065–1082, 2014.

[7] A. Gupta and R. K. Jha, "A Survey of 5G Network: Architecture and Emerging Technologies," *IEEE Access*, vol. 3, pp. 1206–1232, 2015.

[8] T. E. Julsrud and J. M. Denstadli, "Smartphones, travel time-use, and attitudes to public transport services. insights from an explorative study of urban dwellers in two norwegian cities," *International Journal of Sustainable Transportation*, vol. 11, no. 8, pp. 602–610, 2017.

[9] G. Michele, C. de Schietere De Lophem, and C. V. Bave, “Consumer usage patterns of the smartphone: Global mobile consumer survery, belgian editiion,” 2017.

[10] E. ConsumerLab, “Commuters Expect More,” Online, July 2015. [Online]. Available: https://www.ericsson.com/assets/local/news/2015/6/ericsson-consumerlab-commuters-expect-more.pdf

[11] S. S. Jaffry, S. F. Hasan, and X. Gui, “Mobile Cells Assisting Future Cellular Communication,” *IEEE Potentials*, vol. 37, no. 5, pp. 16–20, 2018.

[12] T. S. Rappaport, S. Sun, R. Mayzus, H. Zhao, Y. Azar, K. Wang, G. N. Wong, J. K. Schulz, M. Samimi, and F. Gutierrez, “Millimeter Wave Mobile Communications for 5G Cellular: It Will Work!” *IEEE access*, vol. 1, pp. 335–349, 2013.

[13] I. F. Akyildiz, C. Han, and S. Nie, “Combating the distance problem in the millimeter wave and terahertz frequency bands,” *IEEE Communications Magazine*, vol. 56, no. 6, pp. 102–108, 2018.

[14] Z. Marzi, U. Madhow, and H. Zheng, “Interference analysis for mm-wave picocells,” in *2015 IEEE Global Communications Conference (GLOBECOM)*, Dec 2015, pp. 1–6.

[15] F. Boccardi, R. W. Heath, A. Lozano, T. L. Marzetta, and P. Popovski, “Five disruptive technology directions for 5g,” *IEEE Communications Magazine*, vol. 52, no. 2, pp. 74–80, 2014.

[16] M. Ding, D. Lopez-Perez, H. Claussen, and M. A. Kaafar, “On the fundamental characteristics of ultra-dense small cell networks,” *IEEE Network*, vol. 32, no. 3, pp. 92–100, 2018.

[17] A. Cimmino, T. Pecorella, R. Fantacci, F. Granelli, T. F. Rahman, C. Sacchi, C. Carlini, and P. Harsh, “The role of small cell technology in future smart city applications,” *Transactions on Emerging Telecommunications Technologies*, vol. 25, no. 1, pp. 11–20, 2014.

[18] J. Xu, J. Wang, Y. Zhu, Y. Yang, X. Zheng, S. Wang, L. Liu, K. Horneman, and Y. Teng, “Cooperative distributed optimization for the hyper-dense

small cell deployment," *IEEE Communications Magazine*, vol. 52, no. 5, pp. 61–67, 2014.

[19] Y. Sui, A. Papadogiannis, W. Yang, and T. Svensson, "Performance comparison of fixed and moving relays under co-channel interference," in *Globecom Workshops (GC Wkshps), 2012 IEEE*. IEEE, 2012, pp. 574–579.

[20] R. I. Ansari, C. Chrysostomou, S. A. Hassan, M. Guizani, S. Mumtaz, J. Rodriguez, and J. J. Rodrigues, "5G D2D networks: Techniques, challenges, and future prospects," *IEEE Systems Journal*, 2017.

[21] S. Sesia, M. Baker, and I. Toufik, *LTE-the UMTS long term evolution: from theory to practice*. John Wiley & Sons, 2011.

[22] R. Molina-Masegosa and J. Gozalvez, "LTE-V for Sidelink 5G V2X Vehicular Communications: A New 5G Technology for Short-Range Vehicle-to-Everything Communications," *IEEE Vehicular Technology Magazine*, vol. 12, no. 4, pp. 30–39, 2017.

[23] M. Shin, J. S. Kim, M. Y. Chung, and Y. M. Kwon, "Sidehaul link management scheme for mobile contents caching environments in moving small-cell networks," in *Ubiquitous and Future Networks (ICUFN), 2016 Eighth International Conference on*. IEEE, 2016, pp. 1035–1039.

[24] V. Van Phan, K. Horneman, L. Yu, and J. Vihriala, "Providing enhanced cellular coverage in public transportation with smart relay systems," in *Vehicular Networking Conference (VNC), 2010 IEEE*. IEEE, 2010, pp. 301–308.

[25] F. Jiang, K. Thilakarathna, M. A. Kaafar, F. Rosenbaum, and A. Seneviratne, "A spatio-temporal analysis of mobile internet traffic in public transportation systems: A view of web browsing from the bus," in *Proceedings of the 10th ACM MobiCom Workshop on Challenged Networks*. ACM, 2015, pp. 37–42.

[26] Y. M. Kwon, S.-M. Oh, J. Shin, and M. Y. Chung, "Radio resource management for moving small-cells with proactive content cache," in *TENCON 2015-2015 IEEE Region 10 Conference*. IEEE, 2015, pp. 1–4.

[27] D.-R. Lee, S. Jaffry, S. F. Hasan, Y.-W. Kuo, and X. Gui, "Performance evaluation of handover protocols in software defined networking environment," in *International Conference on Smart Grid Inspired Future Technologies*. Springer, 2018, pp. 240–249.

[28] A. Merwaday and I. Güvenç, "Handover count based velocity estimation and mobility state detection in dense hetnets," *IEEE Transactions on Wireless Communications*, vol. 15, no. 7, pp. 4673–4688, 2016.

[29] Y. Nakayama, K. Maruta, T. Tsutsumi, and K. Sezaki, "Optically backhauled moving network for local trains," in *Proceedings of the 4th ACM Workshop on Hot Topics in Wireless*. ACM, 2017, pp. 31–35.

[30] S. T. Shah, M. Shin, Y. M. Kwon, J. Shin, A.-S. Park, and M. Y. Chung, "Moving personal-cell network: Characteristics and performance evaluation," *China Communications*, vol. 15, no. 12, pp. 159–173, 2018.

[31] A. Khan and A. Jamalipour, "An Outage Performance Analysis With Moving Relays on Suburban Trains for Uplink," *IEEE Transactions on Vehicular Technology*, vol. 66, no. 5, pp. 3966–3975, 2017.

[32] M. Shin, S. T. Shah, M. Y. Chung, S. F. Hasan, B.-C. Seet, and P. H. J. Chong, "Moving small cells in public safety networks," in *2017 International Conference on Information Networking (ICOIN)*, Jan 2017, pp. 564–568.

[33] D. Tsolkas, N. Passas, and L. Merakos, "Device discovery in LTE networks: A radio access perspective," *Computer Networks*, vol. 106, pp. 245–259, 2016.

[34] S. Jaffry, S. F. Hasan, and X. Gui, "Making a case for the moving small cells," in *2016 26th International Telecommunication Networks and Applications Conference (ITNAC)*. IEEE, 2016, pp. 249–251.

[35] S. Jaffry, S. F. Hasan, X. Gui, and Y. W. Kuo, "Distributed device discovery in ProSe environments," in *TENCON 2017-2017 IEEE Region 10 Conference*. IEEE, 2017, pp. 614–618.

[36] S. Jaffry, S. F. Hasan, and X. Gui, "Neighbourhood-aware out-of-network D2D discovery," *Electronics Letters*, vol. 54, no. 8, pp. 507–509, 2018.

[37] S. Jaffry, S. K. Zaidi, S. T. Shah, S. F. Hasan, and X. Gui, "D2D Neighborhood Discovery by a Mobile Device," in *ICC 2019-2019 IEEE International Conference on Communications (ICC).* IEEE, 2019, pp. 1–6.

[38] S. Jaffry, S. F. Hasan, and X. Gui, "Shared Spectrum for Mobile-Cell's Backhaul and Access Link," in *2018 IEEE Global Communications Conference (GLOBECOM).* IEEE, 2018, pp. 1–6.

[39] ——, "Interference Management and Resource Sharing in Moving Networks," *IET Communications*, 2019.

[40] ——, "Efficient Resource-Sharing Algorithms for Mobile-Cell's Sidehaul and Access Links," *IEEE Networking Letters*, vol. 1, no. 2, pp. 72–75, 2019.

[41] E. Tanghe, W. Joseph, L. Verloock, and L. Martens, "Evaluation of vehicle penetration loss at wireless communication frequencies," *IEEE transactions on vehicular technology*, vol. 57, no. 4, pp. 2036–2041, 2008.

[42] "Technical specification group radio access network; mobile relay for evolved universal terrestrial radio access (E-UTRA)," Third Generation Partnetship Project (3GPP), techreport TR 36.836, May 2012.

[43] Y. Sui, A. Papadogiannis, and T. Svensson, "The potential of moving relays - a performance analysis," in *Vehicular Technology Conference (VTC Spring), 2012 IEEE 75th*, May 2012, pp. 1–5.

[44] S. Chae, T. Nguyen, and Y. M. Jang, "A novel handover scheme in moving vehicular femtocell networks," in *Ubiquitous and Future Networks (ICUFN), 2013 Fifth International Conference on.* IEEE, 2013, pp. 144–148.

[45] A. Jaziri, R. Nasri, and T. Chahed, "Offloading traffic hotspots using moving small cells," in *Communications (ICC), 2016 IEEE International Conference on.* IEEE, 2016, pp. 1–6.

[46] H. Yasuda, A. Kishida, J. Shen, Y. Morihiro, Y. Morioka, S. Suyama, A. Yamada, Y. Okumura, and T. Asai, "A study on moving cell in 5G cellular system," in *Vehicular Technology Conference (VTC Fall), 2015 IEEE 82nd.* IEEE, 2015, pp. 1–5.

[47] R. Favraud, A. Apostolaras, N. Nikaein, and T. Korakis, "Toward moving public safety networks," *IEEE Communications Magazine*, vol. 54, no. 3, pp. 14–20, 2016.

[48] Y. Sui, A. Papadogiannis, W. Yang, and T. Svensson, "The energy efficiency potential of moving and fixed relays for vehicular users," in *Vehicular Technology Conference (VTC Fall), 2013 IEEE 78th.* IEEE, 2013, pp. 1–7.

[49] Y.-T. Hsueh, M.-F. Huang, M. Jiang, Y. Shao, K. Kim, and G.-K. Chang, "A novel wireless over fiber access architecture employing moving chain cells and rof technique for broadband wireless applications on the train environment," in *Optical Fiber Communication Conference and Exposition (OFC/NFOEC), 2011 and the National Fiber Optic Engineers Conference.* IEEE, 2011, pp. 1–3.

[50] X. Jiang and D. H. Du, "Bus-vanet: a bus vehicular network integrated with traffic infrastructure," *IEEE Intelligent Transportation Systems Magazine*, vol. 7, no. 2, pp. 47–57, 2015.

[51] J. Hare, L. Hartung, and S. Banerjee, "Beyond deployments and testbeds: experiences with public usage on vehicular wifi hotspots," in *Proceedings of the 10th international conference on Mobile systems, applications, and services.* ACM, 2012, pp. 393–406.

[52] "Public transportation with free wifi," Online. [Online]. Available: http://www.openwifispots.com

[53] H. Cui, V. C. Leung, S. Li, and X. Wang, "Lte in the unlicensed band: Overview, challenges, and opportunities," *IEEE Wireless Communications*, vol. 24, no. 4, pp. 99–105, 2017.

[54] T. Berisha, P. Svoboda, S. Ojak, and C. F. Mecklenbräuker, "Seghyper: Segmentation-and hypothesis based network performance evaluation for high speed train users," in *Communications (ICC), 2017 IEEE International Conference on.* IEEE, 2017, pp. 1–6.

[55] S. Yutao, *Moving Networks, a Better Way to Serve Vehicular Users.* Chalmers University of Technology, 2016.

[56] S. Jangsher and V. O. K. Li, “Resource allocation in cellular networks employing mobile femtocells with deterministic mobility,” in *2013 IEEE Wireless Communications and Networking Conference (WCNC)*, April 2013, pp. 819–824.

[57] A. Khan and A. Jamalipour, “Moving relays in heterogeneous cellular networks—a coverage performance analysis,” *IEEE Transactions on Vehicular Technology*, vol. 65, no. 8, pp. 6128–6135, 2016.

[58] J. Feng, S. Yang, and Z. Feng, “Vehicle-assisted offloading on metropolitan streets: Enhancing geographical fluidity of wireless resources,” *IEEE Wireless Communications Letters*, vol. 6, no. 5, pp. 622–625, 2017.

[59] A. Mastrosimone and D. Panno, “New challenge: Moving network based on mmWave technology for 5G era,” in *Computer, Information and Telecommunication Systems (CITS), 2015 International Conference on*, July 2015, pp. 1–5.

[60] X. Wang, “Moving relays in downlink multiuser networks-a physical-layer security perspective,” in *2018 IEEE 87th Vehicular Technology Conference (VTC Spring)*. IEEE, 2018, pp. 1–5.

[61] 3GPP, “Delivering Public Safety Communications with LTE 3GGP whitepaper.” [Online]. Available: httep;//3gpp.org/Public-safety

[62] L. Li, D. Wen, and D. Yao, “A survey of traffic control with vehicular communications,” *IEEE Transactions on Intelligent Transportation Systems*, vol. 15, no. 1, pp. 425–432, Feb 2014.

[63] 3GPP, “Techniques for D2D Disc,” 3GPP, techreport, aug 2013.

[64] S. E. Roslin, C. Gomathy, and P. Bhuvaneshwari, “A survey on neighborhood dependant topology control in wireless sensor networks,” *Int. J. of Computer Science & Commun*, vol. 1, no. 1, pp. 185–188, 2010.

[65] U. N. Kar and D. K. Sanyal, “An overview of device-to-device communication in cellular networks,” *ICT Express*, 2017.

[66] R. Pozza, M. Nati, S. Georgoulas, K. Moessner, and A. Gluhak, “Neighbor discovery for opportunistic networking in internet of things scenarios: A survey,” *IEEE Access*, vol. 3, pp. 1101–1131, 2015.

[67] S. Vasudevan, M. Adler, D. Goeckel, and D. Towsley, "Efficient algorithms for neighbor discovery in wireless networks," *IEEE/ACM Transactions on Networking*, vol. 21, no. 1, pp. 69–83, 2013.

[68] S. Vasudevan, D. Towsley, D. Goeckel, and R. Khalili, "Neighbor discovery in wireless networks and the coupon collector's problem," in *Proceedings of the 15th annual international conference on Mobile computing and networking*. ACM, 2009, pp. 181–192.

[69] N. K. Pratas and P. Popovski, "Network-Assisted Device-to-Device (D2D) Direct Proximity Discovery with Underlay Communication," in *2015 IEEE Global Communications Conference (GLOBECOM)*. IEEE, 2015, pp. 1–6.

[70] H. Tang, Z. Ding, and B. C. Levy, "Enabling d2d communications through neighbor discovery in lte cellular networks," *IEEE Transactions on Signal Processing*, vol. 62, no. 19, pp. 5157–5170, 2014.

[71] D. Griffith and F. Lyons, "Optimizing the UE Transmission Probability for D2D Direct Discovery," in *Global Communications Conference (GLOBECOM), 2016 IEEE.*

[72] X. Wu, S. Tavildar, S. Shakkottai, T. Richardson, J. Li, R. Laroia, and A. Jovicic, "Flashlinq: A synchronous distributed scheduler for peer-to-peer ad hoc networks," *IEEE/ACM Transactions on Networking (TON)*, vol. 21, no. 4, pp. 1215–1228, 2013.

[73] D. Xenakis, M. Kountouris, L. Merakos, N. Passas, and C. Verikoukis, "On the performance of network-assisted device-to-device discovery," in *2015 IEEE Global Communications Conference (GLOBECOM)*. IEEE, 2015, pp. 1–7.

[74] W. Lee, J. Kim, and S. W. Choi, "New D2D Peer Discovery Scheme based on Spatial Correlation of Wireless Channel," *IEEE Transactions on Vehicular Technology*, vol. PP, no. 99, pp. 1–1, 2016.

[75] 3GPP, "3gpp ts 23.303 version 10.3.0 release 12," 3GPP, Tech. Rep., 2014.

[76] X. Lin, J. Andrews, A. Ghosh, and R. Ratasuk, "An overview of 3GPP device-to-device proximity services," *IEEE Communications Magazine*, vol. 52, no. 4, pp. 40–48, 2014.

[77] K.-H. Lee, K. H. Won, and H.-J. Choi, "Timing synchronization method for device-to-device communication system," in *Proceedings of the 7th International Conference on Ubiquitous Information Management and Communication*. ACM, 2013, p. 105.

[78] 3GPP, "Evolved universal terrestrial radio access (e-utra); radio resource control (rrc); protocol specification- ts:36.331," Technical Report.

[79] Y. Zhao, B. Pelletier, P. Marinier, and D. Pani, "D2D neighbor discovery interference management for LTE systems," in *2013 IEEE Globecom Workshops (GC Wkshps)*. IEEE, 2013, pp. 550–554.

[80] H. Albasry and Q. Z. Ahmed, "Network-assisted d2d discovery method by using efficient power control strategy," in *2016 IEEE 83rd Vehicular Technology Conference (VTC Spring)*, May 2016, pp. 1–5.

[81] J. Hong, S. Park, H. Kim, S. Choi, and K. B. Lee, "Analysis of device-to-device discovery and link setup in lte networks," in *2013 IEEE 24th Annual International Symposium on Personal, Indoor, and Mobile Radio Communications (PIMRC)*, Sept 2013, pp. 2856–2860.

[82] W. Hwang, D. Lee, and H. J. Choi, "A new channel structure and power control strategy for D2D discovery in LTE cellular network," in *The 20th Asia-Pacific Conference on Communication (APCC2014)*, Oct 2014, pp. 150–155.

[83] S. K. Gupta, J. Y. Khan, and D. T. Ngo, "Cluster-based d2d architecture for safety services in vehicular ad hoc networks," in *Wireless Communications and Networking Conference Workshops (WCNCW), 2018 IEEE*. IEEE, 2018, pp. 43–48.

[84] S. Vasudevan, J. Kurose, and D. Towsley, "On neighbor discovery in wireless networks with directional antennas," in *INFOCOM 2005. 24th Annual Joint Conference of the IEEE Computer and Communications Societies. Proceedings IEEE*, vol. 4. IEEE, 2005, pp. 2502–2512.

[85] H. Cai and T. Wolf, "On 2-way neighbor discovery in wireless networks with directional antennas," in *Computer Communications (INFOCOM), 2015 IEEE Conference on*. IEEE, 2015, pp. 702–710.

[86] F. Tian, R. Q. Hu, Y. Qian, B. Rong, B. Liu, and L. Gui, "Pure asynchronous neighbor discovery algorithms in ad hoc networks using directional antennas," in *Global Communications Conference (GLOBECOM), 2013 IEEE*. IEEE, 2013.

[87] F. Tian, B. Liu, H. Cai, H. Zhou, and L. Gui, "Practical asynchronous neighbor discovery in ad hoc networks with directional antennas," *IEEE Transactions on Vehicular Technology*, vol. 65, no. 5, pp. 3614–3627, 2016.

[88] S. Zhao, Y. Liu, T. Yang, Z. Feng, Q. Zhang, and C. Gao, "3-way multi-carrier asynchronous neighbor discovery algorithm using directional antennas," in *Wireless Communications and Networking Conference (WCNC), 2016 IEEE*, 2016.

[89] S.-L. Chao, H.-Y. Lee, C.-C. Chou, and H.-Y. Wei, "Bio-inspired proximity discovery and synchronization for d2d communications," *IEEE communications letters*, vol. 17, no. 12, pp. 2300–2303, 2013.

[90] F. Wu, T. Meng, A. Li, G. Chen, and N. H. Vaidya, "Have you recorded my voice: Toward robust neighbor discovery in mobile wireless networks," *IEEE/ACM Transactions on Networking*, 2018.

[91] T. C.-Y. Chang, C.-Y. Wei, M.-C. Hsu, C.-Y. Lin, and Y. T. Su, "Distributed clustering and spectrum-based proximity device discovery in a wireless network," in *Broadband Multimedia Systems and Broadcasting (BMSB), 2016 IEEE International Symposium on*. IEEE, 2016, pp. 1–4.

[92] B. Zhang, Y. Li, D. Jin, and Z. Han, "Network science approach for device discovery in mobile device-to-device communications," *IEEE Transactions on Vehicular Technology*, vol. 65, no. 7, pp. 5665–5679, 2016.

[93] 3GPP, "3GPP TR 36.843, Study on LTE Device to Device Proximity Services; Radio Aspects," 3rd Generation Partnership Project (3GPP), TR 36.801, 2014.

[94] J. Hong, S. Park, and S. Choi, "Novel power control and collision resolution schemes for device-to-device discovery," *Peer-to-Peer Networking and Applications*, pp. 1–10, 2015.

[95] D. Griffith, A. B. Mosbah, and R. Rouil, “Group discovery time in device-to-device (d2d) proximity services (prose) networks,” in *INFOCOM 2017-IEEE Conference on Computer Communications, IEEE.* IEEE, 2017, pp. 1–9.

[96] A. B. Mosbah, D. Griffith, and R. Rouil, “Enhanced transmission algorithm for dynamic device-to-device direct discovery,” in *Consumer Communications & Networking Conference (CCNC), 2018 15th IEEE Annual.* IEEE, 2018, pp. 1–8.

[97] ——, “A novel adaptive transmission algorithm for device-to-device direct discovery,” in *Wireless Communications and Mobile Computing Conference (IWCMC), 2017 13th International.* IEEE, 2017, pp. 177–182.

[98] A. Asadi, Q. Wang, and V. Mancuso, “A survey on device-to-device communication in cellular networks,” *IEEE Communications Surveys Tutorials*, vol. 16, no. 4, pp. 1801–1819, Fourthquarter 2014.

[99] Y. Wang, W. Wang, and M. Song, “How Durable and Stable Is a File Sharing on the Move in Cellular-Assisted D2D Communications?” in *IEEE GLOBECOM 2017.*

[100] C. Gao, Y. Li, and D. Jin, “Mobility assisted device-to-device communications underlaying cellular networks,” in *2016 International Conference on Computing, Networking and Communications (ICNC).* IEEE, 2016, pp. 1–6.

[101] E. Hossain, M. Rasti, H. Tabassum, and A. Abdelnasser, “Evolution toward 5g multi-tier cellular wireless networks: An interference management perspective,” *IEEE Wireless Communications*, vol. 21, no. 3, pp. 118–127, 2014.

[102] S. Landström, A. Furuskãr, K. Johansson, L. Falconetti, and F. Kronestedt, “Heterogeneous networks–increasing cellular capacity,” *The data boom: opportunities and challenges*, vol. 4, 2011.

[103] J.-B. Park and K. S. Kim, “Load-balancing scheme with small-cell cooperation for clustered heterogeneous cellular networks,” *IEEE Transactions on Vehicular Technology*, vol. 67, no. 1, pp. 633–649, 2018.

[104] J. I. Agbinya, M. C. Aguayo-Torres, and R. Klempous, *4G Wireless Communication Networks: Design Planning and Applications.* River Publishers, 2013.

[105] A. Ghosh, N. Mangalvedhe, R. Ratasuk, B. Mondal, M. Cudak, E. Visotsky, T. A. Thomas, J. G. Andrews, P. Xia, H. S. Jo *et al.*, "Heterogeneous cellular networks: From theory to practice," *IEEE communications magazine*, vol. 50, no. 6, pp. 54–64, 2012.

[106] J. G. Andrews, F. Baccelli, and R. K. Ganti, "A tractable approach to coverage and rate in cellular networks," *IEEE Transactions on Communications*, vol. 59, no. 11, pp. 3122–3134, 2011.

[107] H. S. Dhillon, R. K. Ganti, F. Baccelli, and J. G. Andrews, "Modeling and analysis of k-tier downlink heterogeneous cellular networks," *IEEE Journal on Selected Areas in Communications*, vol. 30, no. 3, pp. 550–560, 2012.

[108] T. D. Novlan, H. S. Dhillon, and J. G. Andrews, "Analytical modeling of uplink cellular networks," *IEEE Transactions on Wireless Communications*, vol. 12, no. 6, pp. 2669–2679, 2013.

[109] J. G. Andrews, R. K. Ganti, M. Haenggi, N. Jindal, and S. Weber, "A primer on spatial modeling and analysis in wireless networks," *IEEE Communications Magazine*, vol. 48, no. 11, pp. 156–163, 2010.

[110] Z. Lin, Y. Gao, B. Gong, X. Zhang, and D. Yang, "Stochastic geometry study on small cell on/off adaptation," in *Communications and Networking in China (CHINACOM), 2014 9th International Conference on.* IEEE, 2014, pp. 331–334.

[111] T. Ding, M. Ding, G. Mao, Z. Lin, D. López-Pérez, and A. Y. Zomaya, "Uplink performance analysis of dense cellular networks with los and nlos transmissions," *IEEE Transactions on Wireless Communications*, vol. 16, no. 4, pp. 2601–2613, 2017.

[112] J. Yoon and G. Hwang, "Distance-based inter-cell interference coordination in small cell networks: Stochastic geometry modeling and analysis," *IEEE Transactions on Wireless Communications*, vol. 17, no. 6, pp. 4089–4103, 2018.

[113] Y. Wang and Q. Zhu, "Modeling and analysis of small cells based on clustered stochastic geometry." *IEEE Communications Letters*, vol. 21, no. 3, pp. 576–579, 2017.

[114] W. C. Cheung, T. Q. Quek, and M. Kountouris, "Throughput optimization, spectrum allocation, and access control in two-tier femtocell networks," *IEEE Journal on Selected Areas in Communications*, vol. 30, no. 3, pp. 561–574, 2012.

[115] G. Salami, S. Burley, O. Durowoju, and C. Kellett, "Lte indoor small cell capacity and coverage comparison," in *Personal, Indoor and Mobile Radio Communications (PIMRC Workshops), 2013 IEEE 24th International Symposium on*. IEEE, 2013, pp. 66–70.

[116] L. Chen, F. R. Yu, H. Ji, G. Liu, and V. Leung, "Distributed virtual resource allocation in small cell networks with full duplex self-backhauls and virtualization," *IEEE Transactions on Vehicular Technology*, vol. PP, no. 99, pp. 1–1, 2015.

[117] S. Sadr and R. S. Adve, "Partially-Distributed Resource Allocation in Small-Cell Networks," *IEEE Transactions on Wireless Communications*, vol. 13, no. 12, pp. 6851–6862, Dec 2014.

[118] L. Cheng, J. Zheng, and J. Xiao, "A distributed downlink resource allocation algorithm for dense small cell networks," in *Wireless Communications Signal Processing (WCSP), 2015 International Conference on*, Oct 2015, pp. 1–6.

[119] A. Abdelnasser, E. Hossain, and D. I. Kim, "Tier-aware resource allocation in ofdma macrocell-small cell networks," *IEEE Transactions on Communications*, vol. 63, no. 3, pp. 695–710, March 2015.

[120] H. Zhang, C. Jiang, N. C. Beaulieu, X. Chu, X. Wang, and T. Q. S. Quek, "Resource Allocation for Cognitive Small Cell Networks: A Cooperative Bargaining Game Theoretic Approach," *IEEE Transactions on Wireless Communications*, vol. 14, no. 6, pp. 3481–3493, June 2015.

[121] P. Semasinghe, K. Zhu, and E. Hossain, "Distributed resource allocation for self-organizing small cell networks: An evolutionary game approach," in *2013 IEEE Globecom Workshops (GC Wkshps)*, Dec 2013, pp. 702–707.

[122] P. Semasinghe, E. Hossain, and K. Zhu, "An evolutionary game for distributed resource allocation in self-organizing small cells," *IEEE Transactions on Mobile Computing*, vol. 14, no. 2, pp. 274–287, Feb 2015.

[123] S. Chae, M. Z. Chowdhury, T. Nguyen, and Y. M. Jang, "A dynamic frequency allocation scheme for moving small-cell networks," in *2012 International Conference on ICT Convergence (ICTC)*, Oct 2012, pp. 125–128.

[124] S. Jangsher and V. O. K. Li, "Resource allocation in cellular networks with moving small cells with probabilistic mobility," in *2014 IEEE 25th Annual International Symposium on Personal, Indoor, and Mobile Radio Communication (PIMRC)*, Sept 2014, pp. 1701–1705.

[125] ——, "Resource Allocation in Moving Small Cell Network," *IEEE Transactions on Wireless Communications*, vol. PP, no. 99, pp. 1–1, 2016.

[126] S. Jangsher and V. Li, "Backhaul resource allocation for existing and newly-arrived moving small cells," *IEEE Transactions on Vehicular Technology*, 2016.

[127] M. Krbalek and P. Seba, "Headway statistics of public transport in mexican cities," *Journal of Physics A: Mathematical and General*, vol. 36, no. 1, p. L7, 2002.

[128] S. N. Chiu, D. Stoyan, W. S. Kendall, and J. Mecke, *Stochastic geometry and its applications.* John Wiley & Sons, 2013.

[129] "Evolved Universal Terrestrial Radio Access (E-UTRA); Radio Resource Control (RRC); Protocol specification- TS:36.331," Third Generation Partnetship Project (3GPP), techreport TR 36.331, 2014.

[130] 3GPP, "LTE; Evolved Universal Terrestrial Radio Access (E-UTRA); (MAC) Protocol specification," 3GPP, TS 36.321, 2014.

[131] M. Hazewinkel, *Encyclopaedia of Mathematics: Volume 6: Subject Index—Author Index.* Springer Science & Business Media, 2013.

[132] G. Fodor, S. Parkvall, S. Sorrentino, P. Wallentin, Q. Lu, and N. Brahmi, "Device-to-device communications for national security and public safety," *IEEE Access*, vol. 2, pp. 1510–1520, 2014.

[133] B. Zhou, H. Hu, S.-Q. Huang, and H.-H. Chen, "Intracluster device-to-device relay algorithm with optimal resource utilization," *IEEE transactions on vehicular technology*, vol. 62, no. 5, pp. 2315–2326, 2013.

[134] M. Ashraf, W.-Y. Yeo, M. Woo, and K.-G. Lee, "Smart energy efficient device-to-multidevice cooperative clustering for multicasting content," *International Journal of Distributed Sensor Networks*, vol. 12, no. 4, p. 3727918, 2016.

[135] A. Paramonov, O. Hussain, K. Samouylov, A. Koucheryavy, R. Kirichek, and Y. Koucheryavy, "Clustering optimization for out-of-band d2d communications," *Wireless Communications and Mobile Computing*, vol. 2017, 2017.

[136] P. Rawat, M. Haddad, and E. Altman, "Towards efficient disaster management: 5g and device to device communication," in *2015 2nd International Conference on Information and Communication Technologies for Disaster Management (ICT-DM)*. IEEE, 2015, pp. 79–87.

[137] J. Harri, F. Filali, and C. Bonnet, "Mobility models for vehicular ad hoc networks: a survey and taxonomy," *IEEE Communications Surveys & Tutorials*, vol. 11, no. 4, pp. 19–41, 2009.

[138] C. Bettstetter, G. Resta, and P. Santi, "The node distribution of the random waypoint mobility model for wireless ad hoc networks," *IEEE Transactions on mobile computing*, no. 3, pp. 257–269, 2003.

[139] C. Bettstetter, H. Hartenstein, and X. Pérez-Costa, "Stochastic properties of the random waypoint mobility model," *Wireless Networks*, vol. 10, no. 5, pp. 555–567, 2004.

[140] J. Philip, *The probability distribution of the distance between two random points in a box*. KTH mathematics, Royal Institute of Technology, 2007.

[141] M. Horowitz, "Probability of random paths across elementary geometrical shapes," *Journal of Applied Probability*, vol. 2, no. 1, pp. 169–177, 1965.

[142] S. B. Provost and K. Yu, "An approximate distribution for the random distance between sets of rectangles," *GSTF Journal of Mathematics, Statistics and Operations Research (JMSOR)*, vol. 2, no. 1, 2018.

[143] Y. Sui, I. Guvenc, and T. Svensson, "On the deployment of moving networks in ultra-dense urban scenarios," in *5G for Ubiquitous Connectivity (5GU), 2014 1st International Conference on*, Nov 2014, pp. 240–245.

[144] S. Jangsher and V. O. Li, "Backhaul Resource Allocation for Existing and Newly Arrived Moving Small Cells," *IEEE Trans. on Vehicular Tech.*, 2017.

[145] M. Duarte et al., "Experiment-driven characterization of full-duplex wireless systems," *IEEE Trans. on Wireless Comm.*, 2012.

[146] Y. Chen, P. Martins, L. Decreusefond, F. Yan, and X. Lagrange, "Stochastic analysis of a cellular network with mobile relays," in *Global Communications Conference (GLOBECOM), 2014 IEEE.* IEEE, 2014, pp. 4758–4763.

[147] S. K. Moore, "Super-accurate GPS Chips Coming to Smartphones in 2018," *IEEE Spectrum, Sept*, vol. 21, 2017.

[148] X. Lin, R. K. Ganti, P. J. Fleming, and J. G. Andrews, "Towards understanding the fundamentals of mobility in cellular networks," *IEEE Transactions on Wireless Communications*, vol. 12, no. 4, pp. 1686–1698, 2013.

[149] W. Ni, "A Self-Learning Based Antenna System for Indoor Wireless Network," *International Journal of Advanced Pervasive and Ubiquitous Computing (IJAPUC)*, vol. 9, no. 4, pp. 78–87, 2017.

[150] A. Goldsmith, *Wireless communications.* Cambridge university press, 2005.

[151] O. Georgiou, S. Wang, M. Z. Bocus, C. P. Dettmann, and J. P. Coon, "Directional antennas improve the link-connectivity of interference limited ad hoc networks," in *2015 IEEE 26th Annual International Symposium on Personal, Indoor, and Mobile Radio Communications (PIMRC).* IEEE, 2015, pp. 1311–1316.

[152] A. B. Constantine *et al.*, "Antenna theory: analysis and design," *MICROSTRIP ANTENNAS, third edition, John wiley & sons*, 2005.

[153] Á. Baricz, *Generalized Bessel functions of the first kind.* Springer, 2010.

[154] I. S. Gradshteyn and I. M. Ryzhik, *Table of integrals, series, and products.* Academic press, 2014.

[155] C. Clapham and J. Nicholson, *The concise Oxford dictionary of mathematics.* OUP Oxford, 2009.

[156] S. Sen, N. Santhapuri, R. R. Choudhury, and S. Nelakuditi, "Successive interference cancellation: A back-of-the-envelope perspective," in *Proceedings of the 9th ACM SIGCOMM Workshop on Hot Topics in Networks.* ACM, 2010, p. 17.

[157] A. Jeffrey and H. H. Dai, *Handbook of mathematical formulas and integrals.* Elsevier, 2008.

[158] K. Kannike, "Notes on feynman parametrisation and the dirac delta function," Online, may 2013. [Online]. Available: http://kodu.ut.ee

[159] "Evolved Universal Terrestrial Radio Access (E-UTRA); Requirements for support of radio resource management," Third Generation Partnetship Project (3GPP), Techreport TS 36.133 12.7.0 R-12, jun 2015.

[160] Y.-J. Yu, W.-C. Tsai, and A.-C. Pang, "Backhaul traffic minimization under cache-enabled comp transmissions over 5g cellular systems," in *2016 IEEE Global Communications Conference (GLOBECOM).* IEEE, 2016, pp. 1–7.

[161] S. Krishnan, M. Afshang, and H. S. Dhillon, "Effect of retransmissions on optimal caching in cache-enabled small cell networks," *IEEE Transactions on Vehicular Technology*, vol. 66, no. 12, pp. 11 383–11 387, 2017.

[162] S. Glass, I. Mahgoub, and M. Rathod, "Leveraging manet-based cooperative cache discovery techniques in vanets: A survey and analysis," *IEEE Communications Surveys & Tutorials*, vol. 19, no. 4, pp. 2640–2661, 2017.

[163] T. Wu, T. S. Rappaport, and C. M. Collins, "The Human Body and Millimeter-wave Wireless Communication Systems: Interactions and Implications," in *Communications (ICC), 2015 IEEE International Conference on.* IEEE, 2015, pp. 2423–2429.

[164] "Technical Specification Group Radio Access Network; Mobile Relay for Evolved Universal Terrestrial Radio Access (E-UTRA)," Third Generation Partnetship Project (3GPP), Techreport TR 36.836, 2012.